



Chair of Chemistry of Polymeric Materials

Doctoral Thesis

SYNTHESIS OF STIMULI-RESPONSIVE
POLYMERS FOR THE PREPARATION OF
COMPLEX 3D OBJECTS WITH SPATIALLY
RESOLVED FUNCTIONALITIES

Ines Cazin, M.Sc.

June 2024



MONTANUNIVERSITÄT LEOBEN
www.unileoben.ac.at

AFFIDAVIT

I declare on oath that I wrote this thesis independently, did not use any sources and aids other than those specified, have fully and truthfully reported the use of generative methods and models of artificial intelligence, and did not otherwise use any other unauthorized aids.

I declare that I have read, understood and complied with the "Good Scientific Practice" of the Montanuniversität Leoben.

Furthermore, I declare that the electronic and printed versions of the submitted thesis are identical in form and content.

Date 11.06.2024

Signature Author
Ines Cazin

The research work was performed within the COMET-Module project “Chemitecture“ (project-no.: 21647048) at the Polymer Competence Center Leoben GmbH (PCCL, Austria) within the framework of the COMET-program of the Federal Ministry for Transport, Innovation and Technology and the Federal Ministry for Digital and Economic Affairs with contributions by Montanuniversitaet Leoben, Politecnico di Torino, Helios TBLUS and bto-epoxy. Funding is provided by the Austrian Government and the State Government of Styria.

To my brother

Acknowledgments

First, I wish to express my gratitude to *Priv.-Doz. Dr. Sandra Schlögl* and *Univ.-Prof. Dr. Wolfgang Kern* for giving me the opportunity to do my PhD research. Especially I want to express my thanks to Dr. Schlögl as my supervisor for her dedicated scientific support, scientific advice, helpful discussions, and patience.

Further, I would like to thank my project partner *Helios TBLUS d.o.o.* for the interesting and useful meetings as well as for hosting me in their synthetic lab. I am grateful that I had the chance to work with *Dr. Martin Ocepek*, *Aleš Stražar*, and *Dipl. ing. Janez Kecelj*. Thank you for sharing your experience and knowledge with me. In addition, I want to thank *Dipl. ing. Aleš Sopčič*, *Miha Kokalj*, and *Dr. Nataša Čuk* for the nice working atmosphere and support.

I am grateful to *Prof. Dr. Marco Sangermano* and *Prof. Dr. Ignazio Roppolo* from Politecnico di Torino, for sharing their knowledge with me, scientific guidance, and experimental support. I would like to thank my colleagues in Italy for their warm welcome and their invaluable assistance in the lab.

Additionally, I would like to thank colleagues from PCCL and Montanuniversität Leoben for their support in the lab over the past four years. Particular gratitude goes to *DI Milena Gleirscher* for her dedicated work on her master thesis, *Evelyn Sattler*, and *Gerald Meier* for their technical support.

My greatest gratitude goes to my family – mother, father, and brother. For their endless love. I would have never made it without their love and encouragement. I am also grateful to my friends *Danica Velimirović*, *Tomislav Knapić*, *Darko Domitrović*, *Daniel Bautista*, *Eliza Truszkiewicz*, *Dr. Sofie Celen*, and *Dr. Sugosh Prabhu* for their life advice, support, and constant encouragement during the hardest time in my life in 2022.

I dedicate this dissertation to my brother *Damir*, who tragically passed away in the Kamnik–Savinja Alps at the beginning of 2022. Damir was a warm-hearted modest man, with an outstanding personality, strong character, and morals, as well as a respected and highly regarded mechanical engineer in his profession. His love for music and mountaineering was an endless source of inspiration, while his support and belief in my potential shaped my path in science. May his legacy live on through this work, serving as a timeless reminder of his extraordinary character and influence on me. I am so proud to have had such an amazing brother.

COOPERATIONS

The results of this thesis were published in four peer-reviewed scientific papers.

- (1) Cazin, I.; Gleirscher, M. O.; Fleisch, M.; Berer, M.; Sangermano, M.; Schlögl, S. Spatially Controlling the Mechanical Properties of 3D Printed Objects by Dual-Wavelength Vat Photopolymerization. *Additive Manufacturing* 2022, 57, 102977. DOI: 10.1016/j.addma.2022.102977.
- (2) Cazin, I.; Plevová, K.; Alabiso, W.; Vidović, E.; Schlögl, S. Dual-Wavelength Vat Photopolymerization 3D Printing with Hybrid Acrylate-Epoxy Resins: Influence of Resin Composition on Microstructure and Mechanical Properties. *Adv Eng Mater* 2024. DOI: 10.1002/adem.202301699.
- (3) Cazin, I.; Ocepek, M.; Kecelj, J.; Stražar, A. S.; Schlögl, S. Synthesis of Bio-Based Polyester Resins for Vat Photopolymerization 3D Printing. *Materials* 2024, 17 (8), 1890. DOI: 10.3390/ma17081890.
- (4) Cazin, I.; Rossegger, E.; Roppolo, I.; Sangermano, M.; Granitzer, P.; Rumpf, K.; Schlögl, S. Digital light processing 3D printing of dynamic magneto-responsive thiol-acrylate composites. *RSC advances* 2023, 13 (26), 17536–17544. DOI: 10.1039/D3RA02504G.

In addition to the publications mentioned above, the following study was also published:

- (1) Cazin, I.; Rossegger, E.; La Guedes de Cruz, G.; Griesser, T.; Schlögl, S. Recent Advances in Functional Polymers Containing Coumarin Chromophores. *Polymers* 2020, 13 (1). DOI: 10.3390/polym13010056.

Two master theses were completed in the course of this research work.

Milena Olga Gleirscher

Additive manufacturing of photopolymers with multi-material properties using dual-wavelength DLP printing, Montanuniversität Leoben, 2021.

Some of the results of this work are presented in Section 3.

Nikola Šebalj

DLP 3D printing of materials with heterogeneous material properties, Faculty of Chemical Engineering and Technology, Zagreb, 2022.

SYNTHESIS OF STIMULI-RESPONSIVE POLYMERS FOR THE PREPARATION OF COMPLEX 3D OBJECTS WITH SPATIALLY RESOLVED FUNCTIONALITIES

ABSTRACT

Light-sensitive resins are commonly used materials in additive manufacturing (AM) processes. Vat photopolymerization is an AM technique that relies on the local solidification of a liquid photopolymer resin by light exposure, forming desired 3D objects in a layer-by-layer manner. Digital light processing (DLP) 3D printing is a type of vat photopolymerization that provides an innovative strategy for producing 3D objects with high resolution, as well as high dimensional accuracy, from versatile feedstock materials. Although the DLP technology offers layer-free, scalable, and rapid production of 3D objects, it is still often limited to a single material. However, multi-functional materials may bring revolutionary solutions in a variety of fields, encompassing soft robotics, electronics, and biomedical engineering. Multi-material vat polymerization brings many challenges, including printing a single photocurable resin where heterogeneous properties of materials can be spatially controlled, forming complex geometries with embedded functionality. In this dissertation, orthogonal photochemistries undergoing independent cross-linking reactions using light with different wavelengths were explored, optimized, and studied in detail. A dual photocurable resin based on commercially available monomers was developed, which consisted of multi-functional acrylates (cured at 405 nm by radical-induced chain growth reaction) and bi-functional epoxy-monomers (additionally cured at 365 nm by cationic curing). Furthermore, the synthetic route for bio-based acrylate-modified polyester resin was optimized with sufficiently low viscosity for processing them with vat photopolymerization 3D printing. In the final part of the thesis, DLP 3D printing of functional polymers was demonstrated by printing magneto-responsive thiol-acrylate composites. Thermo-activated bond exchange reactions were exploited by following catalyzed transesterification to induce a material flow above the networks' topological freezing temperature. The magneto-responsive photocurable resin was optimized in terms of viscosity and stability. Magneto-active objects were printed with a Fe_3O_4 loading up to 6 wt%.

SYNTHESE VON STIMULI-RESPONSIVEN POLYMEREN FÜR DIE HERSTELLUNG KOMPLEXER 3D-OBJEKTE MIT RÄUMLICH AUFGELÖSTEN FUNKTIONALITÄTEN

KURZFASSUNG

Lichtempfindliche Harze sind häufig verwendete Materialien in additiven Fertigungsverfahren (AM). Die badbasierte Photopolymerisation (engl. vat photopolymerization) ist ein AM-Verfahren, das auf der lokalen Verfestigung eines flüssigen Photopolymerharzes durch Lichteinwirkung beruht, wodurch die gewünschten 3D-Objekte Schicht für Schicht entstehen. Der 3D-Druck mit digitaler Lichtverarbeitung (DLP) ist eine Form der badbasierten Photopolymerisation, die eine innovative Strategie zur Herstellung von 3D-Objekten mit hoher Auflösung und hoher Maßgenauigkeit aus vielseitigen Ausgangsmaterialien bietet. Obwohl die DLP-Technologie eine schichtfreie, skalierbare und schnelle Produktion von 3D-Objekten ermöglicht, ist sie häufig auf ein einziges Material beschränkt. Multifunktionale Materialien können jedoch revolutionäre Lösungen in einer Vielzahl von Bereichen wie Soft-Robotik, Elektronik und Biomedizintechnik bieten. Die badbasierte Photopolymerisation mit mehreren Materialien bringt viele Herausforderungen mit sich, wie z. B. das Drucken eines einzigen photohärtbaren Harzes. In dieser Dissertation werden orthogonale Vernetzungsreaktionen unter Verwendung von Licht mit unterschiedlichen Wellenlängen angewendet, optimiert und im Detail untersucht. Ein duales photohärtbares Harz aus kommerziell verfügbaren Monomeren wurde entwickelt, das aus multifunktionalen Acrylaten (gehärtet bei 405 nm durch radikal-induzierte Kettenwachstumsreaktion) und bifunktionalen Epoxy-Monomeren (zusätzlich vernetzt bei 365 nm durch kationische Härtung) besteht. Darüber hinaus wurden die Synthesewege für bio-basierte acryl-modifizierte Polyesterharze mit ausreichend geringer Viskosität für die Verarbeitung im 3D-Druck mittels Vat-Polymerisation optimiert. Im finalen Teil Arbeit wird der DLP-3D-Druck von Funktionspolymeren anhand des Drucks von magneto-responsiven Thiol-Acrylat-Verbundwerkstoffen veranschaulicht. Die thermisch aktivierte Bindungsaustauschreaktionen wurden durch eine katalysierte Umesterung erreicht, um einen Materialfluss oberhalb der topologischen Gefriertemperatur des Netzwerks zu induzieren. Das magneto-responsive, photohärtbare Harz wurde in Bezug auf Viskosität und Stabilität optimiert. Der Anteil an Fe_3O_4 in den gedruckten magnetisch aktiven Objekten betrug bis zu 6 Gew.-%.

Contents

1	General introduction.....	13
2	Motivation and structure of thesis.....	14
3	Theoretical background.....	17
1.1.	Photochemistry.....	17
3.1.1	Light absorption.....	17
3.1.2	Photoinitiators.....	20
3.2	Additive manufacturing.....	26
3.2.1	Fused filament fabrication.....	28
3.2.2	Direct ink writing.....	29
3.2.3	Selective laser sintering.....	29
3.2.4	Stereolithography.....	30
3.2.5	Digital light processing.....	31
3.2.6	Liquid crystal display 3D printing.....	33
3.2.7	Hot lithography.....	34
3.2.8	Two-photon absorption polymerization.....	35
3.2.9	Volumetric 3D printing.....	36
3.3	Vat photopolymerization multi-material additive manufacturing.....	37
3.3.1	Manually and mechanically switching resins/resin vats.....	38
3.3.2	Variation in light intensity and exposure time.....	40
3.3.3	Orthogonal chemistry mechanisms.....	41
3.4	Dynamic covalent networks.....	44
4	Publication I:.....	47
4.1	Abstract.....	48
4.2	Introduction.....	49

4.3	Results and Discussion	51
4.3.1	Network design and cure kinetics	51
4.3.2	Multi-Material DLP 3D printing experiments.....	55
4.3.3	Wavelength dependent thermo-mechanical and mechanical properties	59
4.4	Conclusion	63
4.5	Experimental part	64
4.5.1	Materials and chemicals	64
4.5.2	Preparation of photocurable formulation	64
4.5.3	Characterization of cure kinetics.....	65
4.5.4	Dual wavelength DLP 3D printing.....	65
4.5.5	Characterization of thermomechanical and mechanical properties.....	66
4.5.6	UV-Vis measurements	66
4.6	Acknowledgements	66
4.7	Supporting Information	68
5	Publication II:	72
5.1	Abstract.....	73
5.2	Introduction	74
5.3	Results and discussion	76
5.3.1	Photopolymerization kinetics and photopolymer morphology	76
5.3.2	Photopolymer morphology.....	81
5.3.3	Thermomechanical and mechanical properties	84
5.3.4	Additive manufacturing.....	87
5.4	Conclusion.....	88
5.5	Experimental part	90
5.5.1	Materials and chemicals	90

5.5.2	Preparation of photocurable resin	90
5.5.3	Characterization of cure kinetics and viscosity measurements	91
5.5.4	Equilibrium swelling measurements	91
5.5.5	Photo-differential scanning calorimetry (DSC)	92
5.5.6	Dual wavelength DLP 3D printing.....	92
5.5.7	Characterization of thermomechanical and mechanical properties.....	93
5.5.8	Atomic force microscopy	93
5.6	Acknowledgements	94
6	Publication III:.....	95
6.1	Abstract.....	96
6.2	Introduction	96
6.3	Materials and Methods	99
6.3.1	Materials and Chemicals	99
6.3.2	Polyester synthesis	100
6.3.3	Preparation of Resin Formulations.....	100
6.3.4	Resin Characterization	100
6.3.5	Color Measurement	101
6.3.6	DLP 3D Printing.....	101
6.3.7	Characterization of Mechanical and Thermomechanical Properties.....	102
6.4	Results and Discussion	102
6.4.1	Polyester Synthesis.....	102
6.4.2	Additive Manufacturing	106
6.4.3	Mechanical and Thermomechanical Properties	107
6.5	Conclusions	109
6.6	Acknowledgments	110

6.7	Supporting Information	111
7	Publication IV:	115
7.1	Abstract.....	116
7.2	Introduction	117
7.3	Results and discussion	119
7.3.1	Network design and optimization of the photocurable resin containing Fe ₃ O ₄ nanofillers	119
7.3.2	Printing and material characterization.....	123
7.3.3	Thermal healing and magnetic properties	124
7.4	Experimental.....	127
7.4.1	Materials and chemicals	127
7.4.2	Preparation of resins.....	127
7.4.3	Characterization	127
7.4.4	DLP 3D printing.....	128
7.4.5	Thermo-activated healing.....	128
7.4.6	Welding experiments and magnetic properties	129
7.5	Conclusions	129
7.6	Acknowledgements	129
7.7	Supporting Information	130
8	Conclusions and outlook	132
9	References	136
	Curriculum Vitae.....	157

1 General introduction

Photochemistry is present in everyday life, where in primeval times the only source of energy was from the sun. Synthesis of complex organic molecules such as proteins and nuclear acids is driven by photochemical reactions of simple gas molecules including ammonia, methane, and carbon dioxide. Beyond nature, photochemistry is employed for various applications in science and technology. Photochemistry refreshed synthetic organic chemistry by enabling the synthesis of numerous organic compounds, which could not be produced by dark reactions. There are several advantages that thermal polymerization cannot fulfill, such as low-temperature operation, fast curing, low volatile organic compound emission, energy efficiency, and environmental protection.^[1-3] Some examples of industrially relevant photochemical synthesis routes include the synthesis of vitamin D₂ from ergosterol isolated from fungi and yeast^[4], the synthesis of cubanes (antiviral agents)^[5], and the synthesis of the monomer caprolactam for the production of Nylon 6^[6].

Ancient and historical applications of polymer photochemistry included mummification, photography, and ship sealants. The modern history of photopolymers began in the mid-20th century with the first patents on UV-cured inks based on unsaturated polymers.^[7] Nowadays, photochemical polymers take part in green chemical development and processing, covering applications ranging from biomedicine, stereolithography, optics, biotechnology, microelectronics, photonics, coatings, thin film formation, and energy.^[8,9]

Chemists have searched for decades for a solution to the challenge of controlling chemical reactivity, which is crucial for chemical and biological processes. The key solution is to apply external stimuli without affecting the overall system, which can be accomplished by usage of light.^[10-13] In 1912, one of the pioneers of photochemistry, Giacomo Ciamician, suggested using solar energy as a power source for human communities.^[14] Furthermore, an organic transformation of isomerization of Santonin to Lumisantonin was published in 1958 as one of the earliest examples of light-triggered reactions.^[15]

For many years, photopolymers have found their applications in decorative and protective coating materials. Over the past years, with the high interest in additive manufacturing of 3D objects, photopolymers received much attention in vat photopolymerization technology. Over the past ten years, additive manufacturing (AM), also known as three-dimensional (3D) printing, has attracted a lot of attention from both academia and industry. Vat photopolymerization is one of the AM

methods that use photoreactive resins for the 3D printing process. The prototype of the stereolithography apparatus was designed by A. Herbert, however, the suggested setup was not commercialized.^[16] In 1984 in the United States, Charles Hull^[17] reported a patent on an improved system for stereolithography, which is based on a UV laser for curing photocurable resin and a layer-by-layer approach to building 3D objects. A similar system was reported by Jean-Claude André and co-workers in France^[18]. The big advantage is that AM allows the fabrication of complex geometries without the usage of molds and heavy machining, which opens up new opportunities in the future production industry. The interest is constantly growing in developing functional devices for a wide range of applications in a variety of fields such as soft robotics, healthcare, and electronics. This technique is based on the local solidification of photocurable liquid resins through light exposure. It can be broadly divided into two types: stereolithography (SLA) where 3D objects are generated by using point-wise a scanning laser beam, and digital light processing (DLP) based on layer-by-layer printing, where one layer is printed at a time. Although DLP techniques have advanced over the years to quick, scalable, and even layer-free fabrication of 3D objects, they are still often limited to printing a single material at a time. Multi-material DLP 3D printing can be achieved by exchanging resins or resin vats. However, these methods require time-consuming steps due to cleaning processes with washing and drying steps between an exchange.^[19]

2 Motivation and structure of thesis

It is not surprising that interest in AM technologies is rapidly increasing due to many advantages including being inexpensive, quick, and accurate when producing items with complex geometries. Whilst multi-material structures can be applied in advanced electric and electronic devices, in soft robotics (actuators), in the health care sector (e.g. prosthetics with adaptable mechanical properties), and in integrated sensor technologies, the manufacturing of 3D objects with heterogeneous properties by vat photopolymerization is still challenging. Moreover, nowadays most photopolymers used in vat photopolymerization are derived from fossil fuels. Currently, many research efforts are focused on developing 3D printable bio-based resins from bio-based biodegradable and recyclable materials. To tackle these challenges the thesis addresses the use of orthogonal photoreactions, monomers from bio-based feedstocks and the introduction of dynamic covalent bonds for the next generation of 3D printed multi-material structures.

In the first part of the thesis (Section 3 and 4), orthogonal photochemistries undergoing independent cross-linking reactions using lights with different wavelengths were explored and optimized. An applied dual photocurable resin consisted of multi-functional acrylates (cured at 405 nm by radical-induced chain growth reaction) and bi-functional epoxy-monomers (additionally cured at 365 nm by cationic curing). Wavelength-selective network formation was confirmed by FT-IR experiments, while tensile test and dynamic mechanical analysis showed distinctive difference in the related mechanical properties. Using a single resin vat and a dual-wavelength 3D printer operating at 405 and 365 nm, 3D structures were successfully fabricated with locally controlled mechanical properties. By optimizing the photocurable resin containing 50 wt% acrylate monomers and 50 wt% epoxy monomers, objects with soft ($\varepsilon = 24\%$, $\sigma = 1.0$ MPa) and stiff domains ($\varepsilon = 4\%$, $\sigma = 39.1$ MPa) were 3D printed. Additionally, the influence of resin composition and applied wavelength on cure kinetics, film morphology, (thermo)mechanical properties and printability were studied in detail. Fully separated as well as homogenous network morphologies were obtained depending on the ratio between acrylate and epoxy monomers, cure rate and applied light source (405 versus 365 nm).

The second part of the thesis (Section 5) focused on a synthesis route for photocurable resins where monomeric building blocks were step-wise replaced with bio-based alternatives. The majority commercially available building blocks are derived from petroleum-based precursors. Motivated by environmental concerns, a simple synthesis route for bio-based acrylate-modified polyester resins was optimized with sufficiently low viscosity for processing them with vat photopolymerization 3D printing. The synthesized bio-based acrylic resins were characterized by acid number, color and viscosity. Photocurable formulations were prepared by adding a radical photoinitiator, and polymerization kinetics, and thermomechanical and mechanical properties were then further investigated as a function of the resin structures and benchmarked against a commercially available petroleum-based counterpart. Moreover, printability of the prepared photocurable resins was demonstrated by successfully DLP 3D printing test specimens with a resolution in the millimeter range.

In the third part of the thesis (Section 6), DLP 3D printing of functional polymers was demonstrated by printing magneto-responsive thiol-acrylate composites. Motivated by high interest in processing materials with magnetic properties for 3D printing of functional and stimuli-triggered devices, additionally healing and re-shaping functions were demonstrated. Thermo-activated bond exchange

reactions were exploited by following catalyzed transesterification to induce a material flow above the networks' topological freezing temperature. The magneto-responsive photocurable resin was optimized in terms of viscosity and stability. Magneto-active objects were printed successfully with a Fe_3O_4 loading up to 6 wt%.

3 Theoretical background

1.1. Photochemistry

The driving force in polymer science is the usage of light to control the formation, structure, and biochemomechanical properties of polymeric materials. For processes such as polymer formation, shape change, polymer modification, or inducing smart material response, light is used for manipulation and control of those processes. Most importantly, photochemical reactions offer much greater energy available in a photon as compared to energy available in temperature-driven reactions, leading to a “green” alternative compared to thermal processes. Therefore, it is possible to drive reactions photochemically, which would not be possible to occur at ambient conditions without heating. Although photochemical reactions can proceed at ambient temperature and enable temporal control, one of the biggest benefits of photochemical reactions is spatial control achieved through methods such as photolithography techniques or using masks to selectively expose certain areas to light. Furthermore, spatial control of photochemical reactions can be achieved through the precise position of the light sources (e.g. digital light projectors) or by utilizing photoreactive compounds that react only to specific wavelengths of applied light. The spatiotemporal control of photochemical polymer processes is used in numerous applications ranging from lithography, and photoresist to stereolithography or additive manufacturing, where physicochemical changes occur in the exposed regions, while unexposed regions remain unaffected.^[9,20–22]

3.1.1 Light absorption

There are two basic laws related to photochemical reactions. The first law, called the Grotthus – Draper law states that only light absorbed by a system can start a photoreaction, while the second law, the Stark – Einstein law, also known as the photochemical equivalence law, states that every absorbed photon will cause a chemical reaction.^[23]

To start a photochemical reaction, the molecule must absorb a photon with three following rules: (1) there should be an overlap between the spectral emission of the light source and the absorption spectra of the target chromophore, (2) to start a desired reaction, the absorbed photon must have sufficient energy, and (3) to cause the desired reaction in the target molecule, the energy must ultimately lead to appropriate orbital transitions.^[9]

If all three previously mentioned rules are fulfilled, upon light absorption, an electron transfer from the highest occupied molecular orbital HOMO to the lowest un-occupied molecular orbital LUMO proceeds (Figure 1).

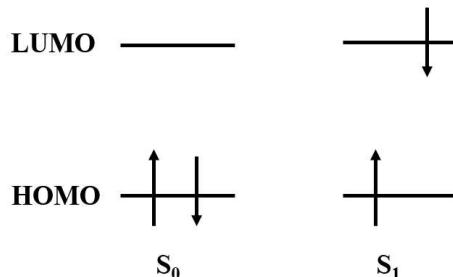


Figure 1. Diagram of HOMO-LUMO transition.^[23]

The Beer-Lambert law describes the light absorption of a single absorbing species:

$$A = \epsilon cd = -\log\left(\frac{I}{I_0}\right) \quad (1)$$

where A represents the absorbance of light within a film, ϵ and c represent molar absorptivity, d is optical path length, I_0 represents the incident light intensity, and I represent the light intensity exiting the film.^[24]

As not each absorbed photon occurs in the photochemical reaction, quantum yield (Φ)^[9] is a measure that helps to quantify the efficiency of photochemical processes. It is a ratio of the number of photons emitted to the number of photons absorbed:

$$\Phi = \frac{N_{Photons\ Emitted}}{N_{Photons\ Absorbed}} \quad (2)$$

The parameters of molar absorption and quantum yield are dependent on the wavelength, a high absorption throughout the film is necessary to achieve a fast reaction rate.

The Planck – Law describes the energy of an absorbed photon:

$$E = h\nu = hc\lambda \quad (3)$$

where the absorbed energy E directly depends on the Planck's constant (h) and photon's frequency (ν). The frequency of the photon (ν) is a function of the speed of light (c) in a vacuum, and the wavelength (λ).

In the 1930s, the Polish physicist Aleksander Jabłoński introduced a graphical representation used in photochemistry to describe the electronic transitions that occur in a molecule after light absorption.^[25] The energy levels of a molecule are represented on the vertical axis, and on the horizontal axis, various electronic states and transitions are represented. Upon exposure to the appropriate wavelength, photon absorption promotes an electron from its ground state (S_0) to its excited state (S_1). From the S_1 energy state, a molecule may return to the ground state (S_0) by emitting a photon of light (fluorescence). Alternatively, if the molecule undergoes intersystem crossing (ISC) to a triplet state (T_1), it can return to the ground state (S_0) by emitting a photon of light (phosphorescence). Fluorescence and phosphorescence processes known as deactivation processes, are in competition with photochemical processes. Additionally, to the deactivation process, the molecule can undergo non-radiative relaxation processes, such as internal conversion (IC), where the molecule returns to the ground state (S_0) without emitting light (the excess energy is dissipated as heat). Intersystem crossing refers to the process where a molecule transitions from a single excited state (S_1) to a triplet excited state (T_1), or vice versa, without emitting light. The described state can lead to different photochemical outcomes.^[9]

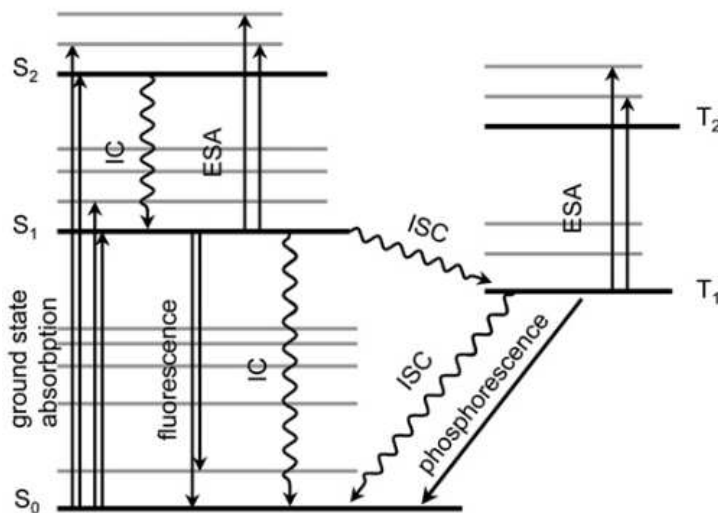


Figure 2. Jablonski diagram: IC – internal conversion, ESA – excited state absorption, ISC – intersystem crossing. Image adapted from ref.^[26].

3.1.2 Photoinitiators

After exposure to visible (Vis, 400 – 700 nm), ultraviolet (UV, mainly below 400 nm), or near-infrared (NIR, usually greater than 700 nm) light of the electromagnetic spectrum (Figure 3), photoinitiators will start photopolymerization by generating reactive species in the form of free radicals, anions, or cations.^[9,27,28] Therefore, photoinitiators can be categorized into radical type^[29,30], cationic type^[31–33], and photobase generators^[34–36].

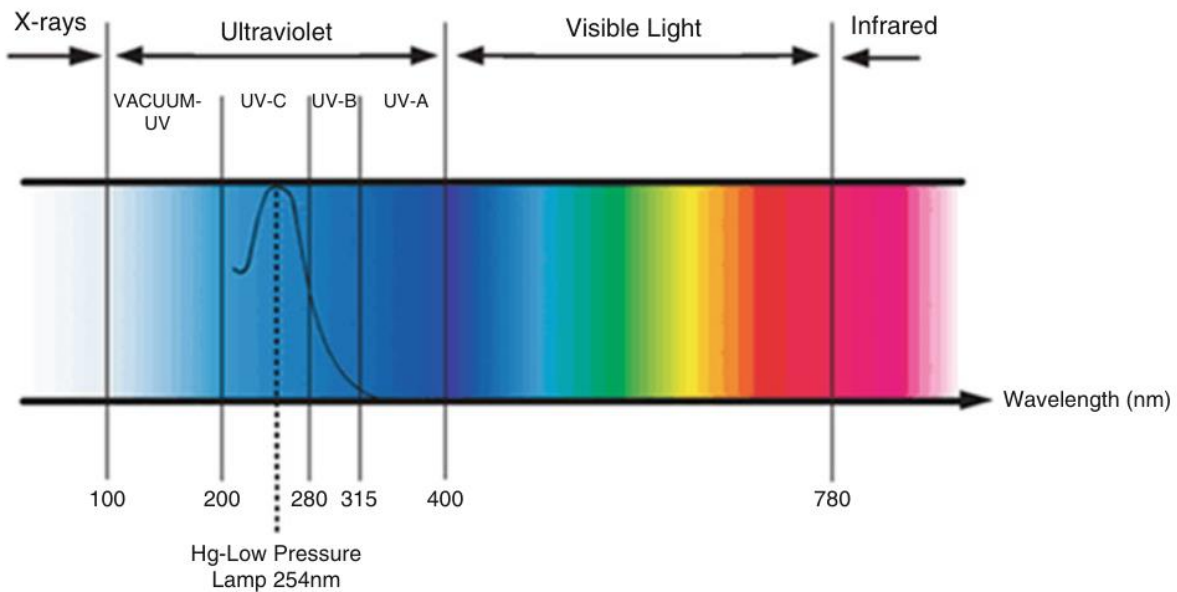


Figure 3. The electromagnetic spectrum of light. Reprinted with permission from ref. ^[28].

Free radical polymerization is based on the generation of free radicals or ions induced by a photoinitiator that is in the ground state before light exposure. Upon light exposure, an electronic transition occurs where the photoinitiator molecule moves from the ground state to an excited state resulting in the generation of active species.

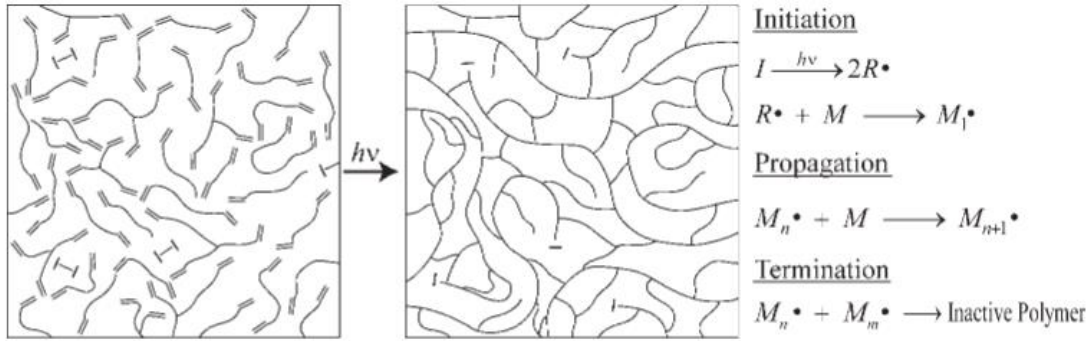


Figure 4. Illustration and steps of a radical photopolymerization reaction.^[37]

Figure 4 shows the steps of radical polymerization, which take place upon light irradiation. The steps are initiation, propagation, and termination. Initiation is the first step of the process and can be divided into two steps. Firstly, from the initiating molecule, one or two radicals are created. The second step includes a transfer of radicals from the initiator molecules to the monomers in the system. In the propagation step, chain propagation occurs by reaction of radicals with more monomers and the polymer with a growing chain length is formed. Termination is the last stage of radical polymerization where termination occurs due to a recombination or disproportionation of radicals.^[9,37]

The initiation rate R_i for radical photoinitiators that form two identical radicals can be calculated from Equation 4:

$$R_i = 2f\Phi I_0 [I]\varepsilon \quad (4)$$

where I_0 is the light intensity, ε is the molar absorptivity, f is the radical efficiency, Φ is the quantum yield, and I represent the concentration of the initiator. It should be noted that Equation 4 is only valid for films that have low light attenuation through their cross-section.^[9]

There are typically two different types of radical photoinitiators: Norrish Type I and Type II photoinitiators. Norrish Type I photoinitiators (α -cleavage) form radicals by following unimolecular bond cleavage. On the other hand, Type II photoinitiators (H-abstraction) follow a bimolecular reaction generating radicals by the interaction between the second molecule and the excited states of the absorbing molecule.^[38] The mechanism of the Norrish Type I reaction is based

on the homolytic cleavage of the weak covalent bonds resulting in formed radicals. Typically, the molecules of this type of photoinitiators includes oxime esters, benzoin, and benzils.^[29,31,39]

Figure 5 shows molecular structures of commercially used Norrish type I photoinitiators with a cleavage mechanism of Irgacure 1173.

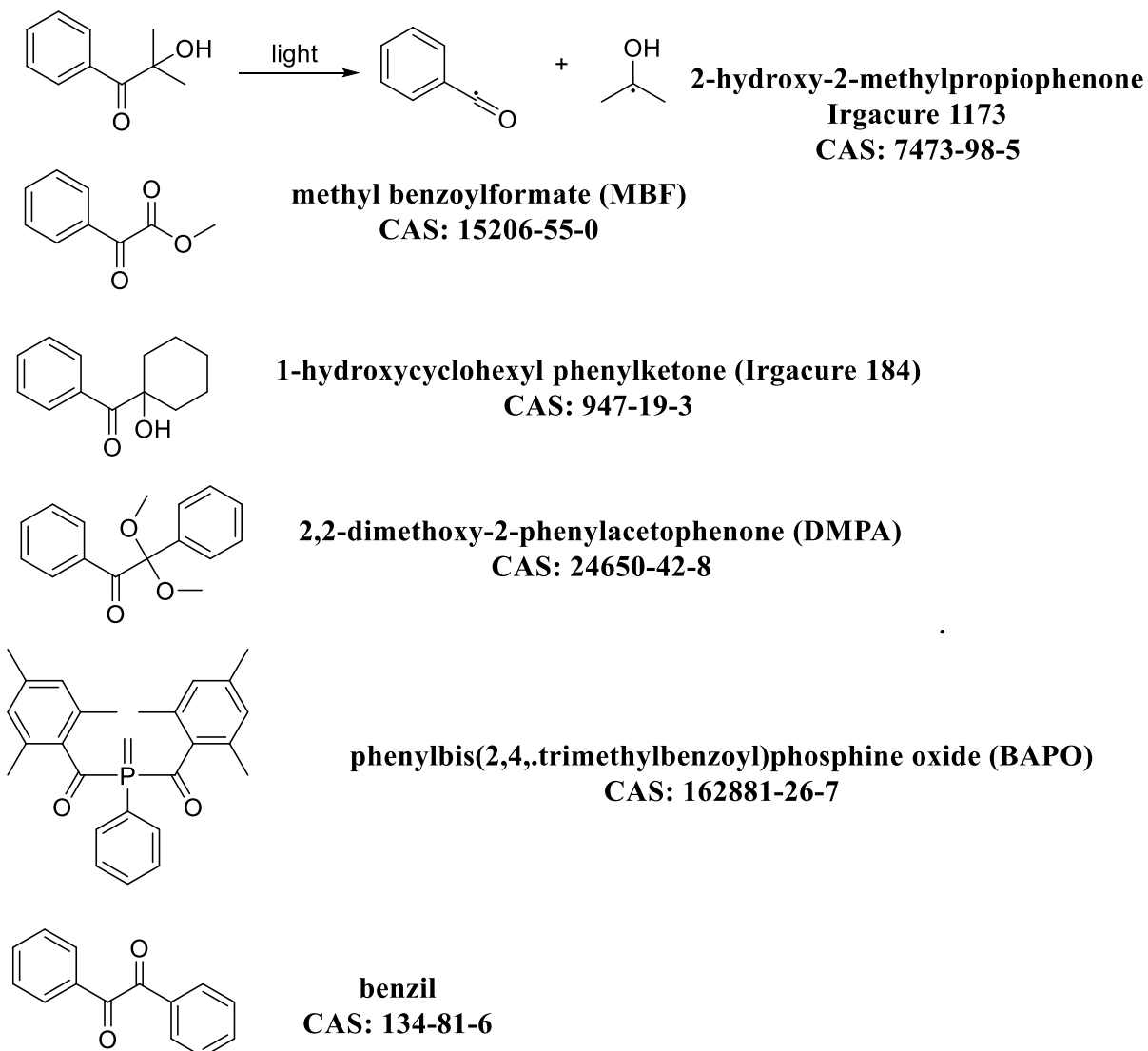


Figure 5. Molecular structures of commercially available Norrish Type I photoinitiators. Adapted with permission from ref. ^[8].

Type II photoinitiators also known as hydrogen abstraction-type trigger the photopolymerization reactions by interacting with hydrogen donors. Type II initiators include molecules such as benzophenone, phenanthrenequinone, 2-methyl anthraquinone, 4,4'-bis(diethylamino)

benzophenone, and 2-isopropylthioxanthone (ITX). Figure 6 shows some molecular structures of commercially available photoinitiators with the initiation mechanism of benzophenone.^[40,41]

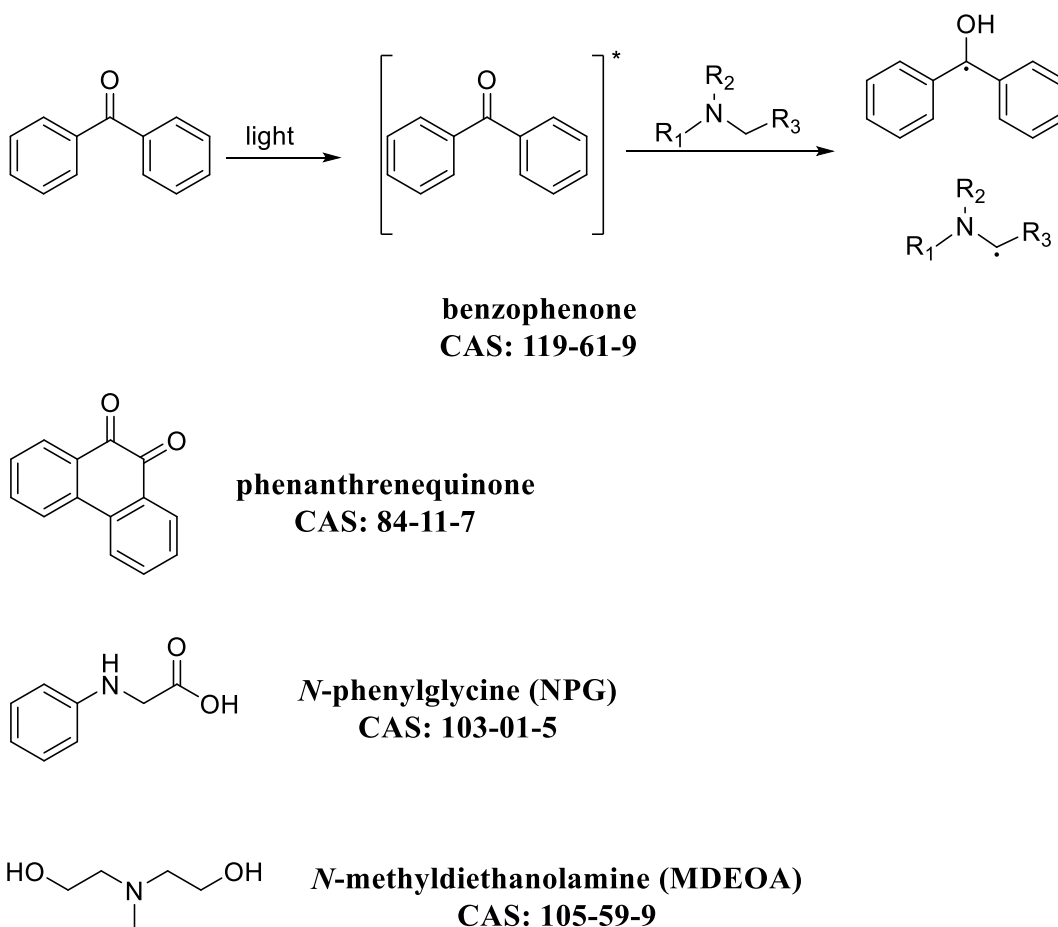


Figure 6. Molecular structures of commercially available Norrish Type II photoinitiators. Adapted with permission from ref. ^[8].

It is important to mention that photosensitizers are added to shift the absorption window of photoinitiators. Photosensitizers are organic or inorganic molecules, dyes, or metal complexes with excellent capacity for light absorption. Upon absorbing the light, the photosensitizer is excited and then transfers the energy to the desired molecule (= photoinitiator). It is interesting to note that Type II photoinitiators can also act as photosensitizers under certain conditions.^[42,43]

In the late 1970s, Crivello and co-workers first described initiators, also known as photoacid generators (PAGs), for cationic polymerization of epoxy and vinyl ether monomers.^[44,45] The mechanism is based on the formation of a Brønsted acid (H^+), generated after light exposure to onium salts and subsequent reactions with monomers or solvents in the formulation. As can be seen

from Figure 7, in the reaction between ethylene oxide and onium salt, a Brønsted acid (H^+) is generated from the decomposition of an onium salt. The released acid further reacts with epoxy monomers through a ring-opening reaction forming new ion pairs. During the propagation process, the chain propagation continues and results in polymer formation.^[46-48] The acidic strength of the formed acid depends on the size of the counter-anion and increases with the nucleophilicity of the counter-anion and size.^[46]

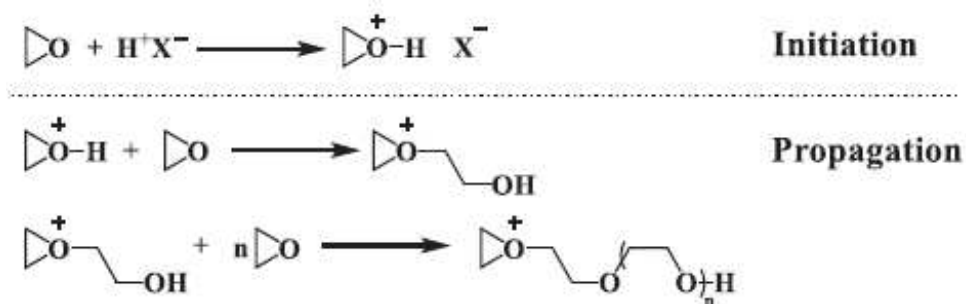


Figure 7. Mechanism of the ring-opening reaction of epoxy monomers. Reprinted with permission from ref. ^[8].

Cationic photoinitiators are divided into two main classes: ionic and nonionic types. The ionic types are based on compounds such as aromatic diaryliodonium salts, diazonium salts and, triaryl sulfonium salts. The nonionic type mainly includes sulfonic ester and triazine compounds (Figure 8).^[32,49]

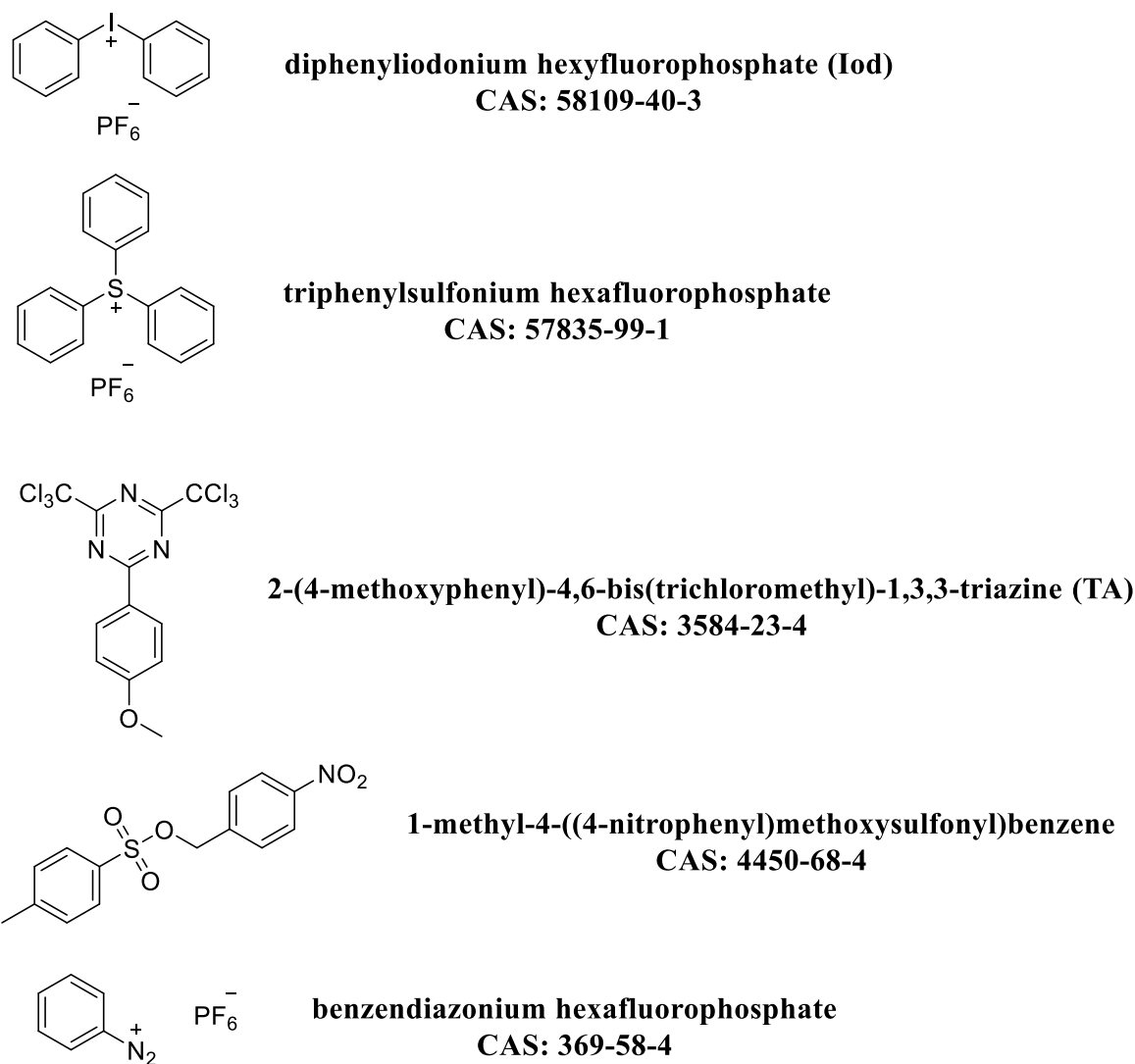


Figure 8. Molecular structures of commonly used commercially available cationic photoinitiators. Adapted with permission from ref. [8].

Using iodonium salts as an example, they undergo homolytic and heterolytic cleavage reactions upon UV light exposure. In the case of homolytic cleavage, a radical cation or an aryl radical pair is formed, while in heterolytic cleavage an aryl cation is generated.^[50]

Triarylsulfonium and diaryliodonium salts have limited absorption within a wavelength range between 200 and 300 nm. The absorption can be shifted to higher wavelengths by free radical induced cationic polymerization if the photoacid generator is mixed with a Type I or Type II photoinitiator. After the generation of free radicals from the radical photoinitiator, in the presence of aryl iodonium salt and radical cations, free radicals are oxidized and initiate cationic

reactions.^[51,52] Another approach to shift the absorption to a higher wavelength is based on the usage of dyes as a sensitizer.^[53]

The main advantages of cationic polymerization are the low viscosity of the monomers, no sensitivity to oxygen, and low shrinkage via ring-opening epoxide reaction.^[54,55]

In contrast to photoacid generators, photobase generators generate bases to trigger a polymerization process upon light exposure.^[56,57] With a wide range of monomers that can be opened (e.g. epoxy, oxetane, vinyl ether), photobase generators possess a better photostability and excellent compatibility compared to photoacid generators.^[58,59] Despite the promotion of ring-opening polymerization, photobase generators also facilitate the Michael addition and the thiol-epoxy click reaction. Commonly used photobase generators are shown in Figure 9.

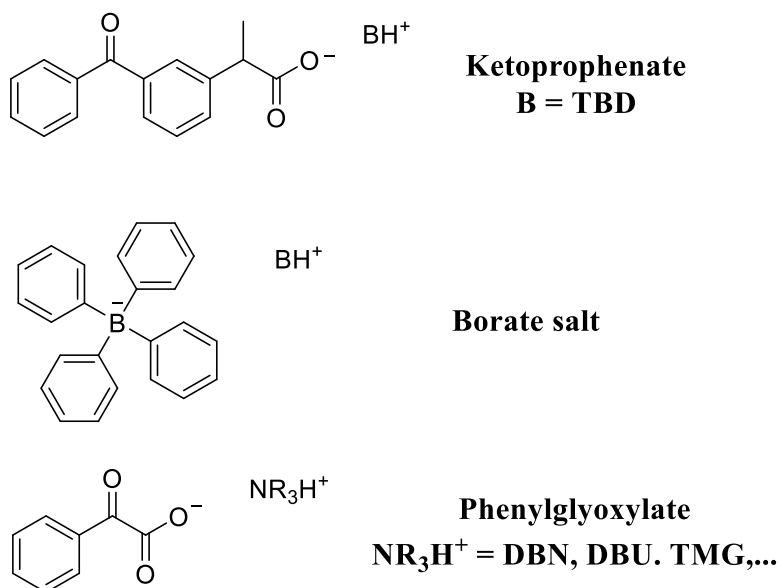


Figure 9. Molecular structures of some photobase generators.^[60]

3.2 Additive manufacturing

Additive manufacturing (AM), also known as three-dimensional (3D) printing, is a revolutionary technology gathering significant attention in both academia and industry. Developed in the 1980s, AM technology has progressed swiftly and paved the way for innovative engineering applications in various industrial sectors. Desired objects are constructed layer-by-layer where each layer represents a thin cross-section of the object which is digitally derived from a 3D computer-aided design (CAD) model. Printed advanced parts, created by depositing, joining, or combining raw

materials directly at the desired location, characterize a high level of complexity in their designed shape, composition, and function.^[61,62] Despite the production of complex geometries, AM technology also offers manufacturing products on demand, minimizes waste production, and accelerates the prototyping process. Due to these advantages, printed products cover a wide spectrum of applications in a variety of fields including aerospace, automotive, dental, medical, consumer electronics, and others.^[63,64] Which method will be chosen for manufacturing 3D objects depends on used raw materials, building time, required final resolution of the object size and performance of the desired object, and the final cost of manufacturing.^[65,66]

Filament fused fabrication, direct ink writing, and selective laser sintering are the techniques that include thermoplastic as used materials which can be malleable and soft upon heating and used in extrusion-based additive manufacturing. Due to the lack of covalent bonds in the thermoplastic materials, they can be re-melted and reused. 3D-printed objects from thermoplastic possess inherent mechanical characteristics and often cannot be used in some applications without adding additives (e.g. reinforcing fillers) to change their characteristics.^[67,68] On the contrary, the materials that produced a covalent cross-linking network through the 3D-printing process cannot be reused due to permanent insoluble bonds. It is typical for cross-linked polymers and thermosets. While curing reactions can be initiated by light or temperature, light-initiated reactions offer spatial control, fast curing at mild conditions, and decreased energy use.^[69,70] In vat photopolymerization, many monomers such as acrylates, methacrylates, unsaturated polyester resins, phenolic polymers, organosilicon, and epoxy resins can be applied. Via the vat photopolymerization process, it is possible to print materials with great mechanical strength and stiffness that can be used in dental applications.^[71] Despite advantages, there are still some challenges that vat photopolymerization 3D printing needs to overcome, such as a limited number of possibly used photopolymers, high viscosity of some materials, printing materials with a suitable resolution, washing material after the print, keeping long-term material properties, as well as developing of reaction orthogonality. Despite the challenges mentioned, vat photopolymerization has drawn much attention in recent years. The most common vat photopolymerization techniques include stereolithography, digital light processing, liquid crystal display, hot lithography, two-photon absorption, and volumetric 3D-printing process.

This section will discuss the most popular AM techniques including filament fused fabrication, direct ink writing, selective laser sintering, liquid crystal display, hot lithography, two-photon polymerization, volumetric 3D printing, stereolithography, and digital light processing.

3.2.1 Fused filament fabrication

The most widely used printing technology for thermoplastic polymers is fused filament fabrication (FFF). The printing process starts with melting polymeric filaments in the extrusion head till a semi-liquid state. Therefore, it is important to choose thermoplastic filaments with low processing temperatures such as polycarbonate (PC), polylactic acid (PLA), and acrylonitrile butadiene styrene (ABS). In the next step, the molten thermoplastic polymers are forced out through the nozzle where they cool down. The 3D desired object is manufactured by the motion of the nozzle in a layer-by-layer manner. Illustration of an FFF based 3D printer is shown in Figure 10.

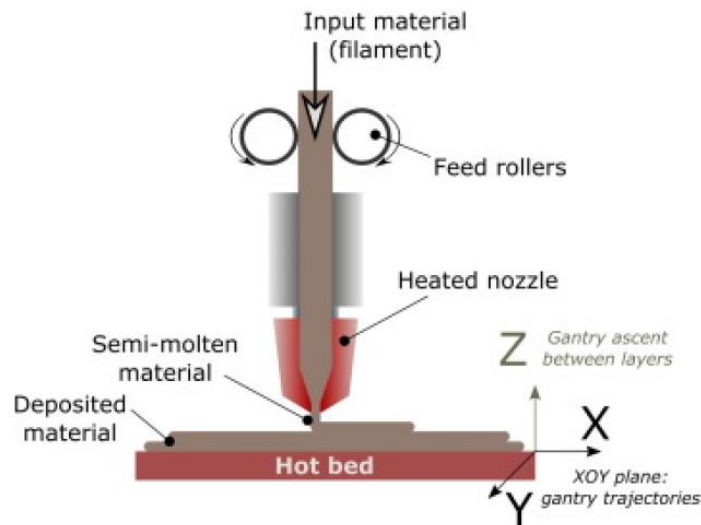


Figure 10. Schematic illustration of filament fused fabrication process. Reprinted with permission from ref. [72].

Printing parameters of this technique, which have to be optimized, are temperature, the thickness of layers, building orientation, width, raster angle, and air gap. Material extrusion or FFF offers low building cost of 3D printing, fast building time, and simple operation. The negative sides are the need for filament forms of used materials, high temperatures, a good range of viscosity for extrusion, and constant material flow during the printing process. [73,74]

3.2.2 Direct ink writing

Direct ink writing (DIW) technology uses a viscoelastic liquid paste extruded through a nozzle while applying pressure. The nozzle moves over the fixed platform and defines the shape of the desired printed object, while the extruded material cools down and solidifies (Figure 11). The quality of layer-by-layer printed structures depends on the speed at which the liquid is extruded as well as its viscosity.^[75,76]

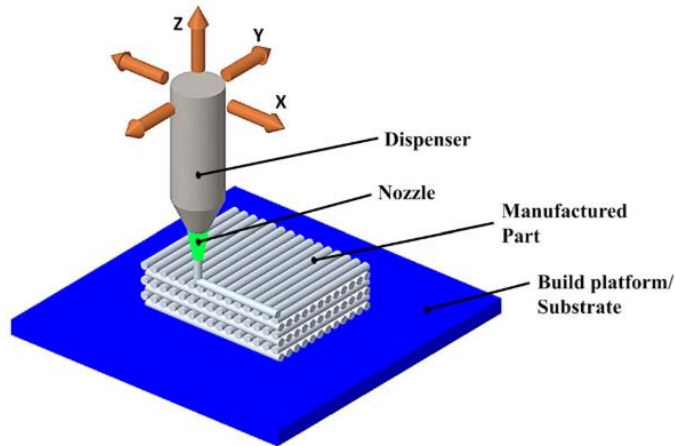


Figure 11. Schematic illustration of direct ink writing process. Reproduced with permission from ref. ^[77].

The benefits of DIW are the simplicity of the process, applied materials can be easily inserted into the nozzle, and a wide range of materials can be used from polymer solutions, pastes to hydrogels. On the other hand, the building of complex objects can be challenging due to the properties of the viscoelastic materials that can collapse during the printing process.

3.2.3 Selective laser sintering

Selective laser sintering (SLS) 3D manufacturing technique uses a solid polymer powder as a material that is melted with a scanning laser and fused over the surface of the build platform. The polymer melts at selected regions due to spatially controlled exposure to laser light, while for the creation of the next layer a piston assembly moves down to collect the polymer powder with a spreading roller's assistance. The process is repeated until the desired 3D object is printed^[78] (Figure 12). To achieve high resolution of the printed objects it is needed to remove unbounded materials at a stage of post-processing step. Important parameters that affect the quality of the printed objects are polymer powder particles' size, speed of scanning, laser intensity, and scan

width and gap.^[79] Commonly used polymeric materials in SLS are polycaprolactone and polyamide.

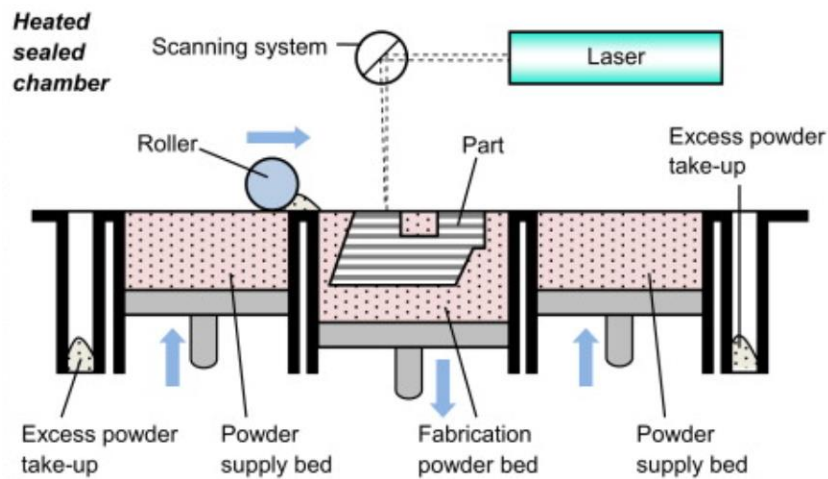


Figure 12. Schematic illustration of selective laser sintering process. Reprinted with permission from ref. ^[80].

3.2.4 Stereolithography

Stereolithography (SLA) is a type of vat photopolymerization where a vat filled with liquid resin is illuminated in a controlled manner. The 3D objects are manufactured with a laser point-by-point^[94,95] (Figure 13). Typically used monomers are acrylates, methacrylates, vinyl, and epoxy monomers. The optimization parameters on which the quality of manufactured structures depends are polymerization kinetics, illumination time, light intensity, chemical functionality, and, resin viscosity. Additionally, photoinitiators are added to the resin to initiate photochemical reactions for solidifying the material upon exposure to the laser. The resolution of the manufactured objects can be improved by the addition of light absorbers.

The SLA technique offers high resolution of the manufactured objects. Since the vat is typically not heated, available photopolymers for SLA are limited by their viscosity at room temperature. It is important to pay attention to unreacted monomers in the printed objects and the irritation potential due to residual acrylate monomers.^[97]

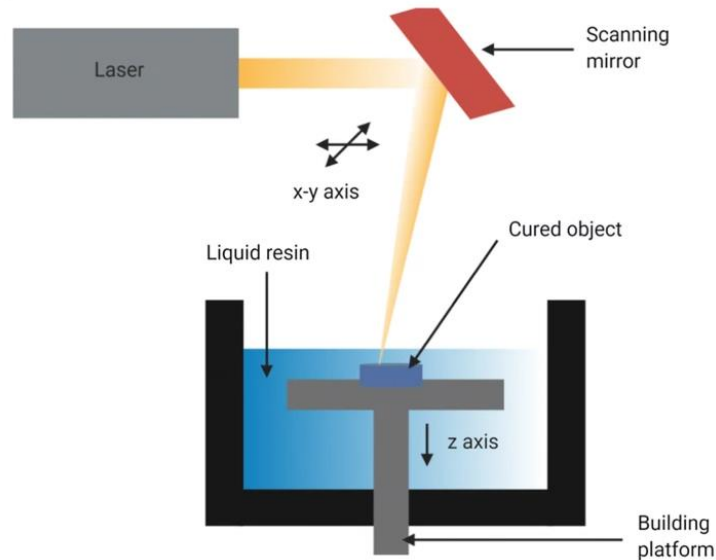


Figure 13. Schematic illustration of the stereolithography process. Reproduced with permission from ref. [96]

3.2.5 Digital light processing

The main difference between SLA and digital light processing (DLP) 3D printing is the way they utilize light to solidify the resin. While in SLA, a laser beam selectively cures liquid resin point-by-point, DLP 3D printing uses a digital light projector to project an entire layer of the object onto the resin surface at once (Figure 14). As each layer is created simultaneously, DLP results in a faster printing speed compared to SLA. However, DLP suffers from a slightly lower resolution and surface quality compared to SLA due to the pixelated nature of the projected image.^[98,99]

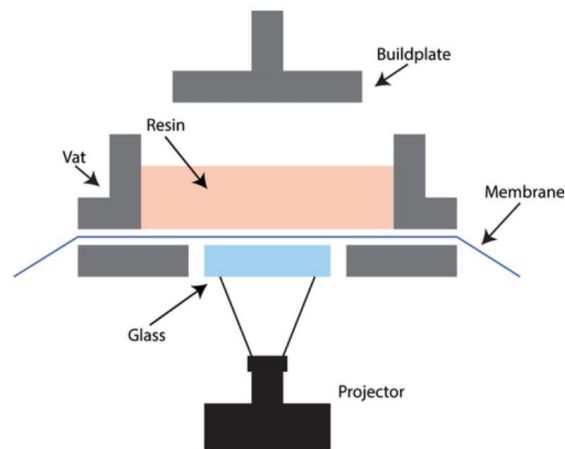


Figure 14. Schematic illustration of digital light processing process. Reproduced with permission from ref. [100].

The photocurable resin typically consists of mono- and multifunctional (meth)acrylate monomers. Once the photoinitiator is exposed to light, radicals are generated resulting in a chain-growth polymerization where high molecular weight polymers and photopolymer networks (in the presence of multi-functional cross-linkers) are rapidly formed. Molecules with a small molecular weight (mono-functional monomers) are often added as reactive diluent to reduce the viscosity of a photocurable system. In contrast, multi-functional monomers with a higher molecular weight provide the desired mechanical properties of printed specimens. Commonly applied acrylates and methacrylates are provided in Figure 15. Isobornyl (meth)acrylate (IBO-(M)A), hydroxyethyl methacrylate (HEMA) decrease the overall cross-linking density, whilst multi-functional and occasionally hyperbranched monomers such as pentaerythritol tetra(meth)acrylate (PET(M)A), 1,6-hexanediol diacrylate (HDDA), and trimethylolpropane tri(meth)acrylate (TMPT(M)-A) improve the cross-linking density.^[101,102] Acrylate-based resins suffer from oxygen inhibition, high shrinkage upon polymerization and low final monomer conversions.^[65,103]

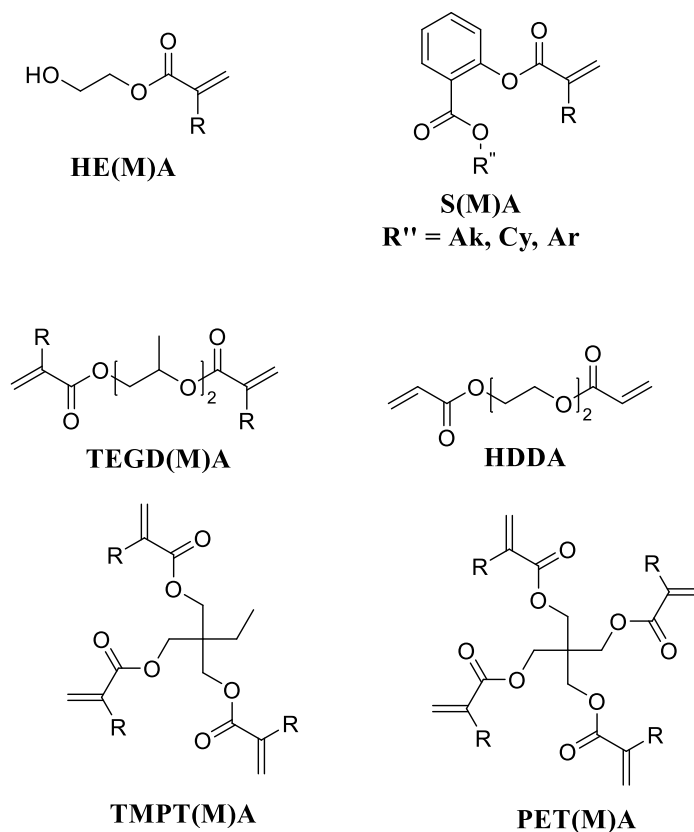


Figure 15. Commonly used acrylate and methacrylate monomers in radical polymerization. Adapted with permission from ref. ^[60].

Along with radical polymerization, cationic polymerization is applied in vat photopolymerization to obtain 3D printed objects. Cationic photoinitiators absorb short-wavelength light and form cationic reactive species upon UV light exposure. In vat photopolymerization 3D printing, the most commonly used cationic photoinitiators are diaryliodonium and triarylsulfonium salts. A wide range of monomers can be activated with cationic photoinitiators. However, oxetanes, mono- and multifunctional epoxides (Figure 16), and vinyl ethers are the most commonly applied monomers in DLP 3D printing.^[104]

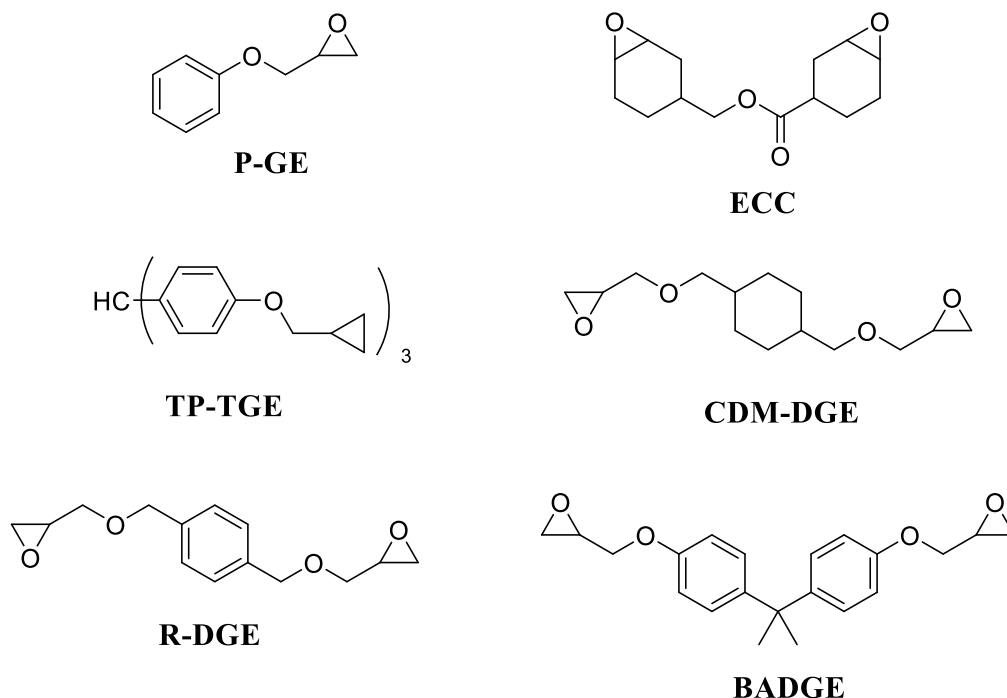


Figure 16. Commonly used epoxide monomers in cationic polymerization. Adapted with permission from ref. ^[60].

3.2.6 Liquid crystal display 3D printing

Liquid crystal display (LCD) is a type of a vat photopolymerization technology, that uses a liquid crystal display for imaging. An applied electric field causes the rearrangements of the liquid crystal molecules, preventing light from passing through selected areas (Figure 17). The desired design of the 3D objects is controlled through a computerized system, and the response is created in the LCD imaging unit. The challenge is to prevent light from passing through the LCD screen when molecular rearrangements are trapped under an applied electric field that results in reduced resolution.^[81]

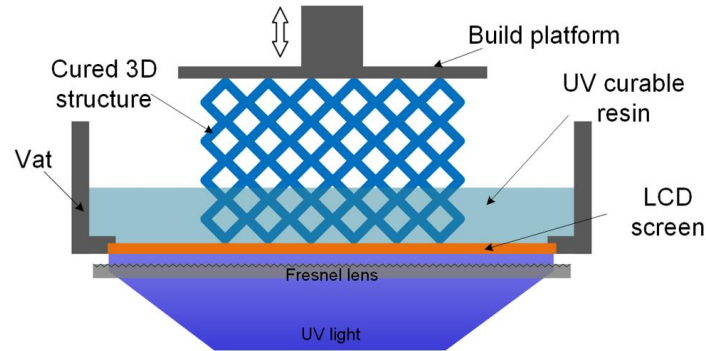


Figure 17. Schematic illustration of liquid crystal display process. Reprinted with permission from ref. [82].

3.2.7 Hot lithography

In the hot lithography process, it is possible to heat the vat during the printing process, while conventional techniques of vat photopolymerization keep the vat at room temperature (Figure 18). In this technique it is possible to use highly viscous resins, since the heat reduces the viscosity and enables the printing process. Moreover, during the applied heat on the vat, the reactivity of monomers also increases and enables polymerization which can be hardly done at room temperature.^[83,84]

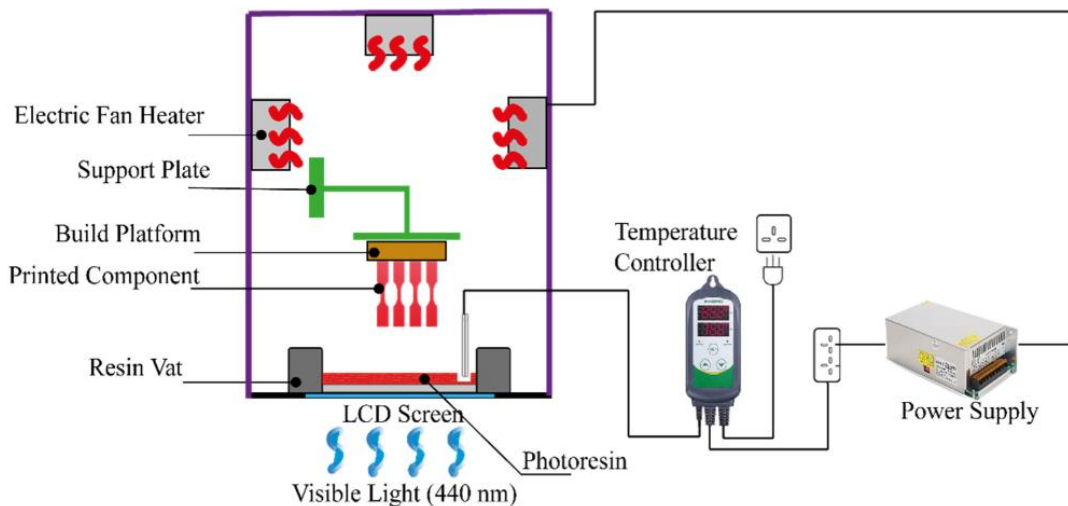


Figure 18. Schematic illustration of hot lithography process. Reprinted with permission from ref. [85].

Compared to typical vat polymerization techniques that work at room temperature such as stereolithography or digital light processing, the usage of heated vat opens many possibilities in terms of monomer selection for 3D printing.^[86]

3.2.8 Two-photon absorption polymerization

Two-photon absorption (TPA) polymerization is a technique that belongs to the family of vat photopolymerization, and it is a well-known approach to manufacture 3D polymer objects at micro- and nanoscale.^[87] For the TPA technique, it is characteristic to use a highly compact laser beam as a light source. Due to very high-power light density in the range of 10^{13} W/ μm^2 over a very limited volume smaller than a cubic wavelength (λ^3), photons are absorbed in a non-linear pattern (two-photon absorption).^[88] Therefore, it is possible to achieve a superb spatial resolution in a nanometer range, far from the optical diffraction limit.^[89] Additionally, the usage of an infrared radiation source enables the deep penetration of the laser light into the bulk of the material, where the loss of absorption is minimized. Additionally, the usage of an infrared radiation source enables the deep penetration of the laser light into the bulk of the material, where the loss of absorption is minimized. When the light is linearly exposed (e.g. lithography), the material response corresponds only to the first order. On the other hand, when two-photon absorption is used, the response is of the second or multiple orders^[89] (Figure 19).

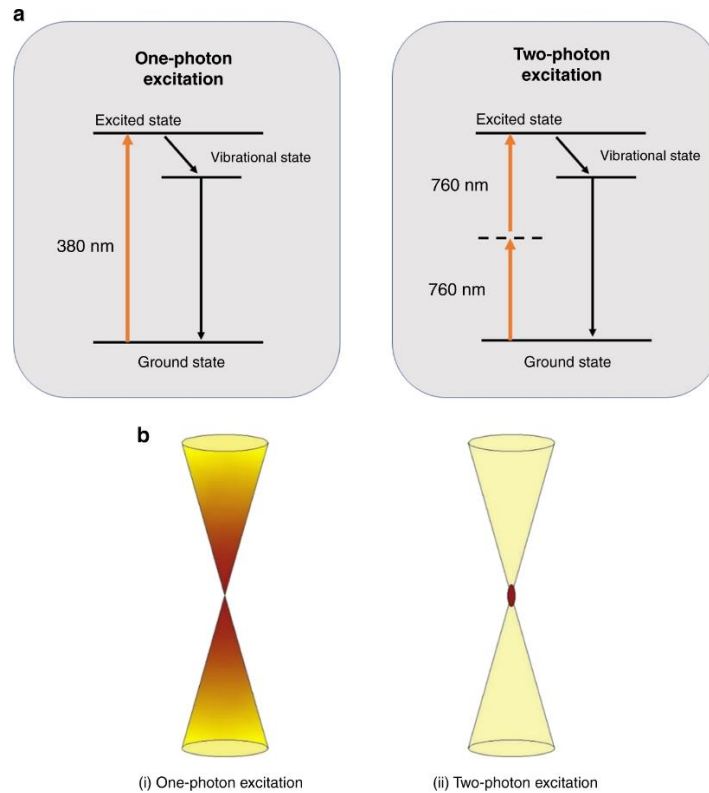


Figure 19. (a) Schematic illustration of the absorption energy of a single photon by UV light and two photons by near-infrared light; (b) Comparison of the (i) excitation volume of one-photon excitation and (ii) two-photon excitation. Reprinted with permission from ref. [90].

The advantage of TPA is a better spatial control of the square light intensity distribution. As a result, the interaction between light and matter is reduced and printing accuracy is improved. In terms of energy absorption, the photoinitiator absorbs two photons in the near-infrared range (NIR), providing as much energy as the single-photon absorption in a photocurable resin. The radicals formed during two-photon polymerization act under the square law of light intensity function. To avoid radical scavengers, e.g. dissolved oxygen from photocurable resin, the radicals remain in areas where the light intensity is higher and the polymerization process occurs.^[38]

3.2.9 Volumetric 3D printing

In volumetric 3D printing, the desired 3D geometry is printed all at once. Therefore, problems that arise in other vat photopolymerization techniques such as surface quality, in volumetric 3D printing are minimized.^[91–93] Figure 20 shows a volumetric 3D printing setup. On the left side, example projections from various angles are presented. As a result, the desired 3D structure is shown on the right side in Figure 24. Volumetric 3D printing, also known as holographic printing or multi-beam

additive manufacturing, offers rapid printing speed, and isotropic mechanical properties. Due to oxygen inhibition, a single illuminated ray cannot polymerize the photocurable resin. This can be overcome with a high concentration of radical species by the superposition of irradiation. The degree of polymerization for each resin can be controlled by manipulating the duration of light exposure and light intensity. Another advantage is the usage of highly viscous resins (up to 90 Pa·s).^[93] Vat photopolymerization technologies based on layer-by-layer printing manner face the problem of printing flexible polymers with an elastic modulus of <10 kPa. These polymers usually find applications in tissue engineering or bio-imprints. The biggest challenge is the frequent breakage between the layers of the desired building structure due to auxiliary and gravitational forces. Since volumetric 3D printing forms the objects all at once, this problem can be overcome.^[38]

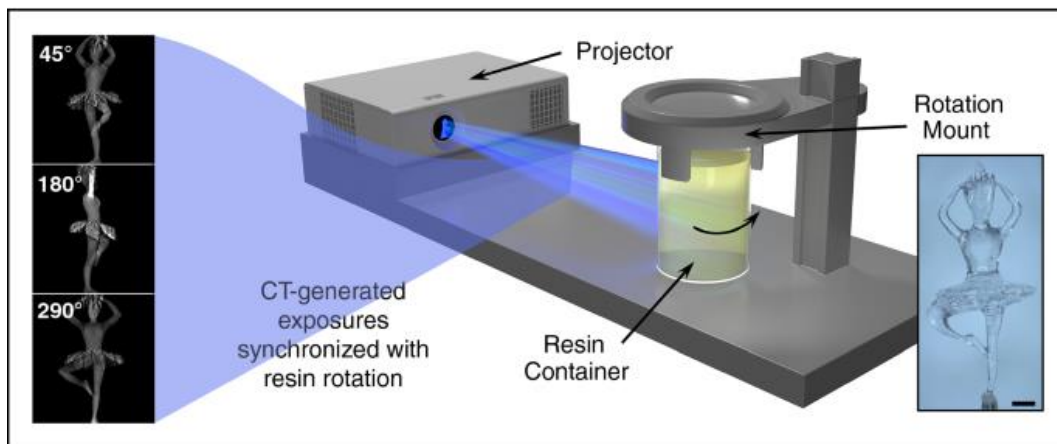


Figure 20. Schematic illustration of volumetric 3D printing. Reprinted with permission from ref.^[91].

3.3 Vat photopolymerization multi-material additive manufacturing

Utilizing multi-material polymers with innovative chemical, physical, mechanical, or biological properties opens new horizons in AM, for example bio-printing and four-dimensional (4D) printing. However, most of the developed AM techniques produce objects by printing a single material only. There are several possibilities to achieve multi-material 3D printing by vat photopolymerization. The first and simplest strategy to produce objects with multi-material properties is based on manually and/or mechanically switching resins or resin vats. The second strategy is based on a variation of light parameters and exposure time during the layer-by-layer printing. The third strategy is based on wavelength-dependent orthogonal chemistries and in the

dual-wavelength approach two orthogonal reactions working at two different wavelengths are exploited. A single developed resin formulation must have miscible orthogonal chemistry precursors and the printer must have integrated more than one wavelength source.^[19,38]

In the following section, several multi-material 3D printing methods for vat photopolymerization explored by the research community will be discussed.

3.3.1 Manually and mechanically switching resins/resin vats

The big advantage of these methods is that a large number of formulations can be used. However, the methods are time-consuming due to cleaning and washing steps between the change of the vats or resins to avoid contaminations of previously used material, and also require extra programming steps to stop the printing and start the printing again at different heights.^[105–109]

The work based on manually switching the resin or resin vats is described in several research papers by the research groups of Bashir^[110–113], Wicker^[114,115], and Roy^[116,117]. Roy and co-workers have tested both DLP- and SLA-based manufacturing of multilayer structures. They found that SLA has the advantage of printing more advanced and complex structures.^[116,117] The examples of switching the resin vats and resins were reported by Mishra et al. and Chan et al., respectively. In the work of Misha et al., the printer was stopped at a certain level, and the vat with the desired resin was then replaced with a new desired vat. On the other hand, Chan et al. used a pipe to introduce the new resin into the vat for each layer (Figure 21).^[111,118]

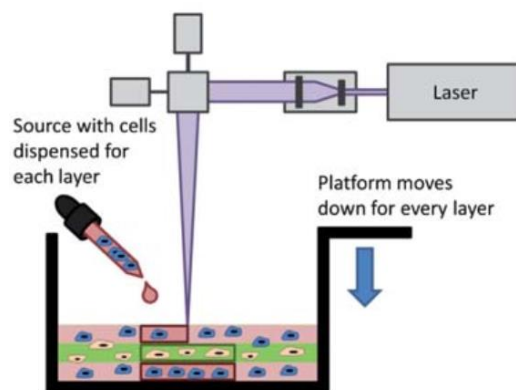


Figure 21. Schematic representation of printing by manually switching the resins by injecting layer-by-layer. Adapted with permission from ref. ^[111].

In 2001, Mauro et al. demonstrated the first work on a micro-stereolithography process where different photocurable resins were printed. In a layer-by-layer manner, two different photocurable

resins were exposed to 325 nm (UV light) and were printed by using two polymer resin-dosing pumps.^[119] In 2004, Wicker et al. reported on multi-material stereolithography based on multi-vat carousel assembly. In total three vats were included in the setup apparatus comprising of two vats with different photocurable resins, and a third vat for the cleaning process where the printed structures were washed and dried.^[120] Additionally, they developed a setup consisting of two building platforms in vats that can be rotated by a mechanical assembly together with a resin vat for multi-material printing. A disadvantage of the built setup was the small building area of 4.5 inches x 4.5 inches (Figure 22).

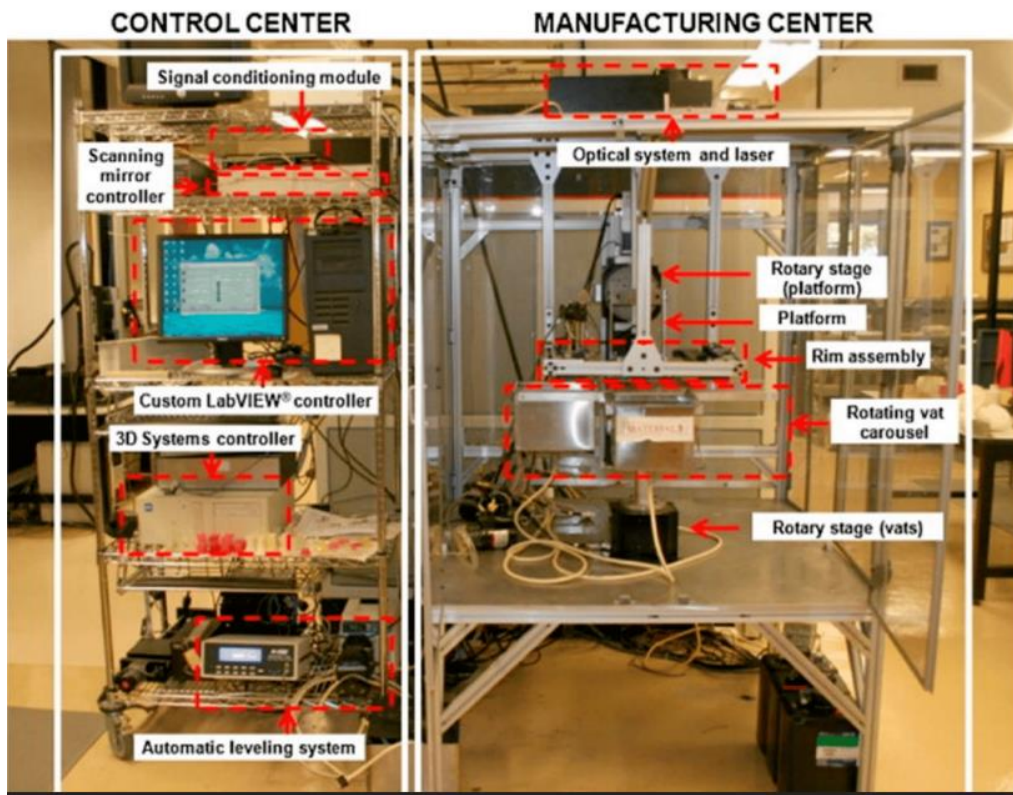


Figure 22. Setup of multi-material SLA 3D printer. Reproduced with permission from ref. ^[94].

They improved the system in a follow-up work by extending the rotary vat assemblies from two to four in the used SLA 3D printer. The capacity of printing resin volumes was up to 9 L (Figure 23).^[94]

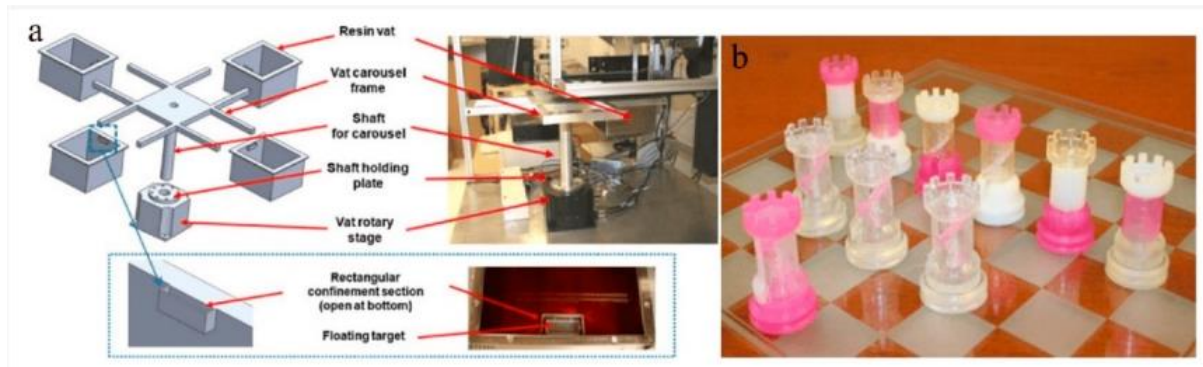


Figure 23. (a) Schematic illustration of multi-material carousel assembly; (b) 3D printed objects with multi-material properties obtained by using SLA. Reproduced with permission from ref. [94].

3.3.2 Variation in light intensity and exposure time

Different mechanical properties within one object can be achieved by controlling the degree of the polymerization process. It is a chemistry-based approach where selected regions are irradiated with varying light intensity and irradiation times to control the cross-linking density.^[121] The biggest advantage of these methods is the usage of single resin formulation. The cross-link density is controlled by using grayscale light projections, which can be achieved by using DLP printers.^[122]

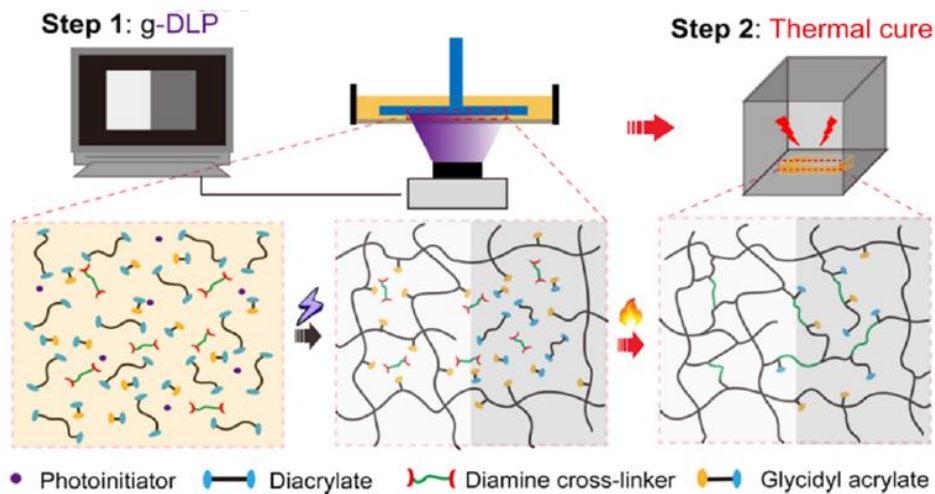


Figure 24. Example of a grayscale DLP setup with final thermal curing step. Reproduced with permission from ref. [122].

The grayscale methodology is based on images scanned under monochromatic light to generate specific properties in each network during the layer-by-layer printing. The goal of using grayscale during the printing process is to vary cross-linking density and thus, stiffness in the printed layers. By using grayscale vat photopolymerization, Kuang et al. successfully printed objects with

heterogeneous properties (Figure 24). The photocurable resin consisted of methacrylate-bearing epoxy moieties, mono-functional and di-functional acrylates, amine cross-linkers, and photoinitiators. The designed structure was fixed with radically photopolymerized acrylates. The unexposed regions consisted of unreacted monomers resulting in different mechanical properties than radically photopolymerized ones. As unreacted monomers give poor mechanical properties, a thermal post-processing step was carried out to cure unreacted monomers and to improve the mechanical properties of unexposed regions.^[123–125] During the post-thermal treatment, the cross-linking reaction of diamine with epoxide and acrylate monomers occurred.^[122] When the grayscale was set to 0%, regions with stiffer properties were formed with a Young's modulus of up to 1.2 GPa. On the other hand, when the grayscale was adjusted to a value of 93%, the formed materials were soft with a Young's modulus up to 1.4 MPa. With the described method, it was possible to produce materials in a T_g range from 14 to 68 °C.^[122]

3.3.3 Orthogonal chemistry mechanisms

In recent years, much attention has been given to the full spectrum of light where responses can be controlled and triggered independently also known as λ -orthogonality.^[126] In 1974, in a New Scientist column by Jone and the reported patent in 1977 by Swason, the two-color 3D printing was mentioned for the first time, although chemical realization was still unclear.^[126] Over the past few years, the interest in adding additional light sources with a different wavelength is constantly growing. The orthogonality approach was first time reported in 1977 by Merrifield and Barany for peptide synthesis, where disparate protecting groups were pulled out in controlled order by successively applying different reaction conditions.^[127] In terms of light-induced 3D printing, the λ -orthogonality concept refers to the selective activation of two photoreactions at different wavelengths, which enables the production of multilateral complex geometries by choosing chromophores, which will result in soft and hard segments, or electrically conducting and insulating properties, respectively.^{[126], [131]} The development of multi-component photocurable resins, which could proceed in a single vat, would significantly impact 3D printing in our daily lives and minimize problems with contaminations from other resins during switching resins or resin vats. To achieve orthogonality in a two- or more-component system, it is necessary to trigger reactions selectively, without activating other monomers. In general, it is possible to apply external stimuli such as light, redox, electrical potential, pH, and heat. Light is the most favorable one, due

to possibly achieving spatial control, ability to utilize independently of other external stimuli, low energy consumption.^[128,129]

There are several reports of selectively using radical and cationic polymerization activated with two different wavelength light sources to create multi-material objects. By applying an additional light source, it is possible to produce soft and hard segments via vat photopolymerization by printing one material only. In 2018, Dolinski et al. printed multi-material objects based on the orthogonality concept by introducing Solution Mask Liquid Lithography (SMaLL), a type of volumetric 3D printing. The mechanical properties of the material were controlled in a single photocurable resin, which was exposed to 530 and 470 nm. Acrylate monomers were selectively polymerized by irradiation with a 530 nm light source, while irradiation with 470 nm induced polymerization of both acrylate and epoxide monomers. 3D-printed structures with soft joints and mechanically reinforced “brick-and-mortar” structures (Figure 25) could be obtained in a high resolution and the printing of objects with well-defined regions of different chemical and mechanical properties was demonstrated.^[130,131]

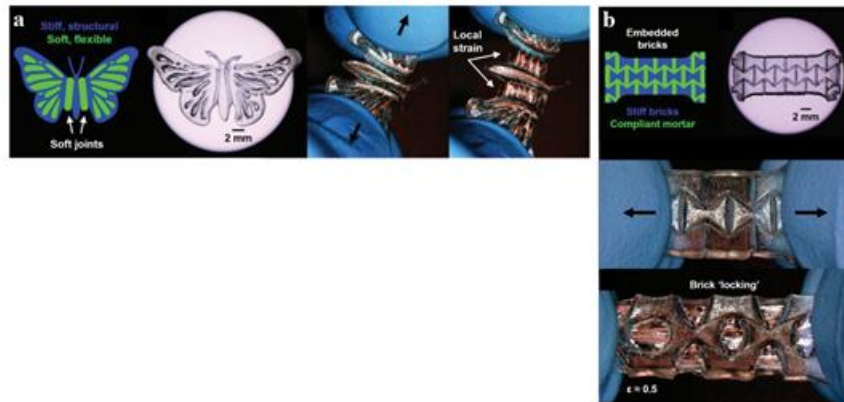


Figure 25. Demonstration of printed structures with SMaLL multi-material printing: (a) Digital butterfly design with stiff (in blue) and soft areas (in green). The printed structure shows selective straining in the soft areas; (b) Demonstration of multi-material brick-and-mortar structures. Digital image with stiff areas (blue bowties) within a compliant green matrix. Images show samples before and after applied tensions. Reproduced with permission from ref.^[130].

In 2019, an interesting similar study based on selective radical and cationic curing of monomers was reported by Schwartz and Boydston. The orthogonal photocurable resin consisted of acrylate (resulting in a soft network) and epoxide monomers (resulting in a stiff network). Upon visible light exposure (405 nm) acrylate monomers were selectively polymerized, while upon UV light exposure (365 nm) both acrylate and epoxide monomers polymerized resulting in an

interpenetrating polymer network with higher cross-link density. They achieved varying materials and properties along all three axes by using their home-built DLP 3D printer (Figure 26). The printing of multi-material objects resulted in a high build speed with cure times of 60 (405 nm irradiation) and 120 s (365 nm irradiation) for 100 μm layer thickness. However, the tensile test of printed specimens showed poor tensile strengths of < 0.5 MPa.^[132]

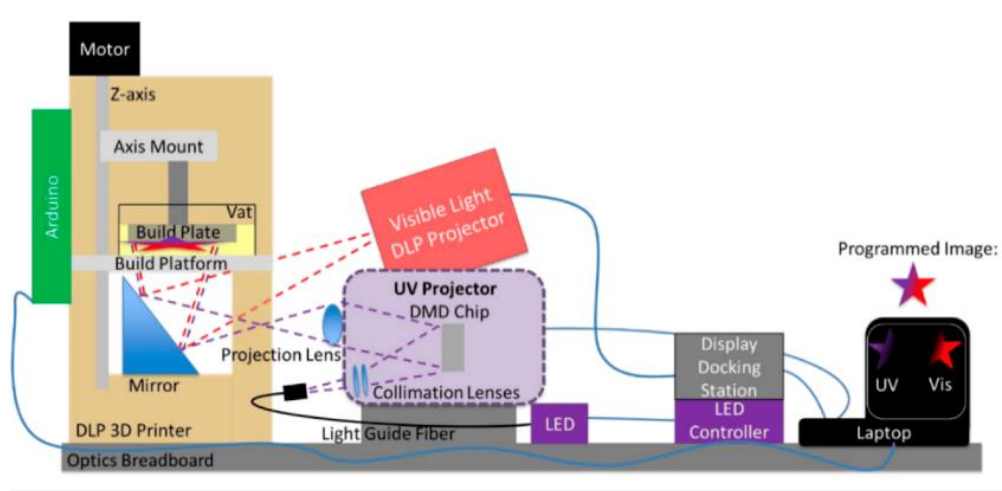


Figure 26. Schematic illustration of multi-material 3D printer with a visible and UV projector. An integrated laptop served as scanning process controller. Reproduced with permission from ref. ^[132].

In 2021, Schlögl and co-workers took advantage of orthogonal chemistry and introduced a spatially activatable photoacid into a photocurable resin consisting of acrylate and thiol monomers. In particular, they added a latent transesterification catalyst (photoacid), which releases a Brønsted acid upon UV exposure. As shown in Figure 27, the optimized resin was processed with a dual-wavelength 3D printer operating at 405 (visible light) and 365 (UV light) nm. By printing in a layer-by-layer approach with selective activation of lights, the activation of the photoacid was controlled in an orthogonal manner, where the activated catalyst initiated dynamic exchange reactions at higher temperatures.^[133]

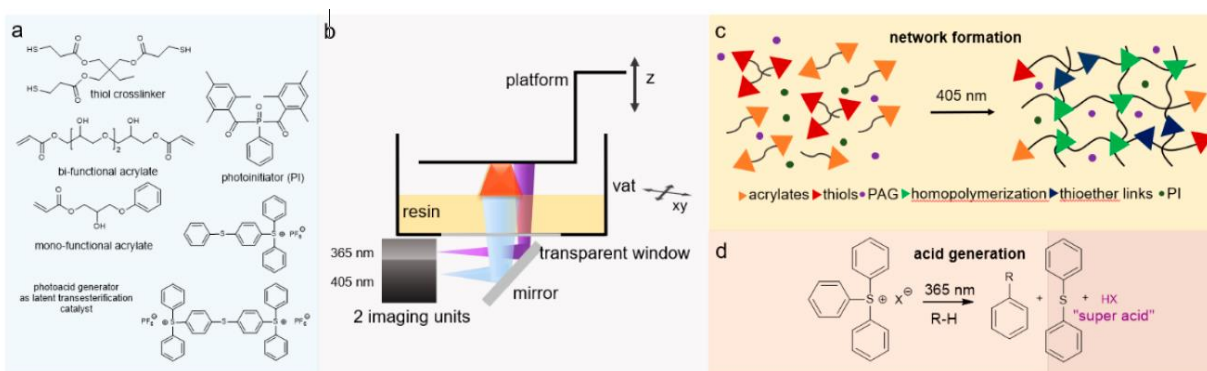


Figure 27. (a) Photocurable composition; (b) schematic illustration of a dual-wavelength DLP setup; (c) illustration of network formation under visible light; (d) illustration of network formation under UV light. Reproduced with permission from ref. [133].

Despite the integration of more than one wavelength light source, it is important to note that orthogonal chemistry and dual-wavelength approach require the miscibility of the used monomers in a dual-curing system. Thus, designing a dual-curing system for the λ -orthogonal 3D manufacturing of multi-lateral structures is still poses a challenge.

3.4 Dynamic covalent networks

The first demonstration of dynamic bonds was done by Lehn et al., by introducing supramolecular chemistry.^[134,135] Supramolecular chemistry is based on non-covalent reversible interactions, such as $\pi - \pi$ stacking, hydrogen bonding, and metal-ligand coordination^[136,137], with an excellent potential for biomedical applications. When exposed to heat, polymers were previously classified as thermoplastic or thermosets, based on the formed insoluble, irreversible, and hard networks connected by covalent bonds. On the other hand, another class of materials, called thermoplastic, can be reshaped and recycled due to formed non-covalent bonds. Due to instability to elevated temperatures and the promptness of exchanges, this class of materials is ideal for smart materials with lower operation temperature compared to thermosets.^[138,139] Dynamic covalent networks (DCNs), also known as covalent adaptable networks (CANs) bridge the gap between thermosets and thermoplastics and are based on two different mechanisms. The first mechanism is based on the associative (bond forming/breaking mechanism), and the second refers to the dissociative (bond breaking/forming mechanism) pathways.

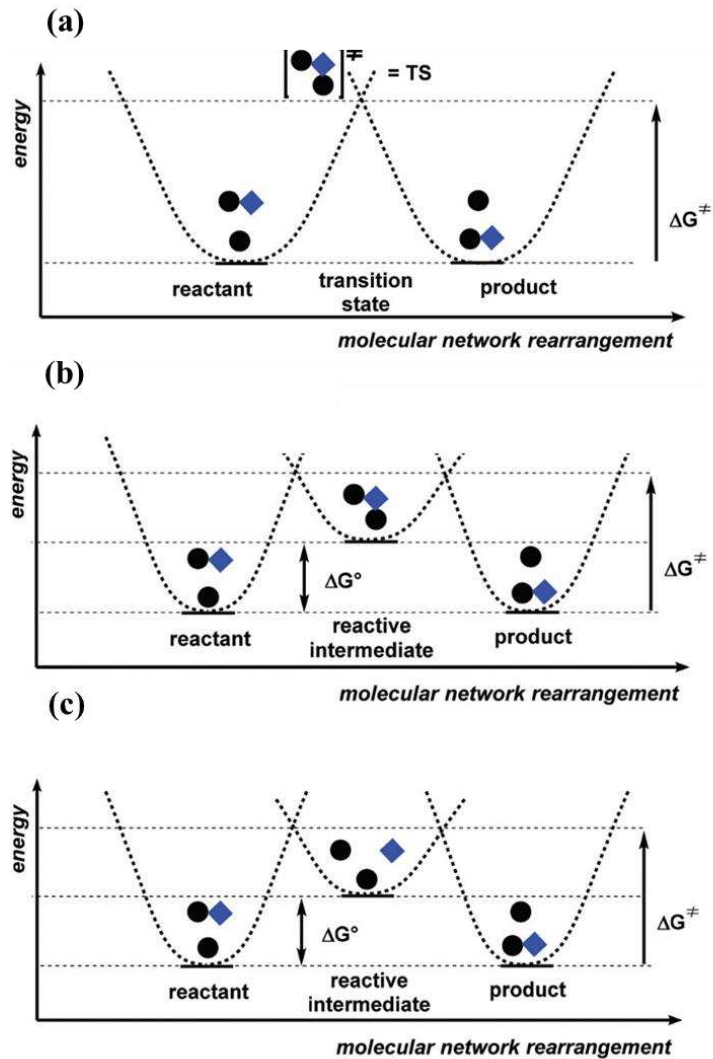


Figure 28. Schematic illustration of molecular network rearrangements: (a) ideal; (b) associative and (c) dissociative mechanisms. Reprinted with permission from ref. ^[140].

Figure 28 shows molecular network rearranges for associative and dissociative pathways when only one reactive intermediate is formed. The bond exchange reaction in associative CANs is based on the temporary formation of an intermediate reactant with increased cross-link density. Soon after that, the formation of a new cross-link occurs when the former bond is cleaved, and constant cross-link density is established.^[140] In contrast in dissociative CANs, bond breakage results in a temporary decrease in viscosity and cross-link density, prior to the formation of a new covalent bond and re-cross-linking.^[141]

Vitrimeres are a type of CANs undergoing associative bond exchange reactions. Their topology is changed under thermally activated bond-exchange reactions. At low temperatures, vitrimers

behave like thermosets due to immeasurably slow (frozen) bond-exchange reactions. On the other hand, at high temperatures, vitrimers flow like viscoelastic liquids. Due to the described properties, vitrimers open a box of new applications of thermosets (e.g. self-healing).^[142]

To sum up, vitrimers can be characterized by the following characteristics: organic network with covalent cross-links following associative dynamic networks when the temperature is applied, the viscosity reduced due to chemical exchange reactions, and follows the Arrhenius law above the topology freezing temperature (T_v). The flow behavior of vitrimers is characterized by their T_v . Above T_v , vitrimers follow the Arrhenius trend resulting in viscoelastic re-shapeable, malleable, and reprocessable fluids. On the other hand, below T_v , they behave like thermosets. The T_v of the dynamic network changes if cross-link density changes. The exchange reaction kinetics are controlled by the chemical reactions between reactants, catalyst load, and thermodynamic factors. The last characteristic of vitrimers includes an average constant cross-link density and material insolubility at all temperature ranges until degradation.^{[140],[141]}

The transesterification reaction is one possibility of dynamic exchange reactions of vitrimers or materials similar to vitrimers.^[142] In the transesterification reaction, the exchange of the organic group of an ester with an alcohol group occurs (Figure 29). The reaction can be catalyzed by organic bases, organo-metallic complexes, or Brønsted acids.

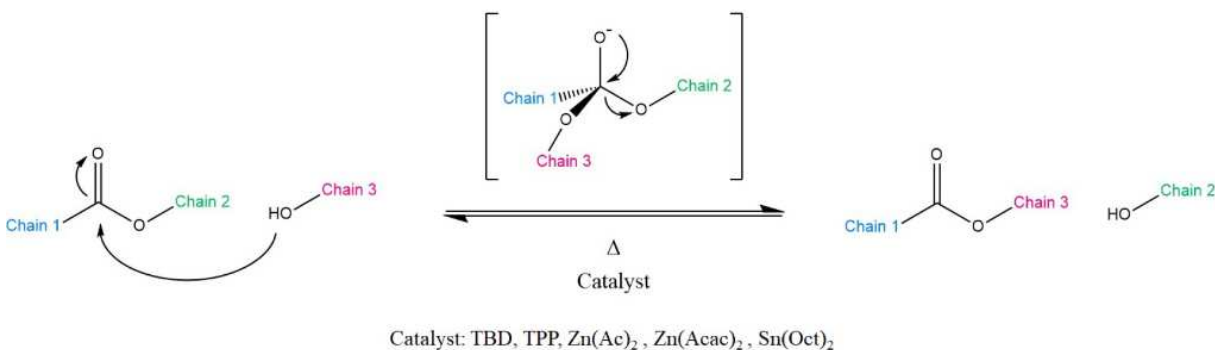


Figure 29. Representation of transesterification reaction. Reprinted with permission from ref. ^[142].

4 Publication I:

*Spatially Controlling the Mechanical Properties of 3D Printed Objects by
Dual-Wavelength Vat Photopolymerization*

Ines Cazin, Milena Olga Gleirscher, Mathias Fleisch, Michael Berer, Marco
Sangermano, Sandra Schlögl

Additive Manufacturing **2022**, 57, 102977,

DOI: 10.1016/j.addma.2022.102977.

The presented manuscript in Section 3 was almost identically published in the above-mentioned paper.

Spatially controlling the mechanical properties of 3D printed objects by dual-wavelength vat photopolymerization

Ines Cazin^a, Milena Olga Gleirscher^b, Mathias Fleisch^a, Michael Berer^a, Marco Sangermano^c, Sandra Schlögl^{a*}

a. Polymer Competence Center Leoben GmbH, Roseggerstrasse 12, A-8700 Leoben, Austria

b. Institute of Chemistry of Polymeric Materials, Montanuniversitaet Leoben, Otto Glöckel-Strasse 2, A-8700 Leoben, Austria

c. Department of Applied Science and Technology, Politecnico di Torino, Duca degli Abruzzi 24, 10124 Torino, Italy

4.1 Abstract

To date, the 3D printing of polymers with heterogeneous and locally controlled material properties is still a challenging area in additive manufacturing. In terms of vat photopolymerization 3D printing, the fabrication of multi-material objects typically relies on an automatic material exchange of different resin vats. However, along with the high complexity of the printing equipment, this technique suffers from a low build speed and often yields 3D printed objects with weak interlayer adhesion across the various material interfaces. Herein, we use chemo-selective wavelengths to fabricate objects with multi-material properties by dual-wavelength vat photopolymerization 3D printing employing a single vat. The photopolymers' stiffness and flexibility are conveniently controlled by two photoreactions working at two different wavelengths. In particular, a dual photocurable resin is applied containing multi-functional acrylates, which are cured by a radical induced chain growth reaction at 405 nm, and bi-functional epoxy monomers, which additionally undergo cationic curing upon UV exposure (365 nm). FT-IR experiments confirm the wavelength selective network formation whilst dynamic mechanical analysis and tensile tests give evidence of the distinctive difference of the related mechanical properties. By being able to produce soft ($\varepsilon = 24\%$, $\sigma = 1.0$ MPa) and stiff ($\varepsilon = 4\%$, $\sigma = 39.1$ MPa) networks with a single resin vat, we demonstrate the efficient fabrication of 3D structures with locally controlled mechanical properties using a dual-wavelength 3D printer operating at 405 and 365 nm. In contrast to previous work in this field, we were able to significantly expand the range of mechanical properties by appropriate selection of the acrylic components and to drastically accelerate the build speed by changing the cationic photoinitiator and using a customized printer with high intensity LED sources.

Key words: dual-wavelength vat photopolymerization 3D printing, heterogeneous properties, photopolymers, locally controlling mechanical performance, dual curable resins

4.2 Introduction

Additive manufacturing (AM), also known as three-dimensional (3D) printing has received high attention in academy and industry over the last decade.^[156–158] From a computer-aided design to a successive building of 3D objects without molds and heavy machining, AM opens up new opportunities in the digitized industry of the future.^[61,159–164] Thus, the interest is still steadily growing in developing functional devices for numerous fields of application such as electronics, soft robotics or biomedical engineering.^[74,165–175] Among the various AM techniques, the 3D printing of polymers by vat photopolymerization offers several advantages by being relatively cheap, fast and precise in the production of objects with a high level of complexity in their designed shapes.^[176] Vat photopolymerization 3D printing relies on the local solidification of a resin formulation by light exposure and can be divided into two main types: stereolithography (SLA), in which the 3D object is formed point-wise via a scanning laser beam, and digital light processing (DLP), in which the structures are fabricated by printing one layer at a time. Over the past years, DLP methods have been advanced for layer-free, scalable and rapid building of 3D objects, but they are typically limited to the printing of a single material.^[4] Facing the growing demand for high functionality and the desire to mimic biological structures, recent research is geared towards multi-material printing, which enables the integration of materials with different chemical, mechanical, electrical or optical properties in one object. Multi-material additive manufacturing (MMAM) is widely used for the fabrication of advanced structures for tissue engineering^[177], biomedical devices, diagnostic arrays and drug delivery.^[107,178] Another exciting application in this field is the fabrication of 3D artificial models used in preclinical or preoperative surgical studies, which significantly reduces the occurrence of errors during medical operations.^[179,180] Besides the medical sector, MMAM is also exploited to enhance the functionality of soft robotic^[181–183] and electronic devices^[184]. Recently, the fabrication of multi-material structures has been reported with nanoscale control over functional and morphological properties by exploiting polymerization induced microphase separation (PIMS) in a commercially available DLP 3D printer.^[185]

One prominent strategy for the fabrication of multi-material objects via DLP is based on a material exchange between different resin vats.^[186] By using a rotational platform^[187] or a delivery system

with microfluidic materials,^[188] 3D structures with heterogeneous material properties can be prepared. However, the build speed is very slow since a cleaning step of the object has to be carried out between each vat change. In addition, the printed objects often suffer from a weak interlayer adhesion between soft and stiffer layers, whilst the design options are limited, as the material properties can be only changed along the z-axis but not in the x,y-plane.

Integrating more than one material along all three axes is quite challenging to achieve. However, innovative AM methods have been recently developed for multi-material fabrication within both individual layers (x,y-homogeneity)^[118,189] and the same layer (x,y-heterogeneity).^[94,190] Printing of multiple materials within the same layer can be achieved by printing multiple layers of the first material all at once, followed by the printing of the second material. The main shortfall is the limited space between the resin vat and the build plate.^[94]

In an elegant approach, Boydston et al. applied grayscale imaging to print heterogeneous objects from acrylate-based systems. By varying the light intensity, they were able to adjust the cross-link density and related mechanical properties in a controlled manner.^[123]

Hawker and co-workers significantly expanded the range of mechanical properties in multi-material printed objects by introducing Solution Mask Liquid Lithography (SMaLL). In SMaLL, photochromic dyes are employed, whose reversible absorption characteristics are used to locally activate or deactivate photoreactions at different wavelengths. By using two orthogonal photocross-linking reactions, they were able to spatially control the fabrication of soft (radical curing of acrylate monomers at 530 nm) and stiff domains (formation of an interpenetrating network by simultaneous radical and cationic curing of the resin at 470 nm). For proof of concept studies, they 3D printed soft joints and mechanically reinforced “brick-and-mortar” structures with high resolution.^[130,131]

In subsequent studies, Boydston and co-workers transferred the concept of wavelength selective photoreactions to DLP 3D printing.^[132] Their resin formulation consisted of low molecular weight acrylates, Irgacure 819 as visible light absorbing radical photoinitiator, 3,4-epoxycyclohexylmethyl-3,4-epoxycyclohexane carboxylate and a triphenylsulfonium salt as cationic photoinitiator, which is transparent in the visible light region. The printing of the multi-material structures was then carried out with a home-built DLP device containing two aligned projectors working with visible and UV light. By visible light exposure, they selectively cured the acrylate resin whilst, upon UV exposure, they cured both the acrylate and the epoxy monomers

obtaining an interpenetrating network with higher cross-link density and related stiffness. The differences in network structure were then exploited for 4D printing of photopolymeric structures through spatially controlled swelling of the visible light cured acrylate domains. Although tensile tests revealed a distinctive wavelength dependent change in the ultimate elongation, the printed objects suffered from poor tensile strengths (< 0.5 MPa) independent of the applied light source. In addition, the build speed was rather low with layer ($100\ \mu\text{m}$) cure times of 60 and 120 s, respectively.

Inspired by this work, we advance the concept of wavelength dependent multi-material DLP 3D printing in the current study towards faster build speed and higher toughness of printed objects. In particular, we optimize the dual curable epoxy-acrylate resin formulation by changing the low-molecular weight acrylates and the cationic initiator. Moreover, a dual-wavelength DLP printer prototype is employed, containing two light engines that operate at 405 and 365 nm and with light intensities of $8\ \text{mW}/\text{cm}^2$. With this combined approach, the layer ($100\ \mu\text{m}$) cure time can be drastically decreased to 1 and 4 s, respectively, whilst the printed parts are characterized by significantly higher tensile strengths. The results clearly show that with the improved set-up of the dual-wavelength DLP 3D printing, an important step towards the fabrication of technically relevant multi-material parts was accomplished.

4.3 Results and Discussion

4.3.1 Network design and cure kinetics

For the local control of mechanical properties during dual-wavelength DLP 3D printing, it is crucial to apply two independent photoreactions, which can be individually switched on by irradiation with two different wavelengths. For this reason, printing experiments were carried out with a dual-wavelength DLP prototype, which was manufactured by way2production GmbH. It contains two high intensity LED light sources operating at 405 nm ($8\ \text{mW}/\text{cm}^2$) and 365 nm ($8\ \text{mW}/\text{cm}^2$), which enable a layer-by-layer printing at two different wavelengths (Figure 1a and 1c). In the current study, we used a dual curable acrylate-epoxy system undergoing a radical induced cross-linking of an acrylate resin upon visible light exposure and cationic curing of an epoxy monomer upon UV exposure (Figure 1b). It has to be considered that both reactions are not fully orthogonal since the applied radical photoinitiator (Irgacure 819) is not only absorbing at 405 nm but also in the UV

spectral region (the absorption spectra of the applied photoinitiators are provided in Figure S1 in supporting information).^[191] Thus, illumination at 365 nm yields a highly cross-linked interpenetrating polymer network formed by simultaneous radical and cationic curing.

Irgacure 819 is a classic radical photoinitiator, which forms up to four radicals by undergoing two subsequent Norrish type I reactions across the σ bond between the carbonyl groups and the phosphor atom.^[192] It is widely used for the photocuring of acrylate, thiol-acrylate and interpenetrating epoxy-acrylate resins as the formed radicals are able to rapidly initiate chain-growth polymerization reactions.^[193–195] However, due to the diffusion control of the curing reaction and rapid gelation, acrylate based photopolymers typically suffer from irregular network structure, high shrinkage stress and low final monomer conversion.^[102] In combination with high cross-link densities, brittle networks with low fracture toughness are obtained. For the design of DLP printable dual curable resins, Boydston and co-workers overcome the networks' brittleness by lowering the cross-link density.^[132] In particular, they applied a high content of mono-functional low-molecular weight acrylates, which in the presence of a bi-functional acrylate cross-linker yielded soft polymer networks with good swelling properties but poor tensile strength.

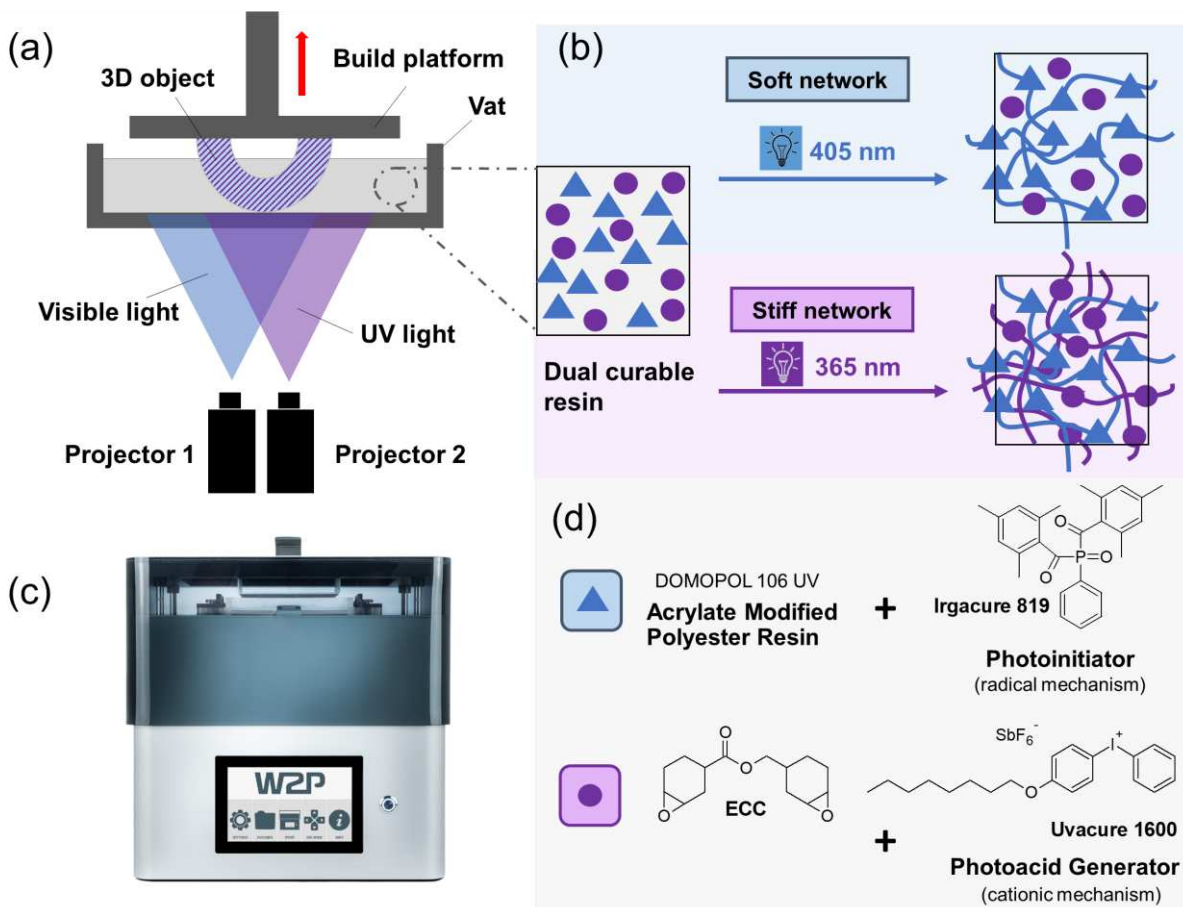


Figure 1. (a) Schematic representation and (c) photograph of the dual-wavelength DLP printer prototype operating at 365 and 405 nm. (b) Schematic representation of the wavelength selective formation of soft and stiff domains. Soft structures are obtained by radical induced curing of the acrylate component upon exposure at 405 nm. Light irradiation at 365 nm yields stiff structures by the formation of a highly cross-linked interpenetrating photopolymer network (simultaneous radical curing of the acrylate component and cationic curing of the epoxy component). (d) Monomers and initiators used for the dual curable resin formulation.

Along with an adjustment of the cross-link density, shrinkage stress and related brittleness of photopolymers can be also reduced by the addition of chain transfer agents (e.g. thiols and allyl sulfides), the use of oligomeric acrylates or the addition of fillers and rubber components.^[196] Herein, we replaced the low-molecular weight acrylate monomers with an acrylate-functional polyester resin (Domopol 106 UV), which - cured as a single resin - gave photopolymer networks with a tensile strength of 1.3 MPa and an ultimate elongation of 9.3% (Figure S2 in supporting information). A drawback of polymeric acrylate resins is their high viscosity, which limits their applicability in DLP printing techniques. However, for the dual curable formulations under

investigation, the viscosity of Domopol 106 UV was conveniently reduced from 2.31 to 0.14 Pas by the addition of the low-molecular weight epoxy monomer ECC.

To accelerate the cationic curing of ECC, we replaced the triphenylsulfonium salt used by Boydston et al., with Uvacure 1600, a diphenyliodonium derivative. Both salts have a poor spectral sensitivity and are transparent at 405 nm. Upon UV exposure, they are cleaved and form cations and strong Brønsted acids by subsequent reaction with solvents or monomers of the formulation, which initiate the cationic curing of ECC.^[197] Account has to be taken into the fact that the acidic strength of the released acid depends on the nucleophilicity of the counter-anion whereas the photochemistry is governed by the organic cation. Whilst both salts have the same anion (SbF_6^-), they differ in their acid quantum yields and reduction potential.^[198] In particular, diphenyliodonium salts have a high reduction potential and can be sensitized via oxidation of free radicals. In this way, reactive cations are formed, which promote radical induced cationic polymerization and the spectral sensitivity of the cationic initiator is significantly expanded to longer wavelengths. To evaluate the orthogonality of the dual curable system under investigation, we spin-cast thin films on Si wafer from dual curable resins containing 50 wt% Domopol 106 UV, 50 wt% ECC, 3 wt% Irgacure 819 and 3 wt% Uvacure 1600 (dual resin-1-1). It should be noted that the content of the photoinitiators is related to the weight of the respective monomers.

Figure 2 displays the conversion of the functional groups as a function of the applied wavelength and irradiation time. It should be noted that a broad $-\text{OH}$ band ($3400 - 3660 \text{ cm}^{-1}$) is already observed in the uncured resin formulation, which is related to the chemical structure of Domopol 106 UV (Figure S3 in supporting information). According to its data sheet, the polyester resin has an acidic value of around 5 mg KOH/g, giving rise to the presence of free carboxylic acid moieties. Upon visible light exposure, a fast conversion of the acrylate groups (depletion of the $\text{C}=\text{C}-\text{H}$ stretching band at $1620-1636 \text{ cm}^{-1}$ and the $\text{C}=\text{C}-\text{H}$ deformation band at 810 cm^{-1}) is obtained whilst the epoxy bands (790 and 745 cm^{-1}) remain unaffected. In addition, there is no significant change of the absorption band related to the $-\text{OH}$ groups, confirming that under the applied irradiation conditions, Irgacure 819 predominately initiates the radical curing of the acrylates and does not simultaneously sensitize any cationic curing. Subsequent UV exposure triggers the cationic cross-linking, which results in a distinctive depletion of the characteristic $\text{C}-\text{O}-\text{C}$ absorption bands of the epoxy groups at 790 and 745 cm^{-1} (Figure S3 in supporting information). At the same time, the –

OH absorption band is significantly increasing confirming the cationic ring opening of the epoxy moieties.

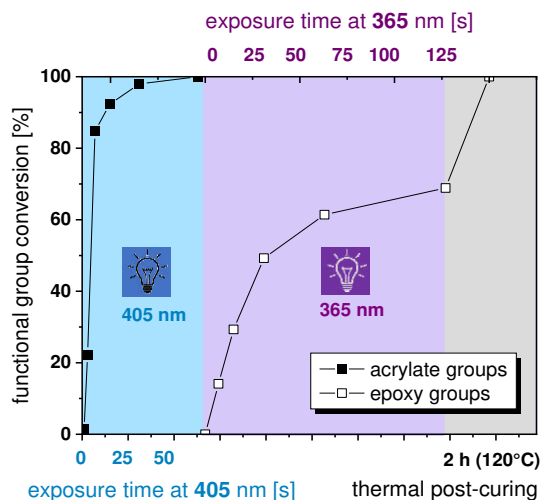


Figure 2. Monitoring the wavelength dependent cure kinetics of (a) dual resin-1-1 (containing 3 wt% Uvacure 1600) by following the depletion of the IR absorption bands related to the acrylate ($1620\text{-}1636\text{ cm}^{-1}$) and epoxy (745 cm^{-1}) groups. The lines are a guide for the eye.

However, the cationic curing is less efficient than the radical mechanism and even after 120 s UV exposure, the final monomer conversion does not exceed 70%. Due to the living nature of the cationic species, full ECC conversion is reached after a thermal post-curing step at $120\text{ }^{\circ}\text{C}$ for 2 h. Summing up, FTIR studies confirm the wavelength selective curing of the dual curable resin formulation, whilst a thermal post-treatment has to be additionally applied to reach a high curing degree of ECC.

4.3.2 Multi-Material DLP 3D printing experiments

In the first step, a series of layer cure times was screened by printing rectangular test specimen ($35\text{ mm} \times 7\text{ mm} \times 22\text{ mm}$) and switching layer wise the LED source. Photographs of the printed test specimen are provided in Figure 3a. It was found that the time window of UV exposure is rather limited since cure times of $> 10\text{ s}$ led to undesired over-curing and loss in resolution.

Although printing within this narrow time window allowed the fabrication of structures with adequate resolution, it was not possible to realize objects with multi-material properties. As shown by FTIR data, the time of the cationic curing is much longer than the radical one and at UV exposure times below 10 s, the ECC conversion is in the range of 10%. In contrast, under the same conditions

(10 s irradiation with UV light), the acrylate conversion amounts to 97% and thus, is mainly dominating the material properties. Irgacure 819 has a higher absorption in the UV than in the visible light spectral region (Figure S1 in supporting information), which explains the faster acrylate conversion upon UV exposure compared to visible light irradiation. As no distinctive change in stiffness was observed, at least when empirically comparing a visible light cured test specimen with a UV cured one, we assume that also the formation of initiating species was too low to reach higher conversions by the subsequent post-baking step.

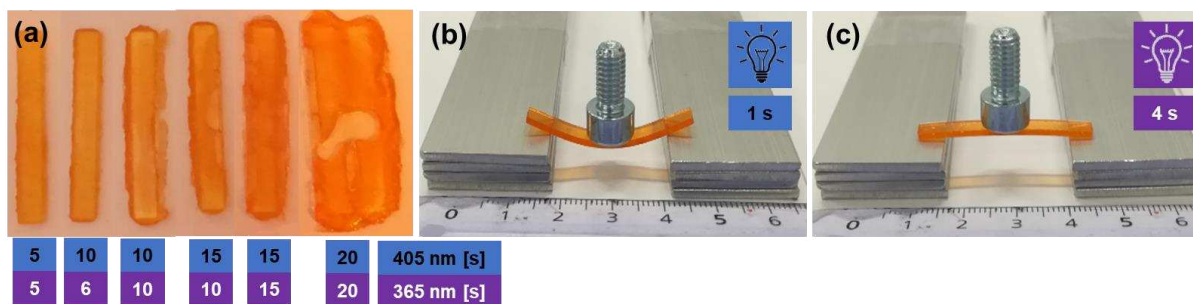


Figure 3. (a) Test specimen fabricated via dual-wavelength DLP printing with dual resin-1-1 using various layer cure times and both wavelengths for printing. Irradiation times for both visible (405 nm) and UV light (365 nm) are represented by the numbers below the figure. Test specimen fabricated via dual-wavelength DLP printing with dual resin-1-2 using either (b) 405 nm or (c) 365 nm. The test specimens were then post-baked at 120 °C for 2 h. The change in stiffness is reflected by the different bending behavior of the test specimen under load (metal screw with 6 g).

To accelerate the cure kinetics, we increased the content of the Uvacure 1600 content from 3 to 10 wt% (dual resin-1-2). FTIR studies revealed that upon short time UV irradiation (4 s), the epoxy group conversion could be more than doubled (Figure S4 in supporting information) at the higher initiator content. As a sufficiently high amount of initiating species is generated within 4 s of UV exposure, full conversion of the epoxy moieties could be reached by the subsequent post-baking step carried out at 120 °C for 2 h. In thicker coatings, such a high amount of cationic photoinitiator would be a drawback to achieve homogeneous conversion, as the chromophores act as internal filter and reduce the penetration depth of the incident light. Due to the low thickness of the single layers (100 μm), this drawback is not relevant for DLP printing and thus, the accelerating effect of the high initiator content on curing kinetics can be fully exploited.

Printing experiments were repeated with dual resin-1-2, using a layer cure time of 1 s at 405 nm, which resulted in complete fixity of the material, and 4 s at 365 nm. In a further step, we evaluated the resolution of dual resin-1-2 with the optimized printing parameters by DLP 3D printing of a

comb-like test structure. Upon either exposure at 405 nm (Figure 4b) or exposure at 365 nm (Figure 4a), all teeth features, with their thickness decreasing from 3 mm to 500 μm , were replicated successfully. However, the printing of holes was more challenging and the structures were not fully replicated. In particular, at 405 nm irradiation, the maximum printable hole diameter is 1 mm, whilst at 365 nm illumination, it increases to 2 mm. In particular, at 365 nm, the holes were also smaller than the CAD drawing, giving rise to undesired over-curing effects.

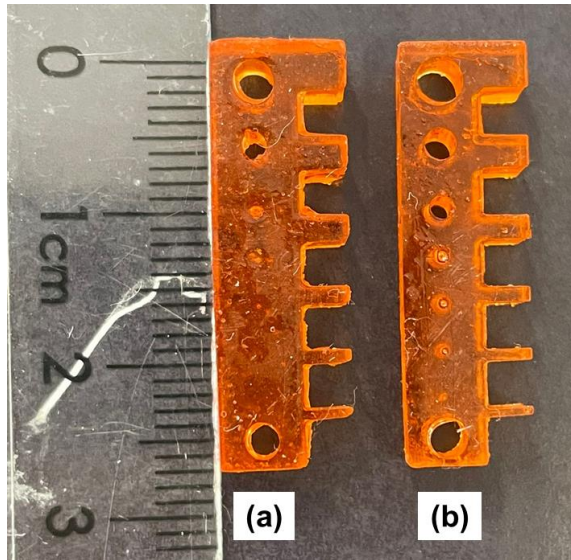


Figure 4. Test specimen DLP 3D printed using dual resin-1-2: (a) exposure at 365 nm (layer cure time: 4 s) and (b) exposure at 405 nm (layer cure time: 1 s).

With this set-up, we were able to print test specimen, whose rigidity was conveniently changed by the wavelength applied in the printing process (Figure 3b and 3c). These heterogeneous properties could be also realized in 3D printed “in-plane hinges” (Figure 5a), in which two rigid domains were connected through a soft domain. The soft centerpiece, irradiated at 405 nm, enabled the elastic bending of the printed hinge, whereas the two stiff domains, irradiated with both lights, gave the structure its stability. Advancing to more complex 3D structures, we further 3D printed a foldable box with soft hinges at the corners and stiff interconnects (Figure 5b). To demonstrate the creation of 3D objects with heterogeneous properties along the z-axis, a comb with a stiff base and soft teeth was printed (Figure 5c).

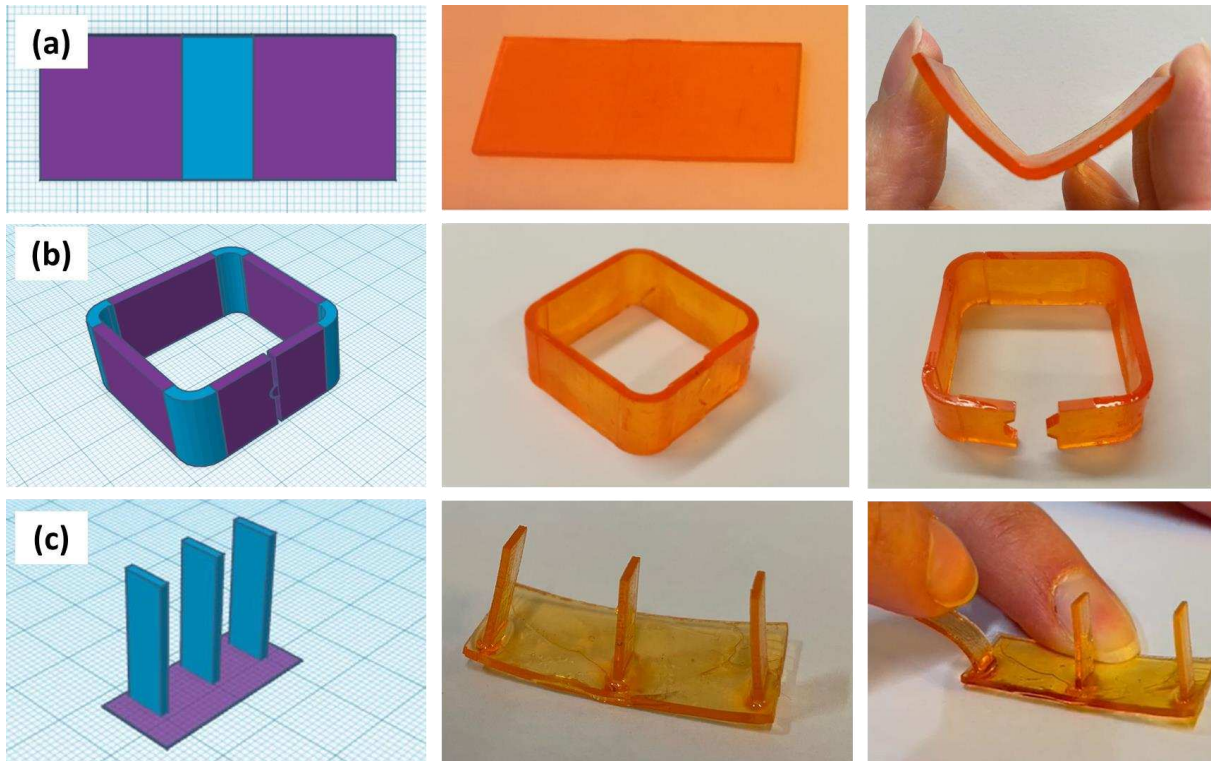


Figure 5. Multi-material test specimen fabricated via dual-wavelength DLP printing with dual resin-1-2: (a) hinge, (b) foldable box and (c) comb. On the left side, the CAD data is shown with the color denoting the different wavelengths (blue: 405 nm, purple: 365 nm), in the middle, the printed part is shown and on the right side, the bending of the structures across the soft domains (illuminated only at 405 nm) is demonstrated.

Compared to the dual-wavelength printer of Schwartz and Boydston, our prototype offers a significantly higher light intensity of the light engines (8 versus 0.75 mW/cm^2), whilst the resin comprises a more efficient photoacid generator for the cationic ring opening of the epoxy monomers.^[44] These two factors significantly increase the building speed of our printer, which requires layer (100 μm) cure time of 1 (405 nm) and 4 s (365 nm), respectively. In contrast, the printer of Schwartz and Boydston needs 60 and 120 s for the curing of the same layer thickness. Another benefit of our system is that the two light sources and the controllers are assembled within one machine, which is expected to ease the handling and also might improve the reproducibility of the printed parts.

However, it should be noted that the resolution of the multi-material domains obtained with our multi-material printer is in the millimeter range, which is mainly a result of the resin properties.

Although printing of sophisticated mechanical metamaterial structures was feasible (Figure S5 in supporting information), we were not able to realize heterogeneous properties of stiff pillars in

combination with soft interconnects (diameter of 0.7 mm).^[199] In this case, we ended up with a 3D object comprising homogenous rigid properties over the whole structure. This can be explained by the exothermicity of the cationic ring opening reaction and the related heat generation, which accelerates the diffusion of the photo-released acids into the soft domains during the printing process. Owing to the longer lifetime of the initiating species, the subsequent thermal post-baking at 120 °C can further promote diffusion of the photo-released acids, which leads to the gradual formation of an interpenetrating network at the interface between soft and rigid structures and in the end in areas exposed with 405 nm only. With the Solution Mask Liquid Lithography (SMaLL) from Hawkers and co-workers, hybrid acrylate-epoxy resins were built with a higher speed (50 cm/h) and also higher resolutions (100 µm) than our system.^[42] However, the system requires use of a diarylethene photoswitch, which undergoes a wavelength-dependent ring opening/ring closure reaction. The synthesis of the photoswitch is quite elaborate and expensive, which is a challenge when it comes to the printing of larger parts and the commercialization of the system. In contrast, our developed resin formulation is exclusively composed of commercially available components, which enables an easier and widespread implementation of multi-material DLP 3D printing in industry.

4.3.3 Wavelength dependent thermo-mechanical and mechanical properties

To study the wavelength selective change in the material performance in more detail, DMA and tensile tests were performed on DPL printed test specimen using the optimized printing parameters (405 nm: 1 s layer exposure time and 365 nm: 4 s layer exposure time). The thermal post-baking step was carried out again at 120 °C for 2 h. In Table 1, the wavelength dependent properties of dual resin-1-2 are compared to the mechanical and thermo-mechanical performance of the single resin components. Domopol UV 106, DLP 3D printed as a single resin at 405 nm and thermally post-baked, comprises a glass transition temperature (T_g) of 19 °C. The post-baking slightly increases both tensile strength and ultimate elongation of the pure Domopol UV 106 resin (Figure S2 in supporting information). This behavior can be explained by the thermally promoted formation of dipolar interactions and H-bonding in the presence of the ester and carboxylic acid moieties, which has been also observed in acrylate-based vitrimers.^[200]

It is interesting to note, that upon 405 nm light exposure and the subsequent post-baking step, dual resin-1-2 exhibits a T_g, which is comparable with pure Domopol UV 106 undergoing the same

curing and post-treatment. Figure 6 shows the related DMA curves, in which only one phase transition related to the T_g is observed, which indicates a similar network structure.

Table 1. Mechanical and thermo-mechanical properties of single and dual curable resins as a function of the applied wavelength used in the dual-wavelength DLP 3D printing process. Dual-wavelength DLP printing was carried out with a layer exposure time of 1 s at 405 nm and 5 s at 365 nm. All samples were post-baked at 120 °C for 2 h.

Formulation	Irradiation	T_g [°C]	E' at 23 °C [MPa]	σ [MPa]	ε [%]
single Domopol UV 106	405 nm	19	54	1.5 ± 0.2	12.0 ± 1.4
dual resin-1-2	405 nm	17	21	1.0 ± 0.11	24.0 ± 0.9
dual resin-1-2	365 nm	70	2050	39.1 ± 3.0	3.8 ± 0.4
single ECC	365 nm	170 ¹	not determined		

¹taken from ^[143]

However, the non-reacted ECC monomers act as plasticizer as the storage modulus of visible light cured dual resin-1-2 is significantly lower than the one of pure Domopol UV 106 (Table 1) cured under the same conditions. This is also endorsed by the results of the tensile tests, which show a distinctive increase in the ultimate elongation (from 12 to 24%) of visible light cured dual resin-1-2 due the presence of free ECC monomers.

By switching the wavelength from 405 to 365 nm, a distinctive increase in T_g from 19 to 70 °C is observed. This is mainly attributed to the additional cationic curing of ECC, which - cured as a single resin - yields rather stiff networks with a T_g around 170 °C.^[143] The DMA data further confirm the formation of a full-interpenetrating network, as only one phase transition can be observed in the loss factor curve. At the same time, the glass transition region became broader indicating a higher network heterogeneity.

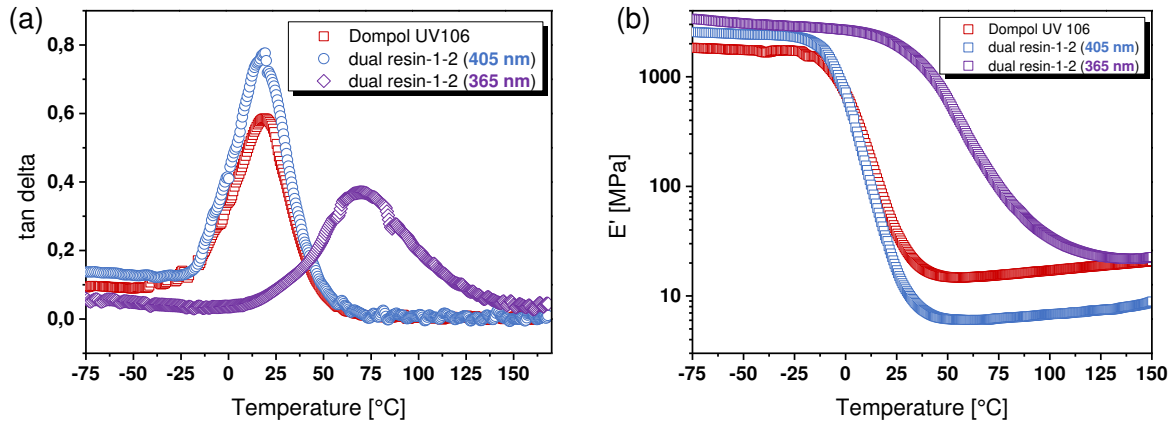


Figure 6. (a) Loss factor ($\tan \delta$) and (b) storage modulus (E') versus temperature as obtained from DMA measurements of dual resin-1-2 compared to single Dompol UV 106. Test specimen were fabricated by dual-wavelength DLP printing using a layer exposure time of 1 s at 405 nm and 4 s at 365 nm. All samples underwent thermal post-baking at 120 °C for 2 h.

Depending on the selected wavelength, the storage moduli could be changed over two orders of magnitude. Whilst at 405 nm, soft networks with $E' = 21$ MPa (at 23 °C) are obtained, the additional cationic curing promoted at 365 nm yields stiff interpenetrating networks with $E' = 2.05$ GPa (at 23 °C), confirming the orthogonality of the two photoreactions under the applied conditions. The reinforcing effect due to the interpenetrated epoxy network is clearly evident also by the occurring of the drop of E' at much higher temperature and reaching a significantly higher rubbery plateau with respect to the formulation cross-linked at longer wavelength.

Along with T_g and moduli, the formation of the interpenetrating network significantly affected the tensile properties. Tensile testing was performed with digital image correlation using Mercury DIC System software and the camera filmed the behavior of the samples during the tensile tests. Whilst the tensile strength increased from 1.0 to 39.1 MPa, the ultimate elongation decreased from 25 to 3.8%. This was accompanied by a distinctive rise in the Young's modulus, which additionally confirmed the wavelength selective switch between soft and rigid material properties by printing with a single vat. The videos of the samples fully printed either with 405 or 365 nm are provided in the supporting information (video S1 and video S2).

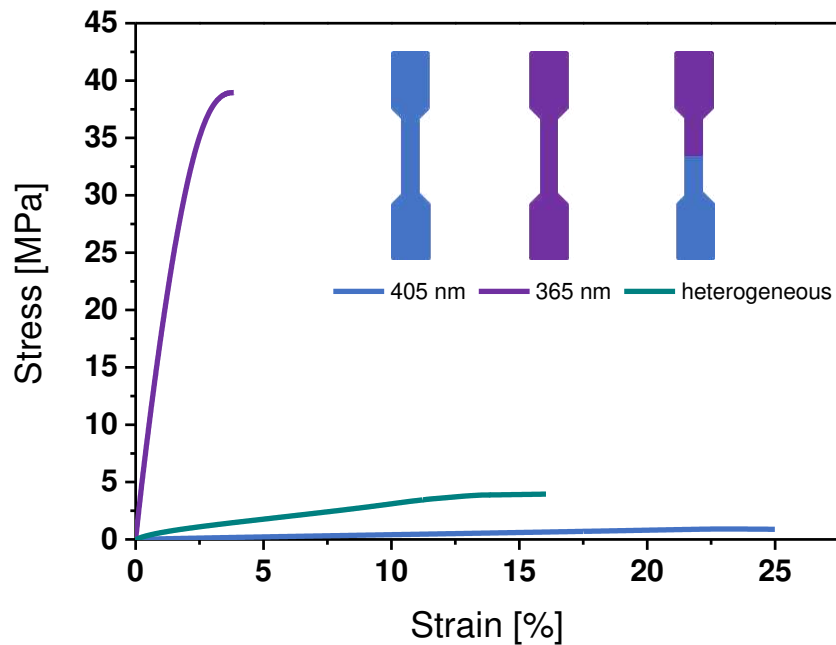


Figure 7. Stress strain curves of dual resin-1-2 after thermal post-baking at 120 °C for 2 h. Test specimen were fabricated by dual-wavelength DLP printing using a layer exposure time of 1 s at 405 nm and 4 s at 365 nm. The blue and purple curve correspond to homogeneous samples, which were fully printed using either 405 or 365 nm. The green curve is related to a sample, in which on half was cured at 405 nm and the other half at 365 nm.

As the pronounced mismatch in mechanical properties can lead to stress concentrations at the interface, we further studied the interlayer adhesion between soft and stiff domains in dual resin-1-2.^[201] In particular, we printed heterogeneous dumbbell shaped test specimen, in which one-half of the sample was printed at 405 nm and the other half at 365 nm (Figure 7). All five tested samples showed cohesive failure in the soft domain giving rise to a superior interlayer adhesion (video S3 in supporting information). The good interlayer adhesion can be explained by the diffusion of the cationic initiating species from rigid areas exposed to 365 nm to soft domains illuminated with 405 nm during printing and the thermal post-baking step. Whilst it compromises on the resolution of the multi-material domains, we assume that the diffusion of the photo-released acids leads to a gradual formation of the cationic cured ECC network across the interface to the soft domains. The related gradient in rigidity at the interface between soft and rigid domains is expected to better distribute internal stresses and improve the interlayer adhesion.

4.4 Conclusion

In the present study, multi-material DLP 3D printing was being advanced by optimizing a dual curable acrylate-epoxy resin towards cure rate and extension of mechanical properties. The resin was processed with a dual-wavelength DLP printer prototype, which operated at 405 and 365 nm. At 405 nm, soft domains were obtained by radical curing of the acrylate component whilst exposure at 365 nm yielded an interpenetrating polymer network formed by additional cationic curing of ECC. The orthogonality of the two photoreactions (under the applied irradiation conditions) was confirmed by FTIR studies. Whilst fast conversion of the acrylate groups was observed, cationic curing of ECC required an additional thermal post-baking step at 120 °C for obtaining a high degree of conversion. Once the printing parameter were optimized, dual-wavelength DLP 3D printing with the optimized resin formulation enabled a fast printing (layer cure time within seconds) of multi-material objects with storage moduli that could be locally adjusted over two orders of magnitude by simply switching the wavelength of the light source. However, due to the thermally promoted diffusion of the photo-released acid, no sharp interface properties were obtained between soft and rigid domains. This compromises on the resolution of the multi-material domains, but also improves the interface properties between soft and rigid parts. One way to overcome the diffusion of the released acid in further work, is the covalent attachment of the photolabile acid within the photopolymer matrix during the visible light induced curing process.

Summing up, with the current set-up, 3D objects with multi-material domains in the mm-range and good interface properties can be easily and efficiently fabricated by using commercially available initiators and resins. These features are of particular interest for introducing stiffness variations and gradients in macroscopic soft actuators and soft robotic systems (e.g. grippers, soft robotic locomotion). Moreover, the ability to locally control the glass transition temperature in the mm-range might offer new possibilities to increase the functionality of shape memory polymers. The spatially controlled movement as a response to temperature might be also interesting for integrated sensor systems. Whilst the resolution of the multi-material domains is not high enough to print composite structures, which mimic biological tissues, the system has a high potential for application in macroscopic composite structures. Examples are functional orthoses and prosthetics, comprising soft areas, which are in contact with the human body, and stiff regions that ensure the structural robustness of the devices. Due to the versatility of the approach, ongoing research is

dedicated to setting up a library of dual curable resin formulations to cover a broad range of material properties, which can be realized by DLP printing using two different wavelengths.

4.5 Experimental part

4.5.1 Materials and chemicals

3,4-Epoxy cyclohexylmethyl-3,4-epoxycyclohexanecarboxylate (ECC) and *p*-(octyloxyphenyl) phenyl iodonium hexafluoroantimonate (Uvacure 1600) were purchased from ABCR (Karlsruhe, Germany). Phenylbis(2,4,6-trimethylbenzoyl) phosphine oxide (Irgacure 819) was supplied by Sigma Aldrich (St. Lois, US). Sudan II was obtained from TCI chemicals (Tokyo, Japan). Acrylate modified polyester resin (Domopol 106 UV) was kindly provided by Helios TBLUS d.o.o. (Ljubljana, Slovenia). All chemicals were used without further purification.

4.5.2 Preparation of photocurable formulation

Photocurable formulations were prepared by mixing an equal amount (50 wt%) of Domopol UV 106 and ECC at room temperature. 3 wt% of Irgacure 809 (calculated according to the acrylate weight), a varying amount of Uvacure 1600 (calculated according to the epoxide weight) and 0.01 wt% of Sudan II were added and the formulations were homogenized with a vortex mixer for three times (1 min at room temperature) until all components were dissolved. The prepared formulations were stored under dark conditions and used within 2 days of preparation. In addition, a single Domopol UV 106 formulation was prepared as reference. The compositions of the resin formulations are summarized in Table 2.

Table 2. Composition of single and dual curable resins under investigation.

Formulation	Domopol UV 106 [wt%]	ECC [wt%]	Irgacure 819 [wt%]	Uvacure 1600 [wt%]	Sudan II [wt%]
single Domopol UV106	100	-	3	-	0.01
dual resin-1-1	50	50	3	3	0.01
dual resin-1-2	50	50	3	10	0.01

4.5.3 Characterization of cure kinetics

Fourier transform infrared spectroscopy was performed on a PerkinElmer Spectrum One spectrometer (Massachusetts, US). Spectra were taken in transmittance mode over a wavenumber range of 4000 to 400 cm^{-1} . All spectra were accumulated from 16 scans at a resolution of 4 cm^{-1} . The conversion of the functional groups was calculated with OPUS software by evaluating the decrease of the characteristic acrylate IR absorption band at 1620-1636 cm^{-1} and the absorption bands of the epoxy moieties at 790 and 750 cm^{-1} . The C=O absorption band at 1730 cm^{-1} was used as reference peak. The degree of conversion (DC) of the curing reaction was calculated using the following equation, in which C_{peak} corresponds to the absorption area of the observed band of the cured sample and $C_{Reference}$ to its reference peak. U_{Peak} and $U_{Reference}$ correspond to the absorption area of the relevant band and reference peak of the uncured sample.

$$DC\% = \left[1 - \left(\frac{C_{Peak}/C_{Reference}}{U_{Peak}/U_{Reference}} \right) \right] \cdot 100$$

For sample preparation, 50 mg of the respective formulation was dissolved in 1 mL of dichloromethane and 40 μL of the prepared solution was spin-cast on a Si wafer (1.5 x 1.5 cm). Spin coating was carried out with a SpinCoater Model 4000 from Electronic Micro Systems Ltd. (Wiltshire, UK) using a speed of 3000 rpm for 60 seconds. Visible light irradiation was performed with a LED curing lamp (zgood® wireless) at 3.6 mW/cm^2 and UV illumination with a Hg lamp (Omnicure Series 1000) at 8 mW/cm^2 . Experiments were carried out under nitrogen atmosphere to prevent oxygen inhibition of the acrylate curing. The light intensity was measured with an EIT (Leesburg, USA) Power Puck II UV radiometer.

4.5.4 Dual wavelength DLP 3D printing

Multi-material DLP 3D printing was performed on a dual-wavelength DLP prototype, which was manufactured by way2production (Austria). The DLP printer operated with two light engines, which contained a 405 and 365 nm LED light source, respectively. Their intensity amounted to 8 mW/cm^2 . The building area of the printer was 67.2 x 37.8 x 130.0 mm with a maximum filling of 400 mL. The layer thickness could be adjusted between 25 and 200 μm . The vat could be heated up to 80 $^{\circ}\text{C}$, but in this study the printing was carried out at room temperature. For the printing of soft domains, the layers (100 μm layer thickness) were illuminated for 1 s with 405 nm, whilst for the fabrication of the stiff domains, the printing of the layers was carried out at 365 nm for 4 s. All

printed objects were rinsed (around 30 s) with isopropanol to remove non-reacted monomers from the surface of DLP 3D printed parts and were post-baked at 120 °C for 2 h.

4.5.5 Characterization of thermomechanical and mechanical properties

Dynamic mechanical analysis (DMA) was carried out on a Mettler Toledo DMA/SDTA861e analyser. Mechanical loss factors ($\tan \delta$) and storage moduli (E') were monitored over a temperature range from -60 to 160 °C at a heating rate of 3 °C/min, with a frequency of 1 Hz, maximum displacement of 3 μm and maximum force of 8 N. The glass transition temperature (T_g) was determined by the temperature at the maximum of the loss factor. For sample preparation, test specimen (35 mm x 7 mm x 22 mm) were fabricated by dual-wavelength DLP 3D printing of dual resin-1-2.

Mechanical properties were characterized by an Instron 5500 (Instron, DEU) Universal Tester, using a 100 N load cell and pneumatic foil grips. Dogbone-shaped rectangles samples, with a size of 2 mm x 12 mm x 0.1 mm, were DLP 3D printed according to ISO 527 type 5B. The test speed was 1 mm/min and the tests were carried out at 23 °C (50% RH). Tensile testing was executed with digital image correlation using Mercury DIC System software version 2.8, a UI-3180CP-M-GL R2.1 camera, and a Componon-S 2.8/50 lens (Schneider Kreuznach, DEU). The gauge length of the extensometer was set at 10 mm.

4.5.6 UV-Vis measurements

UV-Vis experiments were conducted on a Varian (Palo Alto, USA) Cary 50 UV-Visible spectrophotometer in the range of 200-800 nm at a scan rate of 600 nm/min and a recording interval of 1.00 nm, using a quartz cuvette with an optical path length of 10 mm. The photoinitiators were dissolved in acetonitrile resulting in a final concentration of 100 $\mu\text{M}/\text{mL}$.

4.6 Acknowledgements

The research work was performed within the COMET-Module project “Chemitecture“ (project-no.: 21647048) at the Polymer Competence Center Leoben GmbH (PCCL, Austria) within the framework of the COMET-program of the Federal Ministry for Transport, Innovation and Technology and the Federal Ministry for Digital and Economic Affairs with contributions by Montanuniversitaet Leoben, Politecnico di Torino, Helios TBLUS and bto-epoxy. Funding is

provided by the Austrian Government and the State Government of Styria. In addition, the authors thank Gerald Meier (PCCL) for performing the tensile tests.

This paper is dedicated to Damir Cazin, a mechanical engineer, a passionate alpinist and a joyful musician, who tragically lost his life in January 2022 in the Kamnik-Savinja Alps in Slovenia.

4.7 Supporting Information

Spatially controlling the mechanical properties of 3D printed objects by dual-wavelength vat photopolymerization

Ines Cazin^a, Milena Olga Gleirscher^b, Mathias Fleisch^a, Michael Berer^a, Marco Sangermano^c, Sandra Schlögl^{a*}

a. Polymer Competence Center Leoben GmbH, Roseggerstrasse 12, A-8700 Leoben, Austria

b. Institute of Chemistry of Polymeric Materials, Montanuniversitaet Leoben, Otto Glöckel-Strasse 2, A-8700 Leoben, Austria

c. Department of Applied Science and Technology, Politecnico di Torino, Duca degli Abruzzi 24, 10124 Torino, Italy

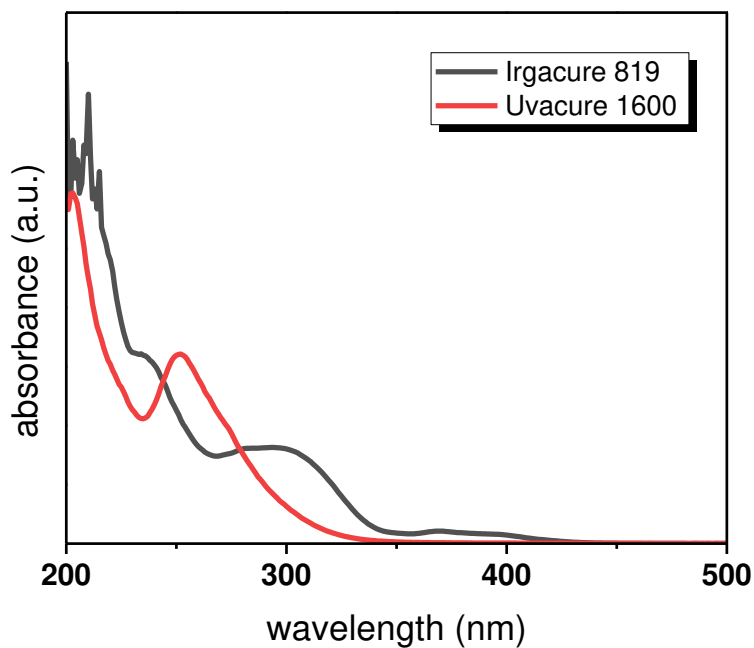


Figure S1: Uv-Vis spectra of Irgacure 819 and Uvacure 1600 (100 μ M/mL in acetonitrile).

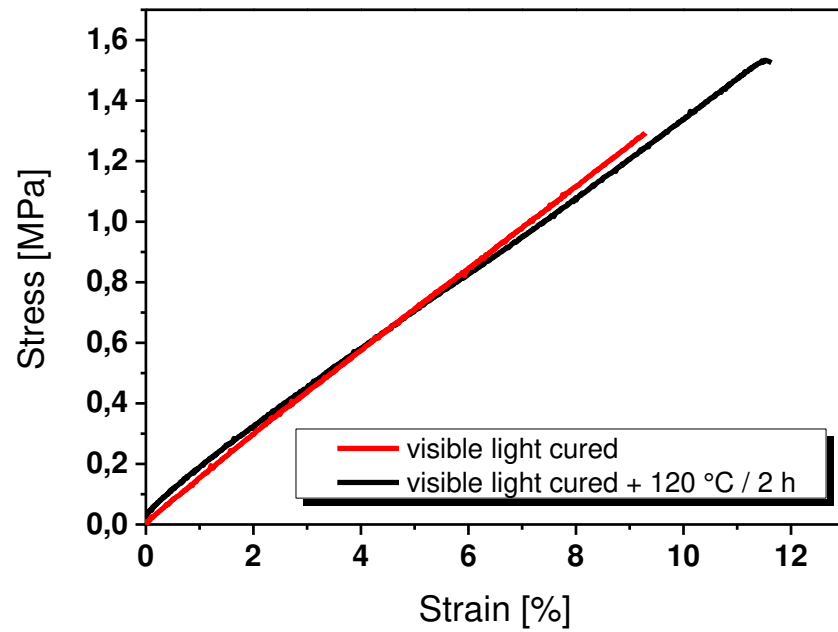


Figure S2: Stress-strain curve of visible light cured Domopol 106 UV containing 3 wt% Irgacure 819 as radical photoinitiator prior to and after a thermal post-baking step (120 °C for 2 h).

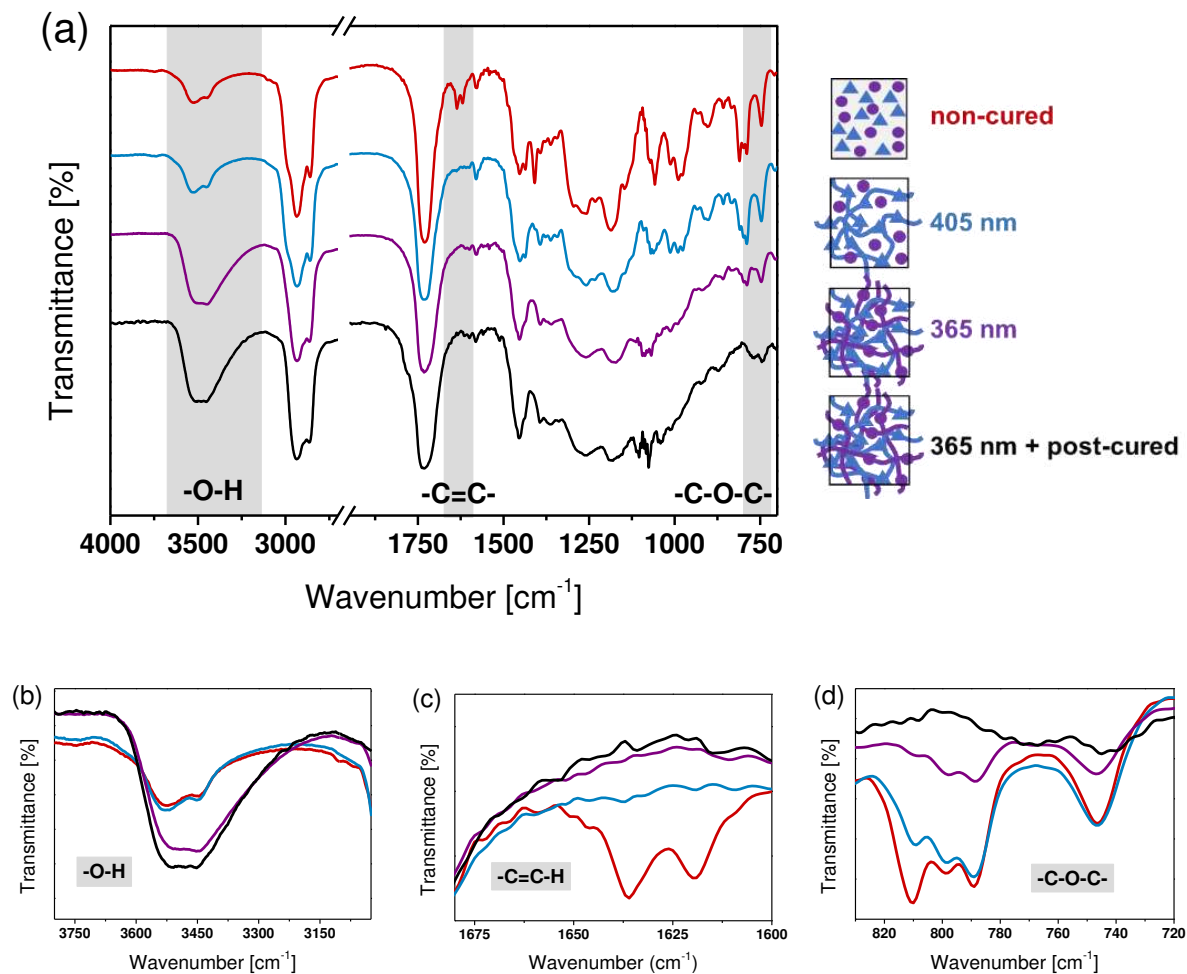


Figure S3. (a) FTIR spectra of dual resin-1-1 prior to and after exposure to visible (405 nm, 3.6 mW cm⁻²) and UV light (365 nm, 8 mW cm⁻²) and subsequent thermal post-curing at 120 °C for 2 h. Magnified area of the (b) -O-H, (c) -C=C-H (acrylate) and (d) -C-O-C- (epoxide) absorption bands.

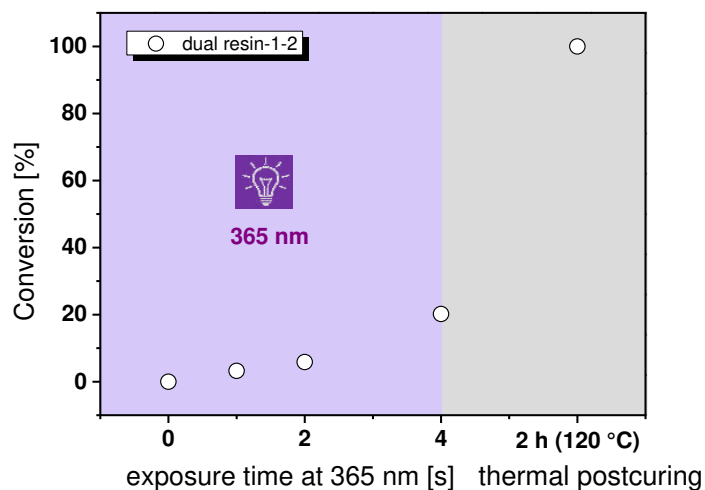


Figure S4. Monitoring the conversion of the epoxy groups (745 cm^{-1}) of dual resin-1-2 (10 wt% Uvacure 1600) by following the depletion of the IR absorption bands. The lines are a guide for the eye.



Figure S5. Multi-material test specimen fabricated via dual-wavelength DLP printing with dual resin-1-2. On the left side, the CAD data is shown with the color denoting the different wavelengths (blue: 365 nm, grey: 405 nm), in the middle and the right side the printed part is shown (sample dimensions: 20 mm x 20 mm x 20 mm).

5 Publication II:

Dual-wavelength vat photopolymerization 3D printing with hybrid acrylate-epoxy resins: influence of resin composition on microstructure and mechanical properties

Ines Cazin, Kateřina Plevová, Walter Alabiso, Elvira Vidović, Sandra Schlögl

Adv Eng Mater, **2024**, 26, 2301699

DOI: 10.1002/adem.202301699.

The presented manuscript in Section 4 was almost identically published in the above-mentioned paper.

Dual-wavelength vat photopolymerization 3D printing with hybrid acrylate-epoxy resins: influence of resin composition on microstructure and mechanical properties

Ines Cazin^a, Kateřina Plevová^b, Walter Alabiso^a, Elvira Vidović^c, Sandra Schlögl^{a*}

a. *Polymer Competence Center Leoben GmbH, Roseggerstrasse 12, A-8700 Leoben, Austria*

b. *Institute of Materials Science and Testing of Polymers, Department of Polymer Engineering and Science, Montanuniversitaet Leoben, Otto Glöckel-Strasse 2, 8700 Leoben, Austria*

c. *University of Zagreb, Faculty of Chemical Engineering and Technology, Trg Marka Marulića 19, HR-10000 Zagreb, Croatia*

5.1 Abstract

Dual-wavelength vat photopolymerization 3D printing represents a convenient technology for the fabrication of objects with heterogeneous and locally controlled mechanical properties. By using two λ -orthogonal cross-linking reactions, it is possible to produce soft and stiff photopolymers with a single resin vat by switching the light source. Herein, hybrid acrylate-epoxy resins are selectively cured by using either visible or UV-light. At 405 nm, a free radical curing of the acrylate monomers is induced whilst irradiation with 365 nm triggers an additional cationic ring opening reaction of the epoxy monomer yielding interpenetrating photopolymer networks. In a comprehensive approach, the influence of the resin composition and the applied wavelength on cure kinetics, film morphology, (thermo)mechanical properties and printability are studied. Fully separated as well as homogenous network morphologies are obtained depending on the ratio between acrylate and epoxy monomers, cure rate and applied light source (405 versus 365 nm). In general, glass transition temperature, stiffness and tensile strength of the photopolymers increase with rising epoxy content. In contrast, a higher epoxy concentration in combination with a higher amount of the cationic photoinitiator compromises on the system's orthogonality, giving rise to the important role of the resin composition in dual-wavelength vat photopolymerization 3D printing.

Key words: Dual-wavelength vat photopolymerization 3D printing, hybrid radical/cationic photopolymers, heterogeneous properties, multi-material, polymer morphology.

5.2 Introduction

Integrating two or more different materials into one object offers numerous advantages for technical applications including certain material choices which can be incorporated in a single print job and improved mechanical properties of target parts of highly complex structures without using high-cost and time-consuming methods.^[202–204] Composites with variations in chemical, physical, mechanical and electrical properties have been developed and implemented in various industrial fields such as biomedicine, electronics or soft robotics.^[19,205,206] Advancing from traditional processing techniques, recent research is geared towards the additive manufacturing of multi-material objects benefiting from a high flexibility in design. Additive manufacturing, also known as three-dimensional (3D) printing, allows the fabrication of complex 3D objects often using a layer-by-layer technique where each layer constitutes a thin cross-section of the desired object designed by 3D computer-aided design (CAD).^[61,123,207,208] In particular, vat photopolymerization enables the printing of photopolymers by selective curing of a liquid resin through light-activated polymerization. It mainly relies on two different techniques: stereolithography (SLA) and digital light processing (DLP). Although both techniques are based on layer-by-layer structure fabrication, in SLA the polymerization process is induced by a laser beam focused onto a photosensitive liquid, while curing a whole layer at a time is characteristic for the DLP technique.^[209,210] Taking advantage of inexpensive, mechanically simple printers, fast and precise scalable building of objects (without the usage of molds, masks and heavy machining) the DLP technology has gained remarkable interest in the last decade.^[132,211] However, most developed 3D printing techniques are limited to fabricating objects with one material only.

Integrating more materials in a spatially controlled manner and, particularly, the building of multi-material printed objects by vat photopolymerization is still challenging. Several techniques have been reported for the printing of complex multi-material structures via vat photopolymerization.^[38] Manually switching resins or resin vats during printing is the simplest method which requires the cleaning of the previously printed part and resin vat before it switches to another resin. Whilst a wide range of resin formulations can be used, the method typically suffers from a very slow printing speed. Further reported limitations include interfacial adhesion between soft and stiff domains, possible issues with printing of entrapped materials and different dimensions between the printed materials.^[105,108,118,212–215] Overprinting is often used in the plastic industry based on the construction of printers with rotating components where the multi-material objects are produced

all-at-once, around other materials, which means the method is not limited to layer-by-layer printing. The printing is significantly faster and light intensity or exposure time can vary within a print. Highly viscous resins are applied with high reactivity and high optical density.^[93]

Along with a mechanical switch of the resin vat, multi-material objects can be fabricated with a single vat by changing the light source (exploiting orthogonal chemistries) or varying the light intensity during the layer by layer printing.^[216] In 2016, Boydston et al. reported the DLP 3D printing of heterogeneous objects by adjusting the cross-link density in acrylate-based photopolymers with different light intensities.^[123] Three years later, they introduced a DLP 3D printer containing two different light sources that operated with visible and UV-light, respectively. Following an orthogonal chemistry approach, they selectively induced different curing reactions in the resin. Visible light exposure activated a radical photoinitiator, which started the free radical polymerization of acrylate monomers. In contrast, irradiation with UV light did not only activate the radical curing of the acrylates but also the cationic cross-linking of epoxy monomers, which were present in the resin formulation. The resulting interpenetrating network was comprised of significantly higher cross-link density and stiffness. By switching the lights from 405 to 365 nm, the build speed for 100 μm layer thickness was 60 and 120 s, respectively.^[132] Sequence dependent orthogonal curing of hybrid epoxy-acrylate resins was also used by Hawker and co-workers in their introduced Solution Mask Liquid Lithography (SMaLL). The resins additionally contained photochromic dyes with reversible absorption characteristics that were employed to locally activate and deactivate photoreactions at different wavelengths (530 and 470 nm).^[130]

Recently, we demonstrated the dual-wavelength DLP 3D printing of multi-material structures with drastically increased build speed by optimizing the composition of the hybrid acrylate-epoxy resin and by using a new DLP 3D printer prototype with high intensity LEDs. By switching the wavelengths during the printing, we were able to produce multi-material objects with storage moduli that could be locally adjusted over two orders of magnitude.^[51] Herein, we studied the influence of the resin composition used in dual-wavelength DLP 3D printing on the phase separation assisted change in material and printing properties in detail. In 2019, Hasa et al. investigated phase separation phenomena in UV cured hybrid acrylate-epoxy systems and their influence on surface roughness and related optical properties. Depending on monomer compositions (molar ratio between acrylate and epoxy monomers amounted to 1:1, 7:3 and 9:1), photoinitiator content and irradiation intensity, they were able to obtain homogenous

interpenetrating networks as well as fully phase-separated systems.^[153] Inspired by this work, in the current study, we investigate how resin composition and related changes in their microstructure affect printability and (thermo)mechanical properties of dual-wavelength DLP 3D printed objects.

5.3 Results and discussion

5.3.1 Photopolymerization kinetics and photopolymer morphology

In previous work, we demonstrated the sequence dependent λ -orthogonal photopolymerization of a hybrid radical/cationic curable resin comprising equal weights of an acrylate modified polyester resin (Domopol 106 UV) having five functional acrylate groups per molecule and a low molecular weight epoxy monomer (3,4-epoxycyclohexylmethyl-3,4-epoxycyclohexanecarboxylate, ECC) with two functional epoxy groups per molecule. Upon visible light exposure (405 nm), the radical photoinitiator phenylbis(2,4,6-trimethylbenzoyl) phosphine oxide (Irgacure 819) was selectively activated and initiated the curing of the acrylate groups yielding a soft network with unreacted epoxy monomers (Figure 1a). In contrast, irradiation with UV-light simultaneously started the radical and cationic curing both of acrylate and epoxy groups (Figure 1b).

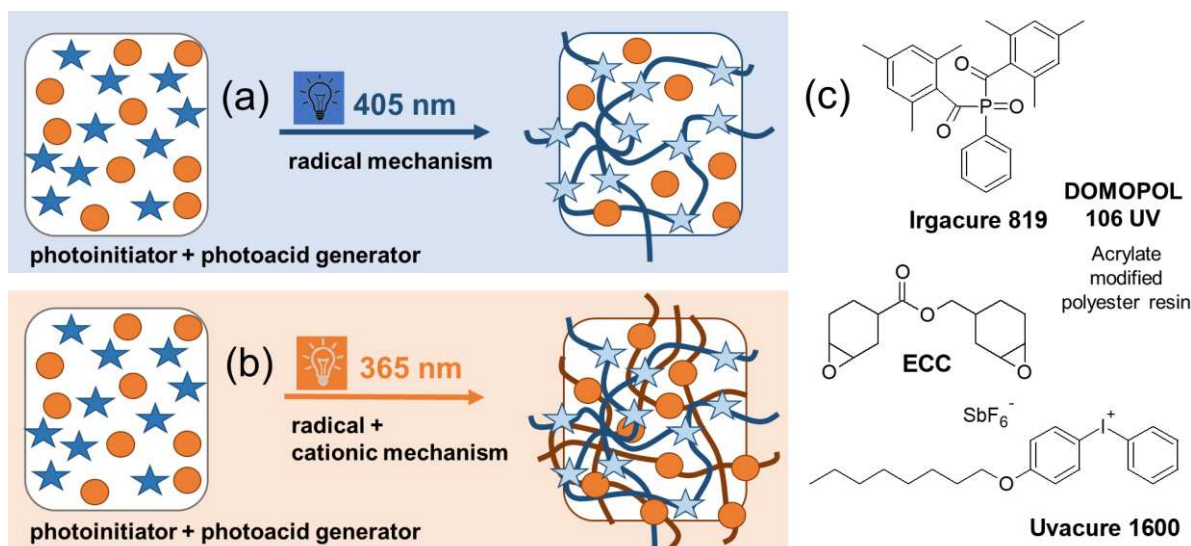


Figure 1. Schematic representation of the wavelength selective (a) radical induced curing of the acrylate upon exposure at visible (405 nm) light and (b) formation of a highly cross-linked interpenetrating photopolymer network formed by simultaneous curing of acrylate and epoxy monomers upon irradiation with UV light (365 nm). (c) Monomers and photoinitiators used for the hybrid acrylate-epoxy systems.

The resulting interpenetrating network was characterized by a significantly higher stiffness and multi-material objects with soft and stiff domains could be fabricated with one resin vat, simply by changing the light source during printing.^[51]

In such hybrid systems, miscibility of the monomers and polymerization kinetics govern phase separation and morphology of the photopolymer networks, which in turn directly affect thermal and mechanical properties of the printed objects.^[151,217] Thus, in a first step, we examined the effect of the resin composition on the orthogonality between the radical and cationic photoreaction by FT-IR studies. Hybrid resins, whose ratio between Domopol 106 UV and ECC varied from D25:E75 to D50:E50 and D75:E25 (w/w), were spin-cast on Si wafer. The related molar ratios amounted to 1:2, 1:6.3, 1:18.8 (mol/mol) giving rise to an excess of epoxy groups in all formulations. The conversion of the functional acrylate (C=C-H stretching band at 1620-1636 cm^{-1} and the C=C-H deformation band at 810 cm^{-1}) and epoxy groups (C-O band at 790 and 745 cm^{-1}) were then followed upon visible and UV light irradiation, respectively. Hybrid resins with an acrylate content of 50 wt% (dual resin-D50:E50, Figure 2b) and above (dual resin-D75:E25, Figure 2a) could be cured in a sequence dependent orthogonal manner. Here, visible light irradiation led to a distinctive conversion of the acrylate groups, whilst the intensity of the epoxy absorption bands remained unaffected. The curing of the acrylates further progressed upon UV exposure, as Irgacure 819 is also strongly absorbing in the UV region and unreacted photoinitiator molecules were activated under these irradiation conditions. At the same time, the cationic photoinitiator was electronically excited and initiated the cationic ring opening of ECC. A light-induced conversion of the epoxy monomers was observed, albeit at much lower rate, as cationic ring opening reactions are typically slower than radical-mediated curing reactions.^[51]

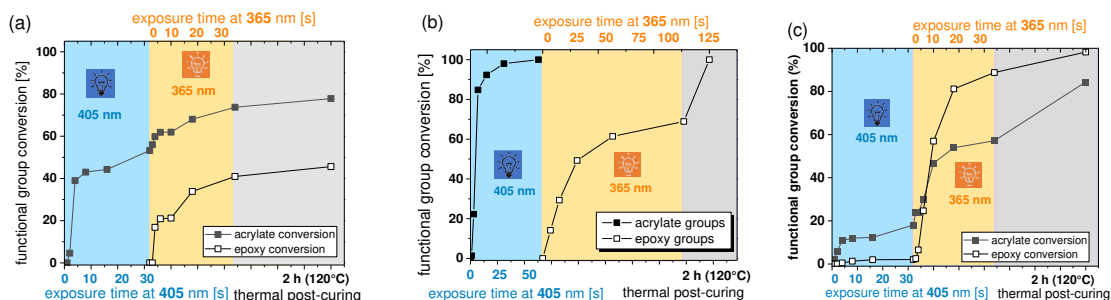


Figure 2. Monitoring the wavelength dependent cure kinetics of (a) dual resin-D75:E25, (b) dual resin-D50:E50 (replotted from Ref ^[51]) and (c) dual resin-D25:E75.

However, in dual resin-D25:E75 comprising an excess of epoxy monomers and a higher amount of the cationic photoinitiator (the weight of the photoinitiator was calculated related to the weight of the respective monomer), the sequence dependent orthogonality between the two reactions was lost (**Figure 2c**) and a slight decrease of the epoxy band ($\sim 2\%$) was already observed upon visible light exposure. To ensure fast cationic curing, which is required for DLP 3D printing with decent build speed, we used a diphenyl iodonium salt as cationic photoinitiator. This family of photoinitiators has a high reduction potential and can be sensitized via the oxidation of free radicals (available in the current system by the visible light induced homolytic cleavage of Irgacure 819) and promote radical induced cationic polymerization.^[218] Whilst the visible light induced conversion of the epoxy groups seems negligible, it should be considered that the samples were thermally post-baked to increase the epoxy conversion by exploiting the living nature of the cationic species. Since both visible and UV cured domains are thermally treated during the post-baking of a multi-material 3D printed structure, the FTIR data suggest that the change in material properties will be less pronounced when using dual resin-D25:E75.

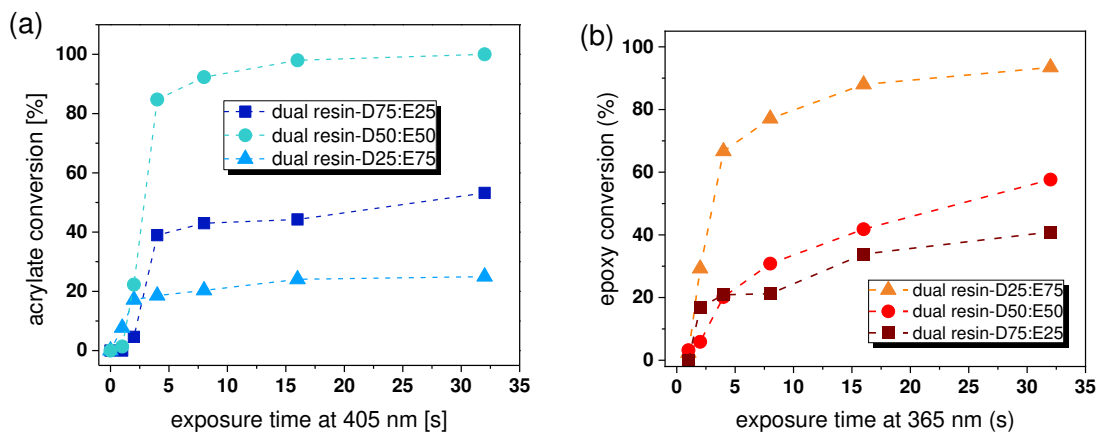


Figure 3. Real-time conversion of hybrid acrylate-epoxy resins with different weight percentage of monomers as obtained from FT-IR spectroscopy: (a) visible light induced conversion of acrylate groups (1627 cm^{-1}) and (b) UV induced conversion of epoxy groups (790 cm^{-1}). The lines are a guide for the eye.

Comparing the cure kinetics of the epoxy groups (Figure 3b) in the three resins under investigation, it is obvious that cure rate and final monomer conversion increase with decreasing amount of Domopol UV 106 in the resin. This trend was also reported by Calvez and co-workers and is related to the higher viscosity of the polyester acrylate (2.31 Pas), which limits diffusion of the reactive groups.^[219] After post-baking full conversion of the epoxy groups was observed for dual resin-

D50:E50 and D25:E75 due to the dark reactions of the cationic species. In terms of dual resin-D75:E25, the high diffusion limitations of the acrylate could not be overcome by the thermal treatment and the epoxy conversion only slightly increased from 41 to 46% after 2 h at 120 °C.

For the acrylate conversion, the dilution with the low viscous ECC (0.4 Pas)^[220] is beneficial as a reduced viscosity facilitates the polymerization rate in free-radical polymerization reactions. The literature on relation between resin viscosity and polymerization rate shows that highly reactive formulations are often obtained by mixing highly viscous monomers with lower ones at specific molar ratios.^[221] In particular, it can be seen that the cure rate of the acrylate groups is the highest in dual resin-D50:E50, reaching full conversion after 30 seconds of visible light irradiation. In contrast in dual resin-D75:E25, a 53% conversion of the acrylate groups is obtained under the same conditions. This can be explained by the higher viscosity of dual resin-D75:E25 (1.1 Pas) compared to dual resin-D50:E50 (0.39 Pas). At higher viscosity values, the propagation step becomes diffusion-limited resulting in decreased polymerization rate.

Interestingly, dual resin-25:75 having the lowest viscosity (0.14 Pas) showed only 18% acrylate conversion upon 30 s visible light exposure. In this case, the high dilution of the resin with epoxy monomers start to negatively affect the diffusion of low number of acrylates in the resin and slows down the cure kinetics. This dilution effect is well studied in literature and was reported for various simultaneously and also sequentially cured epoxy acrylate resin formulations. Herein, this effect might be more pronounced as along with the dilution of the acrylate monomer also the radical photoinitiator becomes more diluted (as its concentration was kept constant in relation to the acrylate content).^[222,223]

Along with FTIR spectroscopy, photo-differential scanning calorimetry (DSC) was performed to investigate the photo-polymerization process of dual curable resins at different wavelengths (Figure 4). Here, the enthalpy of the curing of both monomers was monitored to evaluate the orthogonality and the cure behavior under visible (400-500 nm) and UV light (365 nm). The peak at 5.08 min is related to the radical curing of the acrylates whilst the cationic curing of the epoxy groups is observed at 5.9 min. The results show that the orthogonality of the two reactions is lost at a higher content of epoxy monomers. Upon visible light exposure, no heat release related to the cationic curing of ECC was detected in dual resin-D75:E25. Under the same irradiation conditions, dual resin-D50:E50 and D25:E75 exhibited a distinctive peak at 5.9 min and the related enthalpies amounted to 6.6 and 74.8 J/g, respectively. In contrast to the FTIR experiments, a conversion of

epoxy groups can be also detected in dual resin-D50:E50, which we assume is due to the higher sensitivity of photo-DSC and the longer irradiation time.

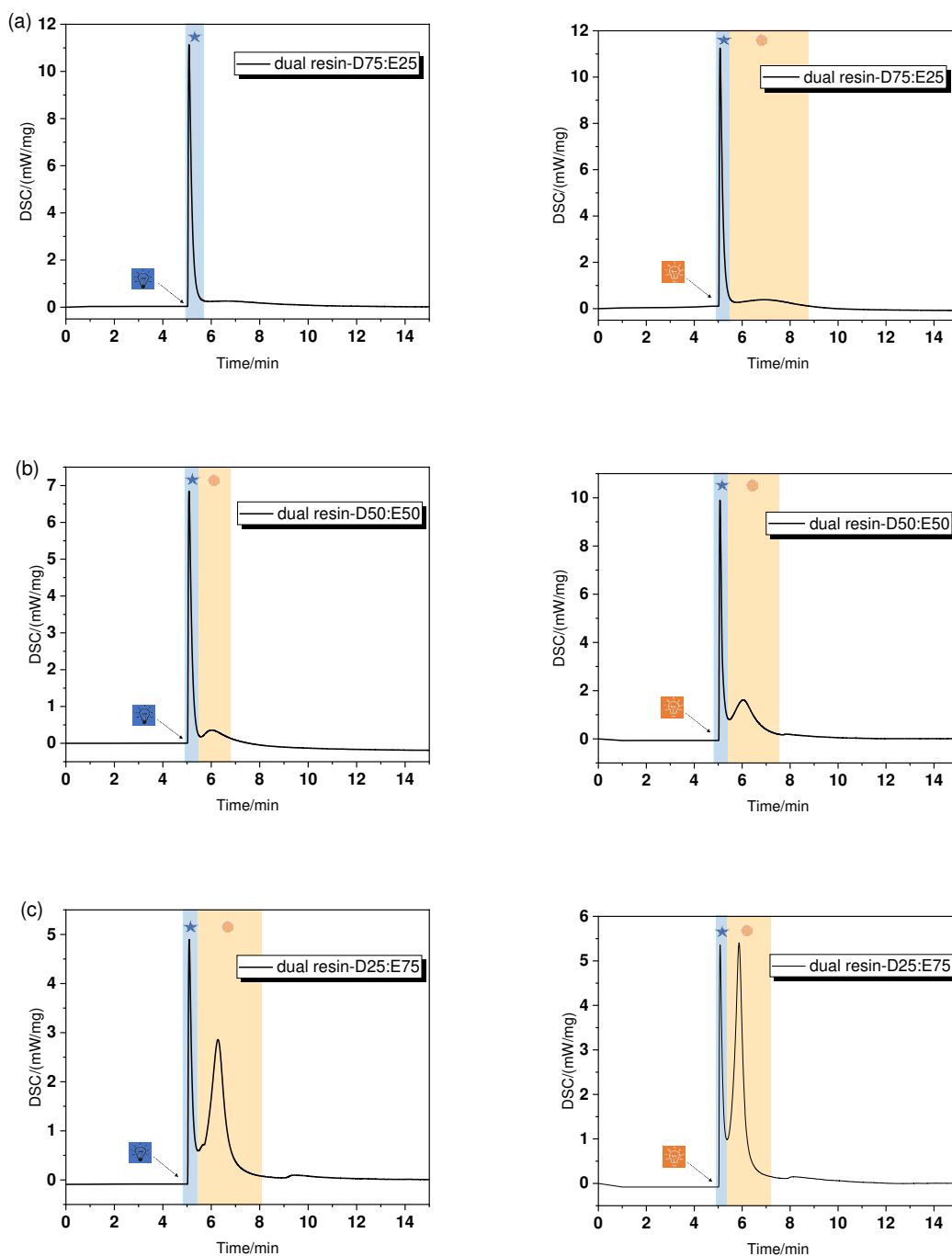


Figure 4. Photo-differential scanning calorimetry (DSC) curves obtained at 25 °C with 400-500 nm (left) and 365 nm (right) irradiation of (a) dual resin-D75:E25, (b) dual resin-D50:E50 and (c) dual resin-D25:E75.

In further experiments, the light-dependent change in the gel fraction and cross-link density (Table 1) were studied on DLP 3D printed samples by carrying out equilibrium swelling measurements. All 3D printed samples were additionally post-baked at 120 °C for 2 h to mimic the conditions of the multi-material domains in dual-wavelength DLP 3D printed structures. Dual resin-D50:E50 showed the highest gel fraction upon exposure at 405 nm, which is in good agreement with the higher acrylate conversion observed in the FTIR kinetics studies. Whilst the final acrylate conversion of dual resin-D25:E75 (irradiated with 405 nm) is significantly lower than the one observed in dual resin-D50:E50, its gel content is only slightly lower (75.2 versus 73.4%). This can be explained by the additional curing of the epoxy monomers and the loss in orthogonality as evidenced by photo-DSC measurements (Figure 4c). Upon exposure at 365 nm, the simultaneous formation of the acrylate and epoxy network resulted in a distinctive increase in the gel fraction which ranged between 81 and 87%.

The cross-link density (ν) obtained from Flory Rehner calculations follows the same trend, albeit the additional cross-linking of the epoxy monomer has a greater effect on the values as it yields a tighter network compared to the acrylate photopolymer. The increase is most visible for dual resin-D25:E75 having the highest amount of epoxy monomers and is in good agreement with the stiffer network properties observed in thermo-mechanical and mechanical tests (section 2.3).

Table 1. Gel fraction and cross-link density (ν) of DLP 3D printed hybrid acrylate-epoxy resins as a function of the applied wavelength.

Formulation	Gel fraction (%)	Gel fraction (%)	Cross-link density (mmol/cm ³)	Cross-link density (mmol/cm ³)
	irradiation with 405 nm	irradiation with 365 nm	irradiated with 405 nm	irradiated with 365 nm
dual resin-D75:E25	68.1 ± 0.8	82.6 ± 0.4	0.78 ± 0.02	2.35 ± 0.13
dual resin-D50:E50	75.2 ± 1.9	81.9 ± 1.5	0.89 ± 0.04	2.21 ± 1.05
dual resin-D25:E75	73.4 ± 2.1	87.1 ± 1.9	1.75 ± 0.63	8.37 ± 1.28

5.3.2 Photopolymer morphology

Considering the orthogonal nature and incompatibilities of the hybrid acrylate-epoxy resins under investigation, photopolymers with varying morphologies (phase separated versus homogenous interpenetrating network) are expected to be formed under the applied curing conditions.^[149,151,153,224] To investigate the effect of different monomer ratios and light sources (405 and 365 nm) on the polymer morphology, the surface of the cured networks (spin-cast on Si wafer)

was studied by atomic force microscopy (AFM). The experiments were carried out in tapping mode with a default oscillation of the cantilever tip to detect different local stiffnesses of phase-separated domains. When the tip approaches the polymer, either attractive or repulsive interaction between the tip and sample occurs. Attractive interaction leads to a positive phase shift and repulsive interaction to a negative phase shift.^[149,153] Typically, softer materials will tend to cause a positive shift and harder materials a negative shift. However, this can be changed by the used scan parameters. Figure 5b provides the phase image and its distribution for photocured dual resin-D50:E50. Significantly different morphologies were observed by altering the light source from visible to UV light. Irradiation at 405 nm led to the formation of a fibril-like surface morphology with uncured soft epoxy monomers (red) distributed within the stiffer cured acrylate (blue) domains.

Along with the AFM micrograph, the phase distribution plot is presented which shows the number of pixels for a specific phase lag degree and with the distribution of peaks giving information about different phases in the network. In visible light cured dual resin-D50:E50, two peaks with a maximum at -26° and -5.3° are observed giving rise to a separated network morphology. In contrast, UV irradiation of the same formulation yielded an interpenetrating network, due to the simultaneous curing of the acrylate and epoxy monomers. In the phase distribution, the phase lag degree is shifted to higher negative values due to the additional formation of the epoxy-based network. One broad peak with two maxima at -60.5° and -51.3° was observed. We assume that the two maxima are related to an acrylate- and an epoxy-rich phase distributed with the formed network, which can be also seen in the related AFM micrograph.

An excess of acrylate monomers (dual resin-D75:E25) facilitated a completely different morphology (Figure 5a). The phase distribution plot of the visible light irradiated sample shows one peak, which is shifted to significantly higher positive values indicating a homogenous, soft photopolymer network. As seen in the related phase image, the film morphology is comprised of evenly distributed domains, which are associated with unreacted acrylate and epoxy monomers distributed within the partly cured acrylate network. It seems that the unreacted acrylates prevent a phase separation of the unreacted ECC monomers and promote a higher homogeneity. In contrast, the UV irradiated dual resin-D75:E25 photopolymers exhibit phase separation, albeit at a lower extend than dual resin-D50:E50 under the same conditions. Due to the higher acrylate content, the

film morphology is dominated by softer (acrylate rich) areas whilst the number of stiffer (epoxy rich) domains is significantly lower.

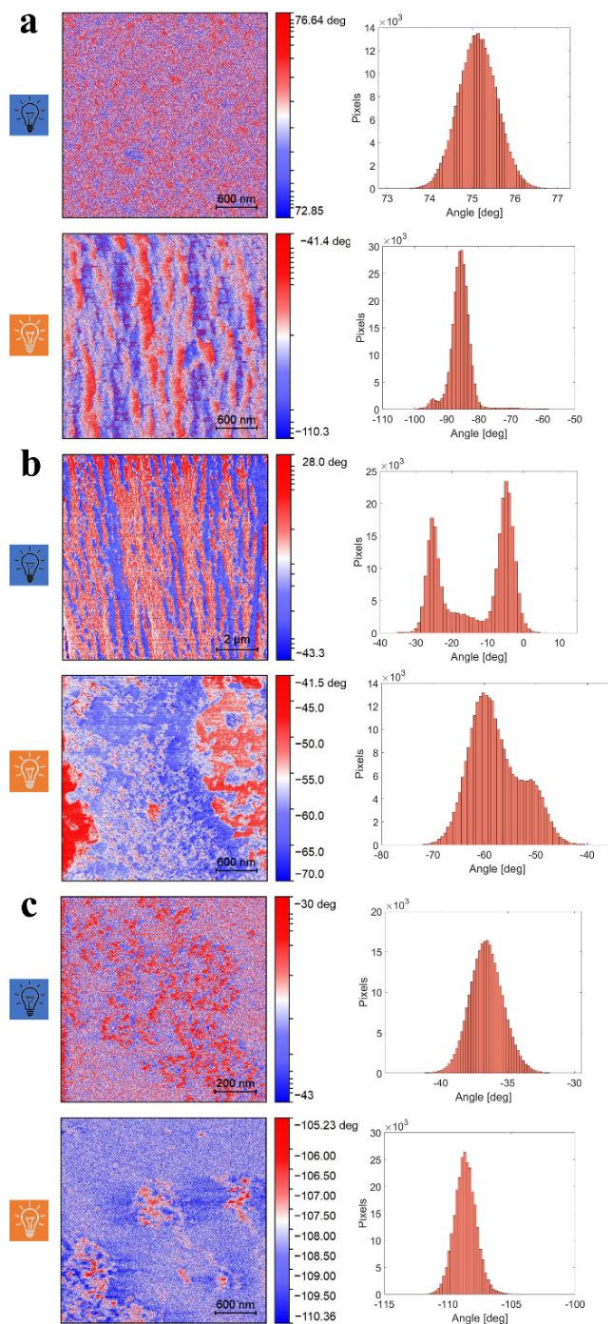


Figure 5. AFM phase images and distributions of (a) dual resin-D75:E25, (b) dual resin-D50:E50, and (c) dual resin D25:E75 illuminated with 405 nm (top) and 365 nm (bottom) light.

An excess of epoxy monomers (dual resin-D25:E75) gives a homogenous network, independent on the applied light source (Figure 5c). Upon visible light irradiation, it seems that the epoxy monomers remain evenly distributed over the film's surface due to the low cure rate of the acrylates

(Figure 4a) in this formulation. Switching to UV light, both monomers cure under the formation of a homogeneous interpenetrating network which is related to a distinctive shift of the phase angle to higher negative values.

5.3.3 Thermomechanical and mechanical properties

The wavelength selective changes in film morphology at varying monomer ratios directly affected the (thermo)mechanical properties of dual-wavelength 3D printed test structures as shown by DMA data (Figure 6). Printing was carried out either at 405 nm or 365 nm, whilst all test specimens were post-baked for 2 hours at 120 °C. Printing at 405 nm yielded networks, whose tan delta peak maximum (i.e. Tg) shifted to higher temperatures at rising ECC concentration. The glass transition of dual resin-D50:E50 and D25:E75 ranged between the Tg of the single acrylate (19 °C) and ECC network (170 °C), which indicates a loss in the orthogonality between the two photoreactions. In dual resin-D75:E25 and D50:E50, an additional maximum at around -50 °C was observed in the tan delta curve, which is related to the melting of unreacted resin components. In addition, all three resins exhibited a distinctive post-curing peak with a maximum at 190 °C together with a significant increase in storage modulus (E'), giving rise to the temperature triggered cationic curing of ECC in the absence of UV exposure. Dual resin-D75:E25 comprised a slightly lower Tg (14 °C) than the pure acrylate network, which is due to the presence of the unreacted epoxy monomers in the system acting as lubricant. This is also evidenced by the lower E' (Table 2) of the network. In contrast, Tg and E' of dual resin-D50:E50 were shifted to higher values compared to the single acrylate networks. This is explained by an additional curing of the epoxide monomers, albeit at a low extend, as shown by photo-DSC experiments.

In dual resin-25:75, a visible light induced conversion of the epoxy groups was already observed in the FTIR spectra (Figure 2c) and a significant curing enthalpy was observed in photo-DSC measurements. The higher ECC conversion facilitated a stronger shift of the Tg (107 °C) and the formation of a second peak maximum at 165 °C, which we assume is the Tg of the epoxy-rich phase observed in the AFM micrographs. The peak is partly overlapping with the post-curing of the epoxy monomer, which is clearly visible in the respective E' curve (Figure 6b) and far more pronounced than in the other two resins under investigation. Moreover, the additional network formation directly affected the width of the loss factor curves (full width at half maximum, FWHM), which gives an indication on the networks' homogeneity. In particular, the FWHM

increased from 70 to around 200 °C by rising the ECC content from 25 to 75 wt% due to the additional curing of the epoxy monomer.

Table 2. Mechanical and thermo-mechanical properties of single and hybrid acrylate-epoxy resins as a function of the applied wavelength used in the dual-wavelength DLP 3D printing process. All samples were post-baked at 120 °C for 2 h.

Formulation	Irradiation	T _g [°C]	E' at 23 °C [MPa]	σ [MPa]	ε [%]
single Domopol UV 106	405 nm	19	54	1.5 ± 0.2	12.0 ± 1.4 ^a
dual resin-D75:E25	405 nm	14	11	0.9 ± 0.1	11.9 ± 1.3
dual resin-D75:E25	365 nm	24	90	1.4 ± 0.2	11.9 ± 1.5
dual resin-D50:E50	405 nm	32	177	1.0 ± 0.11	24.0 ± 0.9 ^a
dual resin-D50:E50	365 nm	74	1571	39.1 ± 3.0	3.8 ± 0.4 ^a
dual resin-D25:E75	405 nm	107	2020	19.3 ± 2.3	4.0 ± 1.5
dual resin-D25:E75	365 nm	137	2259	48.3 ± 5.2	2.3 ± 0.8
single ECC	365 nm	170 ^b	not determined		

taken from: ^a ref [51], ^b ref [143]

The strong contribution of the cationic curing of ECC on thermomechanical properties was confirmed by carrying out the printing experiments at 365 nm (Figure 6c). The simultaneous formation of an acrylate and epoxy network led to stiffer materials with significantly higher T_g compared to the counterparts illuminated at 405 nm (Table 2).

In all three resin formulations, only one tan delta maximum was observed giving rise to a higher conversion of the monomers. However, post-curing of ECC was still observable in the related E' curves (Figure 6d) indicating an incomplete conversion of the epoxy monomers during printing at 365 nm and subsequent post-baking. Summing up, the wavelength selective formation of the photopolymers can be used to significantly alter stiffness and T_g of the printed structures. Whilst dual resin-D50:E50 is not fully orthogonal, the relative shift in thermomechanical properties between 405 and 365 nm was the highest for this network, which also underwent the most distinctive changes in film morphology as seen in AFM studies (Figure 5b). Here it should be noted that the values for the storage modulus at 23 °C of dual resin-50:50 are different compared to our previously published study^[51], as small shifts in the T_g, which is around room temperature, have a strong influence on the E' values.

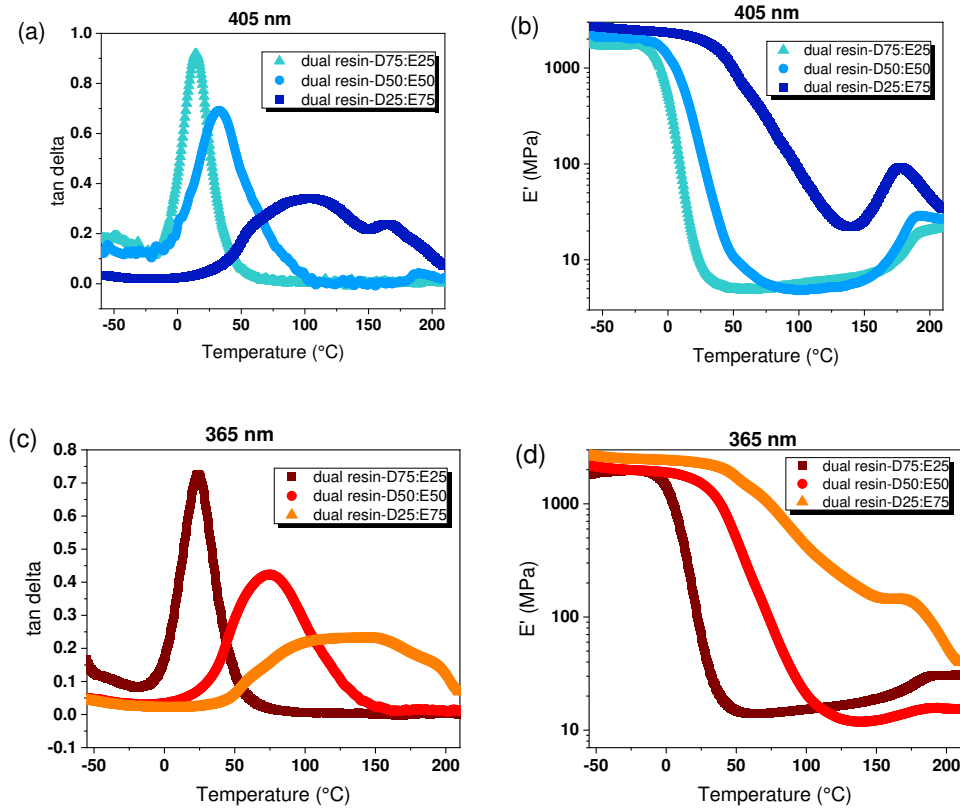


Figure 6. (a, c) Loss factor ($\tan \delta$) and (b, d) storage modulus (E') versus temperature as obtained from DMA measurements of hybrid acrylate-epoxy resins. Test specimens were fabricated by dual-wavelength DLP printing using a layer exposure time of 1 s at 405 nm and 4 s at 365 nm, except dual resin-D25:E75 where the layer exposure time at 405 nm and 365 nm was 4 s. All samples underwent thermal post-baking at 120 °C for 2 h.

As shown in uniaxial tensile tests, dual resin-D50:E50 also exhibited the largest wavelength induced change in tensile properties (Figure 7). In particular, the tensile strength (σ) increased from 1 to 39 MPa, whilst the ultimate elongation (ϵ) decreased from 24.0 to 3.8%. In contrast, the tensile properties of dual resin-75:25 are mainly dominated by the acrylate component and show a negligible change in ϵ and σ depending on the employed light source. Adding a higher amount of ECC to the resin (dual resin-D25:E75) is beneficial for the tensile strength, which amounted to 19.3 and 48.3 MPa at 405 and 365 nm light exposure, respectively. This is not surprising as ring opening reactions typically give tougher networks than free radical cured acrylates, which often suffer from shrinkage stress.^[102] Along with a higher tensile strength, dual resin-D25:E75 comprises a higher stiffness, which is in good agreement with the DMA data, and the network exhibits a lower ultimate elongation than dual resin-D75:E25 and D50:E50. However, the results

also confirm the lack in orthogonality between the two photoreactions as the tensile strength of the visible light cured network is significantly higher (19.3 MPa) than the pure Domopol UV 106 (1.5 MPa), whilst the ultimate elongation is lower (12 versus 4.0%). Thus, the wavelength dependent switch in mechanical properties is less pronounced as observed for dual resin-D50:E50.

Moreover, we tested the interlayer adhesion between soft and stiff domains between different monomer ratios in 3D-printed structures. For this, heterogeneous dumbbell shaped test specimens were printed, in which one-half of the sample was printed at 405 nm and the other half at 365 nm. The heterogeneous printed dumbbell shaped test specimens showed good interlayer adhesion and were predominately breaking in the middle of the softer domain. The high adhesion was already observed in our previous study^[51] and is mainly related to the diffusion of photo-released acid which initiates curing of epoxy monomers across the interface to the soft domains.

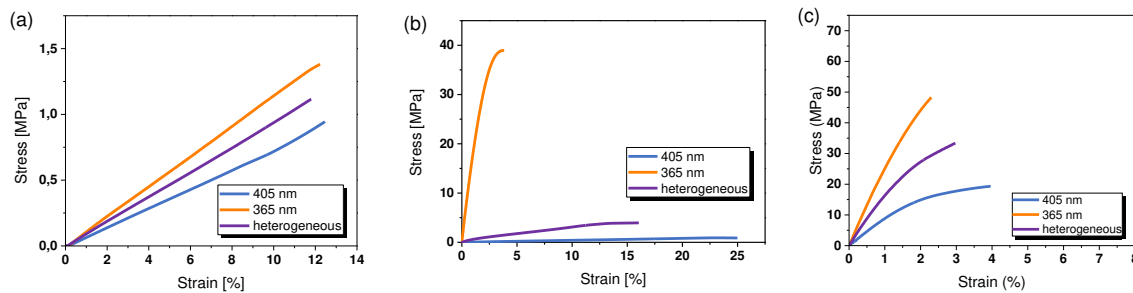


Figure 7. Stress strain curves for dual-wavelength 3D printed (a) dual resin-D75:E25, (b) dual resin-D50:E50 (replotted from Ref ^[51]) and (c) dual resin-D25:E75 obtained under different irradiation conditions (405 and 365 nm). Heterogenous samples were prepared by printing one-half of the sample at 405 nm and the other half at 365 nm.

5.3.4 Additive manufacturing

For dual resin-D50:E50 and D75:E25, the test specimens were printed with a layer thickness of 100 μm and with a cure time of 1 s (405 nm) and 4 s (365 nm), respectively. Due to the slow cure kinetics of dual resin D25:E75, a longer printing time (4 s) with visible light (405 nm) was required whilst the irradiation at 365 nm was kept at 4 s. The intensity of both light sources was 8 mW/cm^2 . The resolution of the 3D printed specimens using the dual-curable resins under investigation was in the millimeter range (Figure 8). In all samples, a decrease in the resolution was observed when the printing was carried out at 365 nm, which is mainly related to dark polymerization of the epoxy monomer ECC. Thus, this effect become more pronounced at higher ECC content and the best replication of the CAD data was observed for visible light cured dual resin-D75:E25.

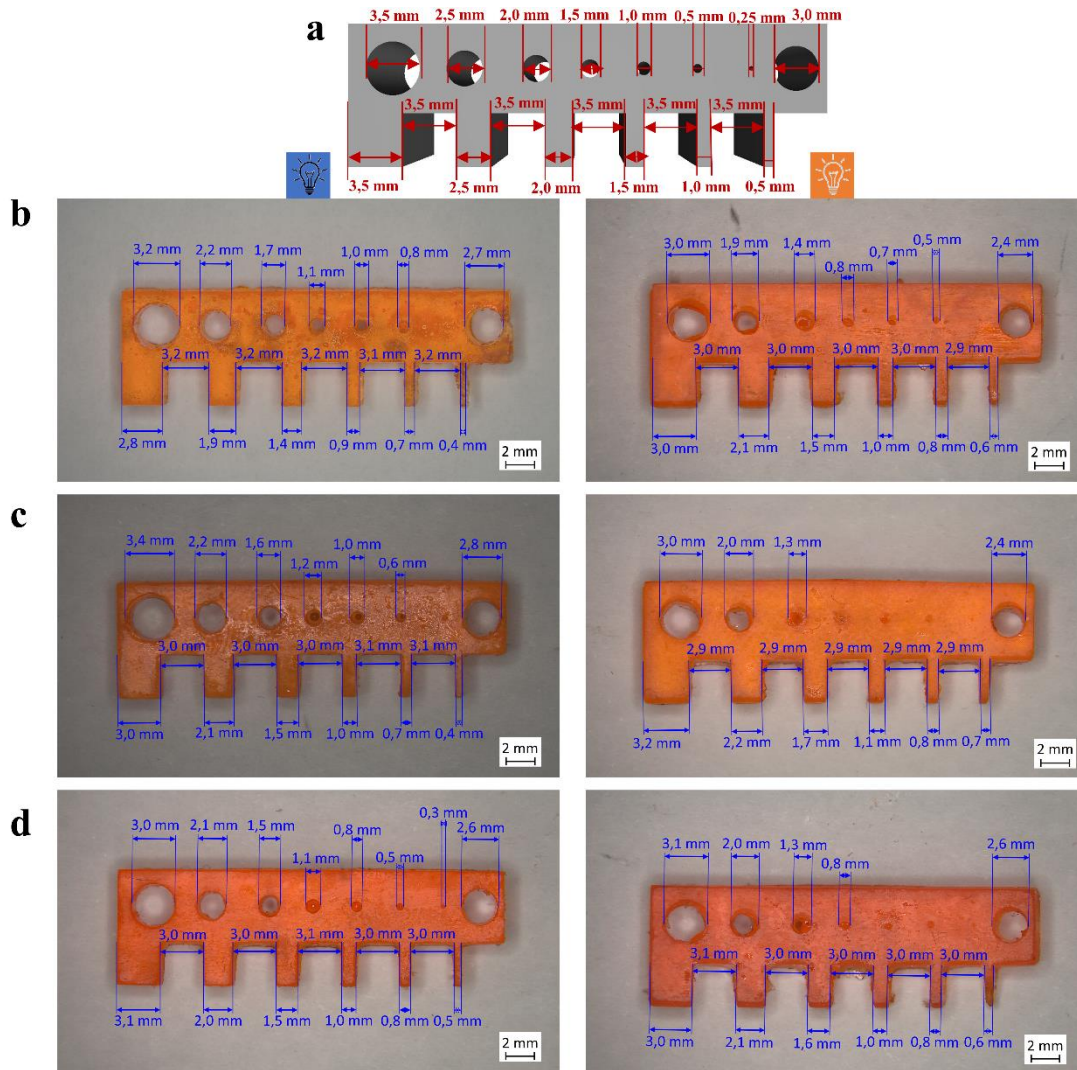


Figure 8. (a) CAD data of a comb-like test structure and related DLP 3D printed objects using (b) dual resin-D75:E25, (c) dual resin-D50:E50 and (d) dual resin-D25:E75. Printing was carried out either with 405 nm (left) or 365 nm (right).

5.4 Conclusion

Having resins in varying stages of cure is a common concept in DLP 3D printing to realize multi-material structures by using either different irradiation intensities or wavelengths during printing. Herein, the crucial influence of resin composition and light source on the microscopic film morphology and macroscopic thermomechanical and mechanical properties of dual-wavelength DLP 3D printed objects has been studied in detail. Using hybrid acrylate-epoxy resins with varying monomer ratios, it has been shown that the cure rate of epoxy monomers increases with rising epoxy concentration. In contrast, the cure kinetics of the acrylate groups is more complex and

reaches a maximum in dual resin-D50:E50, whilst diffusion limitations and the dilution effect negatively affect the cure kinetics at higher or lower concentrations, respectively. However, at the same time a higher epoxy content compromised on the orthogonality between the two photoreactions and cationic curing started already upon visible light exposure. This is mainly related to the high amount of photoacid generator (whose weight was calculated according to the weight of ECC) which has a high reduction potential and is able to be sensitized via oxidation of free radicals from Irgacure 819. The phase distribution images obtained by atomic force microscopy did show significant differences in the film morphology as a function of resin composition and applied wavelength. Depending on the cure degree and presence of uncured monomer, heterogeneous networks with distinctive phase separation (visible light cured dual resin-D50:E50) as well as interpenetrating networks with a homogenous morphology were obtained. The UV induced formation of the epoxy network significantly affected mechanical and thermomechanical properties. With rising ECC content, T_g and E' shifted to higher values. This trend has already been observed in visible light cured films as part of the epoxy monomers started to react under the applied conditions (in dual resin-D50:E50 and D25:E75). The higher stiffness was also observed in uniaxial tensile tests, which revealed an increase in tensile strength and a decrease in ultimate elongation with increasing ECC concentration and by switching the light source from 405 to 365 nm. The most pronounced wavelength dependent difference in mechanical properties could be obtained with dual resin-D50:E50. At a higher acrylate content, the performance was mainly influenced by the acrylate component and the change in the performance was negligible. At a higher epoxide content, a change in the (thermo)mechanical properties was observed, albeit at a lower extent than in dual resin-D50:E50, due to the loss in the orthogonality between the two photoreactions. For technical applications, it should be noted that unreacted monomers might migrate and can affect the long-term performance of 3D printed multi-material structures, particularly at higher temperature (e.g. due to post-polymerization reactions). At room temperature, the multi-material domains of DLP 3D printed structures, which have been investigated in the current study, remained stable at least for 2 months (the materials properties were not monitored over a longer period of time).

5.5 Experimental part

5.5.1 Materials and chemicals

Acrylate modified polyester resin (Domopol 106 UV) with a molecular weight of 1,540 g/mol contained an average number of 5 functional acrylate groups per molecule and was kindly provided by Helios TBLUS d.o.o. (Ljubljana, Slovenia). The epoxy monomer 3,4-epoxycyclohexylmethyl-3,4-epoxycyclohexanecarboxylate (ECC) and the cationic initiator *p*-(octyloxyphenyl) phenyl iodonium hexafluoroantimonate (Uvacure 1600) were purchased from ABCR (Karlsruhe, Germany). The radical photoinitiator phenylbis(2,4,6-trimethylbenzoyl) phosphine oxide (Irgacure 819) was supplied by Sigma Aldrich (St. Lois, US). Sudan II was obtained from TCI chemicals (Tokyo, Japan). All chemicals were used without further purification.

5.5.2 Preparation of photocurable resin

Photocurable dual resins were prepared with DOM:ECC ratios of 75:25, 50:50 and 25:75 (w/w), which relate to molar ratios of 1:2, 1:6.3, 1:18.8 (mol/mol). The concentration of the radical (Irgacure 819) and cationic photoinitiator (Uvacure 1600) for each formulation was calculated according to the weight of the monomer in the investigated formulation. Finally, 0.01 wt% of Sudan II as a photo absorber were added and the formulations were stirred at room temperature until all components were dissolved. Light absorbers regulate light absorption and control the penetration depth of incident light which helps to increase the resolution in z-direction.^[225] The compositions of the resin formulations together with optimized printing parameters (layer thickness of 100 μm) are summarized in Table 3.

Table 3. Composition and printing parameters of dual curable resins under investigation.

Formulation	Domopol UV 106 [wt%]	ECC [wt%]	Irgacure 819 [wt% ^a]	Uvacure 1600 [wt% ^b]	Sudan II [wt%]	Exposure	Exposure
						time [s] at 405 nm	time [s] at 365 nm
dual resin-D75:E25	75	25	3	10	0.01	1	4
dual resin-D50:E50	50	50	3	10	0.01	1	4
dual resin-D25:E75	25	75	3	10	0.01	4	4

^a related to the Domopol UV 106 content, ^b related to the ECC content

5.5.3 Characterization of cure kinetics and viscosity measurements

Light-induced curing of dual resins was monitored by Fourier transform infrared spectroscopy (FTIR) on a PerkinElmer Spectrum One spectrometer (Massachusetts, US). Spectra were taken in transmittance mode over a wavenumber range of 4000 to 600 cm^{-1} . All spectra were accumulated from 16 scans at a resolution of 4 cm^{-1} . The conversion of the functional groups was calculated with OPUS software by evaluating the decrease of the characteristic acrylate IR absorption band at 1620-1636 cm^{-1} and the absorption bands of the epoxy moieties at 790 and 750 cm^{-1} . The degree of conversion (DC) of the curing reaction was calculated using the following equation, in which C_{Peak} corresponds to the absorption area of the observed band of the cured sample and $C_{\text{Reference}}$ to its reference peak. U_{Peak} and $U_{\text{Reference}}$ are the absorption area of the relevant band and reference peak of the uncured sample, respectively.

$$\text{DC}\% = \left[1 - \left(\frac{C_{\text{Peak}}/C_{\text{Reference}}}{U_{\text{Peak}}/U_{\text{Reference}}} \right) \right] \cdot 100$$

For sample preparation, 50 mg of the respective formulation was dissolved in 1 mL of dichloromethane and 40 μL of the prepared solution was spin-cast on a Si wafer (1.5 x 1.5 cm). Spin coating was carried out with a SpinCoater Model 4000 from Electronic Micro Systems Ltd. (Wiltshire, UK) using a speed of 3000 rpm for 60 seconds. Due to the low viscosity of the dual curing resin-D25:E75, the prepared formulation was directly coated on a Si wafer. Visible light irradiation was performed with a LED curing lamp (405 nm) at 8 mW/cm^2 and UV illumination with a Hg lamp (Omnicure Series 1000) at 8 mW/cm^2 . Experiments were carried out under nitrogen atmosphere to prevent oxygen inhibition of the acrylate curing. The light intensity was measured with an STS-UV Miniature Spectrometer (Ocean Insight).

The viscosity of the resins was determined by using a modular compact rheometer MCR 102 from Anton Paar (Austria) with a CP/PP 7 plate. Each measurement was carried out with 1 mL resin at room temperature and a shear rate of 300 s^{-1} .

5.5.4 Equilibrium swelling measurements

The gel fraction was measured by immersing DLP 3D printed samples (2 mm x 12 mm x 0.1 mm) in tetrahydrofuran (THF) at room temperature for 48 h. Printing was carried out as described in section 4.6 and the samples were post-baked at 120 $^{\circ}\text{C}$ for 2 h. After 48 h, the samples were removed from the solvent and the excess solvent was dried from the surface with tissue paper. The swollen samples were placed in the oven at 70 $^{\circ}\text{C}$ until constant weight was obtained (2 days). The

gel fraction was calculated by m_{dr}/m_{ini} , where m_{dr} represents the weight of the dried sample and m_{ini} is the weight of the initial sample. For each cured network, 3 samples were measured and the arithmetic average was taken.

The cross-link density was calculated using the Flory – Rehner equation;^[226]

$$\nu = \frac{\ln(1 - \phi) + \phi + \chi\phi}{V\left(\frac{\phi}{2} - \phi^{\frac{1}{3}}\right)}$$

where ν corresponds to the effective cross-link density in mmol/cm³, V presents the molar volume of tetrahydrofuran, χ presents the polymer-solvent interaction parameter for the epoxy network with tetrahydrofuran, while ϕ is the volume fraction of the epoxy resin. Considering that the χ value is larger than 0.5, χ was calculated from the following equation;^[226]

$$\chi = \frac{1}{2} + \frac{\phi}{3}$$

The volume fraction of the epoxy (ϕ) is given by

$$\phi \approx \left[1 + \left(\frac{W_{eq} - W_0}{W_0}\right) \left(\frac{\rho_2}{\rho_1}\right)\right]^{-1}$$

Here, W_0 and W_{eq} represent the weight of the weight of the epoxy resin before and after the swelling, while ρ_1 and ρ_2 are the mass density of tetrahydrofuran and the polymer network, respectively.

5.5.5 Photo-differential scanning calorimetry (DSC)

The photo-DSC setup consisted of a Netzsch Phoenix F1 machine and an Omnicure® S1500 light source. Intensity of both spectral regions (400-500 nm and 365 nm) was 8 mW/cm². Prior to each measurement, the DSC device was equilibrated at 25 °C for 5 min under a nitrogen atmosphere (50 mL/min flow rate).

5.5.6 Dual wavelength DLP 3D printing

Multi-material DLP 3D printing was performed on a dual-wavelength DLP prototype, which was manufactured by way2production (Austria). The DLP 3D printer operated with two light engines, which contained a 405 and 365 nm LED light source, respectively. Their intensity amounted to 8 mW/cm². The test specimens of dual resin-D75:E25 and dual resin-D50:E50 were printed with a layer thickness of 100 µm using an illumination time of 1 s for 405 nm and 4 s for 365 nm. The

test specimens of dual resin-D25:E75 required an illumination time of 4 s for 405 nm and 4 s for 365 nm. All printed specimens were post-baked at 120 °C for 2 h.

5.5.7 Characterization of thermomechanical and mechanical properties

Dynamic mechanical analysis (DMA) was carried out on a Mettler Toledo DMA/SDTA861e analyser. Mechanical loss factors ($\tan \delta$) and storage moduli (E') were monitored over a temperature range from -60 to 220 °C at a heating rate of 3 °C/min. The glass transition temperature (T_g) was determined by the temperature at the maximum of the loss factor. For sample preparation, test specimen (35 mm x 7 mm x 22 mm) were fabricated by dual-wavelength DLP 3D printing.

Mechanical properties were characterized by tensile tests on an Instron 5500 (Instron, DEU) Universal Tester, using a 100 N load cell and pneumatic foil grips. Dogbone-shaped rectangles samples (2 mm x 12 mm x 0.1 mm) were dual-wavelength DLP 3D printed according to ISO 527 type 5B. The test speed was 1 mm/min. Tensile testing was executed with digital image correlation using Mercury DIC System software version 2.8, a UI-3180CP-M-GL R2.1 camera, and a Componon-S 2.8/50 lens (Schneider Kreuznach, DEU). The gauge length of the extensometer was set at 10 mm. The average of at least 5 samples was taken for each series.

5.5.8 Atomic force microscopy

The AFM samples comprised a thickness of 0.2 mm and were printed with the dual-wavelength DLP 3D printer (see 4.6). The test specimens of dual resin-D75:E25 and dual resin-D50:E50 were printed using an illumination time of 1 s for 405 nm and 4 s for 365 nm. The test specimens printed with dual resin-D25:E75 required an illumination time of 4 s for 405 nm and 4 s for 365 nm. All printed specimens were post-baked at 120 °C for 2 h. The film morphology was examined using an AFM-IR VistaScope 75 (Anfatec Instruments AG, Oelsnitz/V., DE). A silicon tip with gold coating were used as a probe with force constants of 10–130 N/m, resonance frequencies of 204–497 kHz, and a typical radius of curvature <10 nm. The images were recorded with a resolution of 512 x 512 pixels. The AFM microscope was operated in photo-induced force mode (PiFM). The PiFM images were scanned at 1607 or 1578 cm^{-1} as some difference can be observed between the two phases at these wavelengths.

5.6 Acknowledgements

The research work was performed within the COMET-Module project “Chemitecture“ (project-no.: 21647048) at the Polymer Competence Center Leoben GmbH (PCCL, Austria) within the framework of the COMET-program of the Federal Ministry for Transport, Innovation and Technology and the Federal Ministry for Digital and Economic Affairs with contributions by Montanuniversitaet Leoben, Politecnico di Torino, Helios TBLUS and bto-epoxy. Funding is provided by the Austrian Government and the State Government of Styria. In addition, the authors thank Gerald Meier (PCCL) for performing the tensile tests and Siegfried Hasil (PCCL) for performing the photo-DSC measurements.

6 Publication III:

Synthesis of Bio-Based Polyester Resins for Vat Photopolymerization 3D Printing

Ines Cazin, Martin Ocepek , Janez Kecelj , Aleš Stanislav Stražar and Sandra Schlögl

Materials **2024**, *17* (8), 1890

DOI: 10.3390/ma17081890.

The presented manuscript in Section 5 was almost identically published in the above-mentioned paper.

Synthesis of Bio-Based Polyester Resins for Vat Photopolymerization 3D Printing

Ines Cazin^a, Martin Ocepek^b, Janez Kecelj^b, Aleš Stanislav Stražar^b and Sandra Schlögl^{1a*}

a. Polymer Competence Center Leoben GmbH, Sauraugasse 1, A-8700 Leoben, Austria

b. Helios Resins, Količevo 65, 1230 Domžale, Slovenia

6.1 Abstract

Driven by environmental considerations, the scientific community has directed great effort towards the synthesis of new materials derived from renewable resources. However, for photocurable resins, most commercially available building blocks still rely on petroleum-based precursors. Herein, we present a simple synthesis route for bio-based acrylate-modified polyester resins, whose viscosity is sufficiently low for processing them with vat photopolymerization 3D printing. The established synthesis route enables the gradual substitution of fossil-based raw materials with bio-based alternatives. The acid number, color and viscosity of the bio-based acrylic resins are characterized and photocurable formulations are prepared by adding a radical photoinitiator. The photopolymerization kinetics, and thermomechanical and mechanical properties of the photopolymers are investigated as a function of the resin structure and benchmarked against a commercially available petroleum-based counterpart. Finally, the processability of the new bio-based resins via digital light processing 3D printing is demonstrated and test specimens are successfully 3D printed with a resolution in the millimeter range.

Keywords: additive manufacturing; vat photopolymerization 3D printing; bio-based polymers; photocuring; polyester resins

6.2 Introduction

Additive manufacturing (AM), or three-dimensional (3D) printing, is a technique that offers design freedom of 3D objects with high complexity and diverse properties.^[61] Virtually designed 3D models can be built up into an object by using different processes of AM, such as extrusion, direct energy deposition, powder solidification, sheet lamination, and photopolymerization.^[227] The interest for AM is steadily growing, and by the end of 2029 the worldwide revenues for materials

produced by AM techniques are forecast to grow to \$23 billion in the market shares of automotive, defense, aerospace, medical and dental industries.^[228] Polymers take the largest fraction of those produced materials.^[229] Conventional microfabrication techniques such as replication methods, photolithography and subtractive processes are typical time-consuming operating procedures, which require tedious assembly and bonding for making multi-layered three-dimensional objects. In contrast, 3D-printing is based on a layer-by-layer approach that creates an object directly converted from computer-aided-design to hardware. Complex 3D objects are printed without any need for bonding or alignment during the printing process.^[81,230] Among the several polymeric AM-methods, digital light processing (DLP) 3D printing has attracted significant attention over the past decade, due to the possibility of producing complex shaped objects and its high flexibility.^[231] As an optical 3D printing technology, DLP is based on a light beam, which is focused on the bottom surface of a vat filled with a photocurable resin. Due to a local solidification, the desired geometry is built up layer-by-layer.^[232] With the DLP process, it is possible to reach a precision of tens of micrometers in x-, y-, and z-direction, and to print objects with high surface quality.^[233,234] Despite the high precision that can be achieved, due to the limited size of the projection, only small-sized objects can be printed, which limits the applications in some fields.^[235] Moreover, the technique requires a photoreactive component which limits the choice of material, while the viscosity of the resin should be in the range of 0.25 to 5 Pa·s. A fast curing speed is important to ensure a quick build speed of the object. In addition, a slow curing speed can cause printing defects such as warping, sagging, or layer misalignment.

Based on the previously described advantages, it is not surprising that applications for DLP 3D-printed objects continue to grow rapidly and range from soft robotics, sensors, and wearable electronics to biomimetic devices.^[236,237]

For DLP 3D printing, photocurable resins are required, which typically contain (meth)acrylate or multifunctional epoxy monomers/oligomers. Local solidification of the resin is obtained by light triggered polymerization and curing reactions. (Meth)acrylate resins are cured via a radical chain-growth polymerization, whilst epoxy resins are polymerized in a step-growth manner following a cationic mechanism.^[102] However, the majority of commercial photocurable resins are derived from non-renewable building blocks.^[238] Implementing bio-resins for DLP 3D printing brings many ecological and economic benefits, such as high biodegradability and low toxicity, multiple recycling options and reduction of greenhouse gas emissions.^[239]

Thus, in the last few years, great effort has been devoted to the development of 3D printable resins that are replacing petroleum-derived precursors with materials derived from renewable resources.^[228] Some reported renewable building blocks include lignin, rosin and various carbohydrates.^[240–242] The most accessible and non-expensive choice is plant oils (e.g. soybean, castor and linseed oil), which can be easily converted into UV-curable oligomers across their triglyceride structure.^[243–246] One of the most promising derivatives from this category is castor oil, which has been used in the synthesis of UV-curable polyurethanes. The natural hydroxyl groups of castor oil undergo polyaddition with isocyanates resulting in the formation of hard segments that yield polymers with excellent mechanical strength, while superior flexibility is achieved by the long flexible fatty acid structures of castor oil.^[247–249] However, the long aliphatic chain of plant based oils compromise on material properties, and polymers often suffer from low glass transition temperature (T_g), which limits their technical applications. Terpene monomers are another reported renewable source, which can be cured by light-induced thiol-ene chemistry^[250]. However, the printed photopolymers also suffered from a low T_g .^[251]

Recently, research on bio-based unsaturated polyester resins (UPRs) has become popular due to low cost, simple curing process, good balance of durability and mechanical properties.^[252,253] UPR resins generally consist of unsaturated polyester (UP) and a free-radical polymerizable diluent such as styrene. Several studies describe the decrease and replacement of styrene by reactive diluents derived from less toxic and/or bio-based materials.^[254,255] UPs are typically obtained by the polycondensation of diols and unsaturated dicarboxylic acids or anhydrides, which can be taken from renewable feedstocks.^[256] Prominent bio-based feedstock for UPR include acids such as sebacic acid, succinic acid, adipic acid, gluconic acid, itaconic acid or levulinic acid, and glycols (1,3-propanediol, isosorbide, 1,4-butanediol, sorbitol, ethylene glycol, etc.).^[257–262]

Whilst bio-based polymers often suffer from poor mechanical properties^[263], several publications reported on UPRs derived from itaconic acid that benefit from both a high bio-based content and improved mechanical properties.^{[264–268],[269–272]} In this context, in the last few years, there has been a growing interest in the use of itaconic acid, which is composed of two carboxylic acid functionalities, an α,β -unsaturated double bond and two carboxyl groups, which make it highly flexible for UPR chemistry. First, itaconic acid was synthesized by the thermal decarboxylation of citric acid in 1837.^[264,273] Today, it is produced on an industrial scale *via* fermentation with *Aspergillus terreus* using glucose as a carbon source.^[274]

Recently, Čuk et al. replaced raw materials of synthetic polyester polyol with their bio-based alternatives and developed a synthetic route for a fully bio-based and solvent-free version of polyester polyol which can be used in combination with acrylic polyol for high-solid two-component polyurethane protective coatings for metal surfaces. The synthesized bio-based polyester polyol shows a high potential in the coating industry where the properties were comparable to the properties of synthetic counterparts.^[275]

Herein, we present the synthesis and characterization of photocurable bio-based polyester resins for their use in 3D printing with vat photopolymerization. Using commercially Synthetic Polyester-Acrylate (PEA) as a synthetic benchmark, monomeric building blocks are step-wise replaced with bio-based alternatives such as 1,3-propanediol, sebacic acid, succinic acid, isosorbide and itaconic acid. In a comprehensive way, the influence of the building blocks on molecular weight, viscosity and cure kinetics of the polyester resins are studied to assess their applicability for 3D printing. In this work, bio-based resins showed fast curing speed, which enables printing of 3D objects with an acceptable resolution for applications in several fields, e.g. printing of medical devices.

6.3 Materials and Methods

6.3.1 Materials and Chemicals

For the synthesis, the following monomers were used: succinic acid (99.5%) from Roquette (Lestrem, France), sebacic acid (99.5%) from Arkem (Colombes, France), 1,3-propanediol (99.9%) from Covation Biomaterials (Newark, DE, USA), cyclohexandimethanol (Eastman, TN, USA 98.5%), acrylic acid (Arkema, Colombes, France, 99.5%), itaconic acid (Novasol Chemicals, Kraainem, The Netherlands, 99.7%), isosorbide (Ecogreen Oleochemicals, Singapore, 99%), hypophosphorous acid, 2,6-di-tert-butyl-4-methylphenol (99.8% Oxiris Chemicals, S.A., Barcelona, Spain) and 4-methoxyphenol (HQMME) (98+%, BASF) and phthalic acid anhydride (Atmosa Petrochemie GmbH, Vienna, Austria 99.7%). Phenylbis(2,4,6-trimethylbenzoyl) phosphine oxide (Irgacure 819) was used as a radical photoinitiator supplied by Sigma Aldrich (St. Louis, MO, USA). Sudan II was obtained from TCI chemicals (Tokyo, Japan). All chemicals were used without further purification.

6.3.2 Polyester synthesis

All bio-based polyester resins were synthesized in two steps. For the first step, the following materials were used:

- PEA-BIO-1: cyclohexanedimethanol, 1,3 propanediol, sebacic acid, succinic acid, hypophosphorous acid, phthalic acid anhydride.
- PEA-BIO-2 and PEA-BIO-3: isosorbide, 1,3 propanediol, sebacic acid, succinic acid, hypophosphorous acid, phthalic acid anhydride.

The listed materials were directly introduced into a 6 L three-necked glass reactor equipped with a mechanical stirrer, thermometer, condenser, water trap, nitrogen inlet and external heating. The reactor was charged with raw materials and the system was heated to 210 °C under constant nitrogen flux. Toluene was used as reflux solvent for water removal. The progress of the reaction was monitored by acid value titration until the acid value was below 3 mg KOH/g. Toluene was removed using a vacuum. The resin was cooled to room temperature.

The second step included the addition of acrylic acid (for PEA-BIO-1 and PEA-BIO-2) and itaconic acid (PEA-BIO-3) and the addition of 2,6-di-tert-butyl-4-methylphenol and HQMME. The system was heated to 120 °C under constant oxygen flux until the reaction mixture reached an acid value of around 10. The mixture was cooled to room temperature and filtered through a 190 µm filter.

6.3.3 Preparation of Resin Formulations

Photocurable formulations were prepared by mixing the respective resin with 3 wt.% of Irgacure 809 and 0.01 wt.% Sudan II. The formulations were homogenized with a vortex mixture two times (1 min at room temperature) until all components were dissolved.

6.3.4 Resin Characterization

The viscosity of the prepared resins was measured by using a modular compact rheometer MCR 102 from Anton Paar (Graz, Austria) with a CP/PP 7 plate. Each measurement was carried out with 1 mL resin at room temperature and a shear rate of 300 s⁻¹.

The curing kinetics of the prepared resins were studied by Fourier-transform infrared spectroscopy (FTIR) on a PerkinElmer Spectrum One spectrometer (Hopkinton; MA, USA). All spectra were taken in transmittance mode over a wavenumber range of 4000 to 800 cm⁻¹. Spectra were accumulated from 16 scans at a resolution of 4 cm⁻¹ and the absorption peak areas were calculated

with OPUS software (version 2.0). All samples were prepared by drop casting of 1.5 μL of resin between two CaF_2 discs. The samples were then irradiated with an LED curing lamp (405 nm, Opsytec Dr. Gröbel, Ettlingen, Germany) at 8 mW/cm^2 . The conversion of acrylate functional group was calculated with OPUS software by evaluating the decrease in the characteristic IR absorption band at 1620–1636 cm^{-1} . The degree of conversion (DC) was calculated from the following equation:

$$\text{DC}\% = \left[1 - \left(\frac{C_{\text{Peak}}/C_{\text{Reference}}}{U_{\text{Peak}}/U_{\text{Reference}}} \right) \right] \cdot 100 \quad (1)$$

where C_{peak} corresponds to the absorption area of the observed band of the cured sample and $C_{\text{reference}}$ to its reference peak. U_{peak} and $U_{\text{reference}}$ are the absorption area of the relevant band and reference peak of the uncured sample, respectively.

Gel permeation chromatography (GPC) was performed on a Knauer Azura GPC (Berlin, Germany) system equipped with a differential refractive detector and an AppliChrom StyDiViBe-P 5 μm columns. The polymer solution (7 mg mL^{-1} , 100 μL) was injected into the GPC system using tetrahydrofuran eluent at a flow rate of 1 mL min^{-1} .

$^1\text{H-NMR}$ spectra were recorded on a Bruker (300 MHz) spectrometer (Billerica, MA, USA) using $\text{DMSO-}d_6$ as the solvent. $^1\text{H-NMR}$ shifts of synthesized polymers are reported in ppm (δ) downfield from tetramethylsilane (TMS) and were determined by referring to the solvent peak $\text{DMSO-}d_6$ for hydrogen atoms.

6.3.5 Color Measurement

The color of the prepared polyesters was measured according to the SIST EN ISO 6271 standard using the spectroscopic method [61]. Measurements were performed on a Hach Lico 690 spectral colorimeter (Loveland, CO, USA). The resins were placed in a glass cuvette which was inserted into the measuring instrument. The color value was read from the screen of the instrument according to the platinum-cobalt (Hazen) scale.

6.3.6 DLP 3D Printing

The samples obtained from PEA, PEA-BIO-1 and PEA-BIO-2 were printed with an Anycubic Photo Mono S printer (Shenzhen, China) using a 405 nm LED as the light source. Then, 0.01 wt.% of Sudan II was added and the formulation was homogenized with a vortex mixer two times (1 min

at room temperature) until the components were dissolved. The printing parameters are presented in Table 1.

Table 1. Printing parameters.

	PEA	PEA-BIO-2	PEA-BIO-3
Time of three bottom exposure layers:	13 s	20 s	24 s
Exposure time:	10 s	15 s	17 s

PEA-BIO-3 was prepared in the same way as the previously described resins but DLP 3D printing was performed on a Doppio printer operating at 405 nm (intensity was 30 mW/cm²) manufactured by way2production (Vienna, Austria). The resin vat was heated at 50 °C during the printing process. The objects were printed with three different bottom exposure layer times: 100, 75 and 50 s.

6.3.7 Characterization of Mechanical and Thermomechanical Properties

The mechanical properties were characterized by a ZwickRoell (Ulm, Germany) Z1.0b static materials testing machine with a crosshead speed of 250 mm min⁻¹. The dimensions of the DLP 3D-printed tensile specimens were 75 mm × 12.5 mm × 2 mm.

Dynamic mechanical analysis (DMA) was carried out on a Mettler Toledo (Greifensee, Switzerland) DMA/SDTA861e analyzer. Mechanical loss factors ($\tan \delta$) and storage moduli (E') were monitored over a temperature range from -45 to 100 °C at a heating rate of 3 °C/min. The glass transition temperature (T_g) was determined by the temperature at the maximum of the loss factor. For sample preparation, test specimens (30 mm × 4 mm × 1 mm) were fabricated by an Anycubic printer (Shenzhen, China). The printing conditions are shown in Table 1.

6.4 Results and Discussion

6.4.1 Polyester Synthesis

The main goal of the research was to develop bio-based acrylate-functional polyester resins as a greener alternative to commercially available derivatives. For this study, a commercially available synthetic resin PEA was used as a benchmark, which is derived from 1,6-hexanediol, cyclohexanedimethanol, adipic and acrylic acid. Three different resins were synthesized by

selectively replacing the components of PEA with bio-based alcohols and carboxylic acids as building blocks (composition is shown in Table 2).

Table 2. Used monomers in the synthesis of synthetic and bio-based resins.

PEA	PEA-BIO-1	PEA-BIO-2	PEA-BIO-3
cyclohexanedimethanol	cyclohexanedimethanol	isororbide	isororbide
1,6-hexanediol	1,3-propanediol	1,3-propanediol	1,3-propanediol
adipic acid	sebacic acid	sebacic acid	sebacic acid
	succinic acid	succinic acid	succinic acid
phtalic acid anhydride	phtalic acid anhydride	phtalic acid anhydride	phtalic acid anhydride
acrylic acid	acrylic acid	acrylic acid	itaconic acid
0% bio-based	40 wt.% bio-based	60 wt.% bio-based	95 wt.% bio-based

In PEA-BIO-1, adipic acid was replaced with sebacic and succinic acid, and 1,6-hexanediol was replaced with 1,3-propanediol. In PEA-BIO-2, isororbide was introduced instead of cyclohexanedimethanol, and in PEA-BIO-3, acrylic acid was additionally replaced by itaconic acid, yielding a polyester with the highest bio-based content (Figure 1).

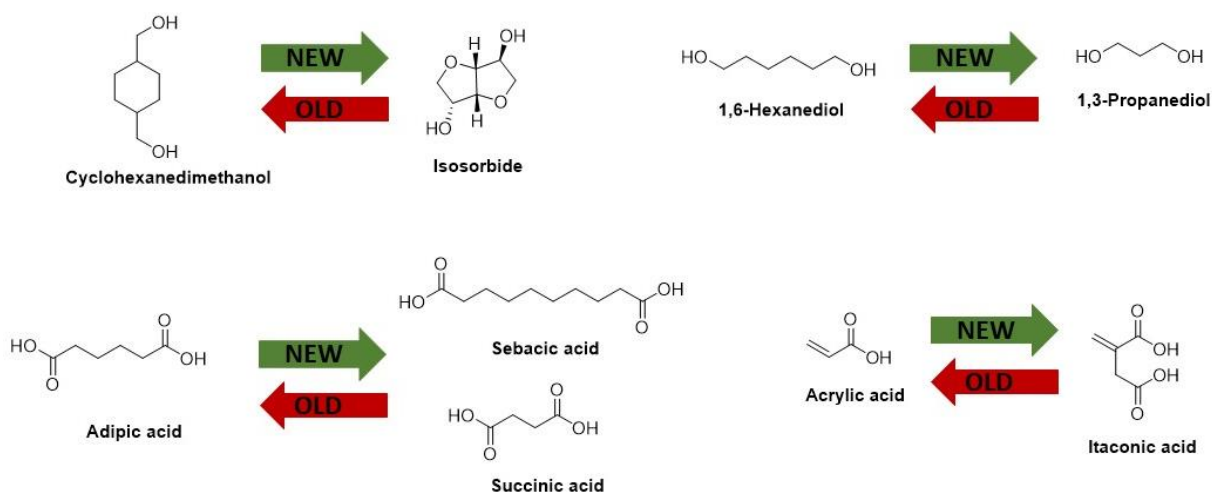


Figure 1. Representation of monomer structures.

The prepared acrylate polyesters were further characterized by ATR Fourier-transform infrared (FTIR) spectroscopy, and the most important vibrations are marked in Figure 2. The signals at 1619-1635 and 810 cm^{-1} correspond to C=C stretch and C=C deformation vibrations of the carbon double bonds, while the signal at 1730 cm^{-1} is assigned to the C=O stretching vibration of the ester group. The broad signal at 3500 cm^{-1} is related to the -OH groups of free carboxylic acid moieties.^[276–278]

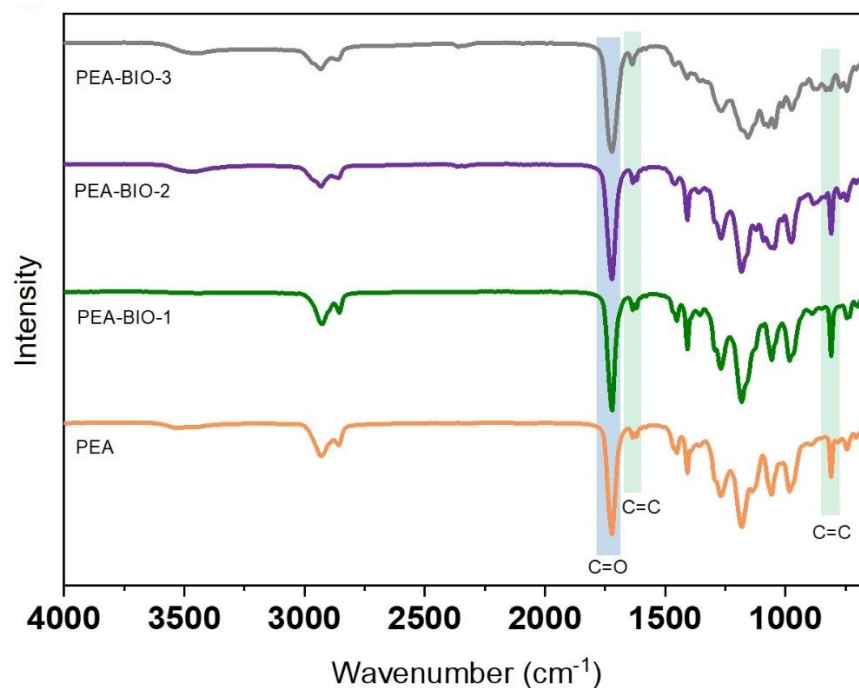


Figure 2. ATR FTIR spectra of synthesized PEA-BIO resins and the commercially available PEA resin.

The ¹H-NMR spectra of the synthetic and bio-based resins are shown in Figure S1 in the Supporting Information. From these spectra, successful polymerization can be confirmed by the observed peaks around 4.0–4.3 ppm (highlighted in blue) which correspond to the protons of C(O)OCH₂- groups. The protons assigned to the -CH₂- group of 1,3-propanediol are observed between 1.5 and 2.5 ppm. The resonance signal at 2.6 ppm belongs to the -OC(O)CH₂- group of succinic acid, while the corresponding peak of sebacic acid is located around 2.3 ppm. Two signals at 1.3 and 1.6 ppm correspond to the methylene groups of sebacic acid.

The average molecular weight (M_w) of the synthetic and bio-based resins was analyzed by gel permeation chromatography (GPC) and the spectra are provided in the Supporting Information (Figure S3). The determined values are as follows: 1543 g/mol (PEA), 936 g/mol (PEA-BIO-1), 665 g/mol (PEA-BIO-2) and 1001 g/mol (PEA-BIO-3).

It was also found that the replacement of adipic acid (PEA) with sebacic and succinic acid (PEA-BIO-1) resulted in a decrease in the viscosity from 2.31 Pa·s to 0.27 Pa·s. By introducing isosorbide into the structure (PEA-BIO-2), the viscosity increases to 0.96 Pa·s. This can be explained by the cyclic and relatively rigid structure of isosorbide, which makes the related polymer chains less flexible and therefore causes an increase in viscosity. In PEA-BIO-3, the acrylic acid was

additionally replaced with itaconic acid as a green alternative, which resulted in a significantly higher viscosity of 91.78 Pa·s. Compared to acrylic acid, itaconic acid contains two carboxylic acid groups which can cause increased viscosity through a higher number of hydrogen bonding and intermolecular interactions. It should be noted that for DLP 3D printing, the viscosity of PEA-BIO-3 was reduced by adding a bio-based reactive diluent. In particular, acrylated eugenol (AEUG) was used in a mass ratio of 1:1, yielding a viscosity of 0.36 Pa·s.

Higher molecular weight often leads to higher viscosity due to increased chain entanglements, resulting in more resistance to flow. By introducing itaconic acid (PEA-BIO-3), the viscosity significantly increased due to the bifunctional structure of itaconic acid. Instead of one carboxylic group (acrylic acid), two carboxylic groups of itaconic acid participate in cross-linking reactions. There is a significant change in the color of synthetic and bio-based polyester-acrylate resins. Synthetic resin PEA resulted in 3 Gardner, while bio-based resins PEA-BIO-1 and PEA-BIO-2 resulted in 5 and 5.5 Gardner, respectively (Figure S2). The properties of the synthetic and bio-based polyester-acrylate resins are summarized in Table 3.

Table 3. Properties of synthetic and bio-based polyester-acrylate.

	PEA	PEA-BIO-1	PEA-BIO-2	PEA-BIO-3
Acid number (mg KOH/g)	5.0	9.0	13.9	83.4
Viscosity 23 °C (Pa·s)	2.31	0.27	0.96	91.78
Color (Gardner)	3	5	5.5	N/A (turbid)
Molecular weight (g/mol)	1543	936	665	1001

Photocurable resin formulations were then prepared by mixing the newly synthesized polyester resins with 3 wt.% of phenylbis(2,4,6-trimethylbenzoyl) phosphine oxide (Irgacure 819) as a radical photoinitiator. The cure kinetics was studied by FTIR spectroscopy in transmission mode, and the C=C-H stretching band of the acrylate (1619 and 1634 cm⁻¹) and vinyl groups (1637 cm⁻¹) was monitored upon exposure at 405 nm (Figure 3). The results show that the introduction of bio-based alcohols in the polyester structure slows down the reaction kinetics. For the synthetic PEA, full conversion of the acrylate groups was observed after 128 s of light exposure. In contrast, the bio-based resins PEA-BIO-1 and PEA-BIO-2 reached a conversion of 100% and 95% after 512 s of light exposure, respectively. Along with a significant reduction in viscosity, we expected that the addition of the low-molecular-weight reactive diluent AEUG accelerates the cure kinetics of PEA-BIO-3. However, the results clearly show that the replacement of acrylic acid with the less reactive itaconic acid considerably slows down the curing reactions and the functional group

conversion only amounts to 65% after 512 s of light exposure. The observed results can be explained by the lower reactivity of bio-based monomers which slow down the polymerization process compared to petroleum-based monomers due to their different chemical structures. Resin PEA-BIO-3 is itaconic acid modified, while PEA, PEA-BIO-1 and PEA-BIO-2 are acrylic acid-modified unsaturated polyester resin. The difference in polymerization kinetics between acrylic- and itaconic-modified unsaturated polyester resins can be affected by chemical structure, functional groups and steric hindrance. The acrylic acid has a linear structure with one carbonyl group, while itaconic acid has a cyclic structure with two carboxyl groups. One ester group of acrylic acid easily undergoes polymerization reaction, while itaconic acid has additional functional groups such as carbon double bonds. The combined steric and electronic effects are expected to slow down the propagation of the chain-growth reaction.^[279]

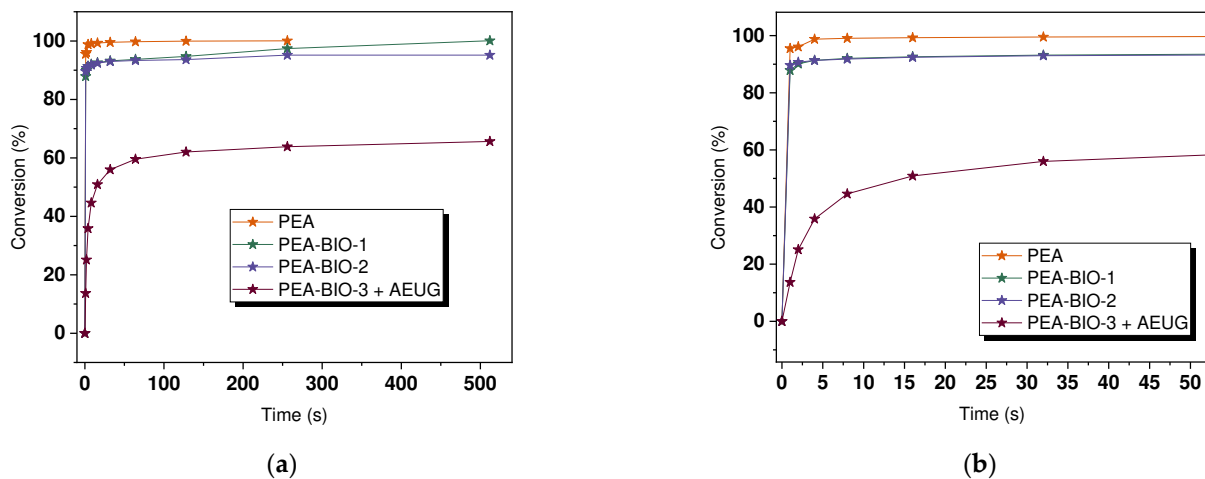


Figure 3. (a) Monitoring the acrylate conversion of synthetic (PEA) and bio-based resins (PEA-BIO-1, PEA-BIO-2 and PEA-BIO-3 + AEUG) upon irradiation with 405 nm, (b) the irradiation time between 0 and 50 s.

6.4.2 Additive Manufacturing

To evaluate the printability of the resins and the resolution of the DLP 3D-printed objects, the resins were cured with a commercial Anycubic Photo Mono printer in layers of 100 μm with a cure time of 10 s per layer for resin PEA, 15 s per layer for resin PEA-BIO-1 and 17 s per layer for resin PEA-BIO-2. As can be seen from Figure 4, the printed specimens showed a resolution in the millimeter range. A decrease in resolution was observed when the content of bio-based alternatives was higher, which is related to their slower cure kinetics.

Due to the slow polymerization reaction and high viscosity value, the printing with PEA-BIO-3 was carried out with another printer (Doppio), which enabled printing at higher light intensity (30 mW/cm²) and the vat was heated at 50 °C. However, the printed specimens were full of bubbles and required a high curing time >30 s per layer (Figure S4 in the Supporting Information). Therefore, it was not possible to print specimens for resolution experiments and subsequently for thermomechanical and mechanical testing.

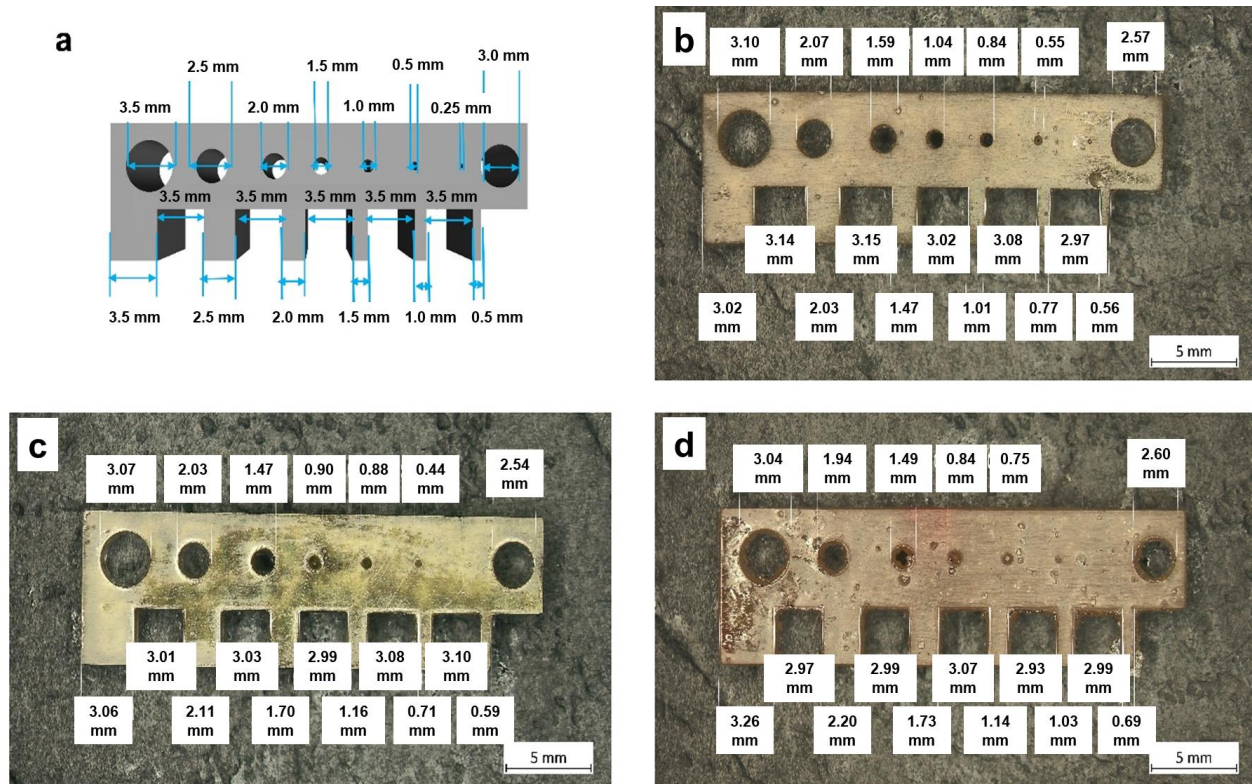


Figure 4. (a) CAD data of a comb-like test structure and DLP 3D-printed objects using different resins: (b) PEA, (c) PEA-BIO-1, (d) PEA-BIO-2.

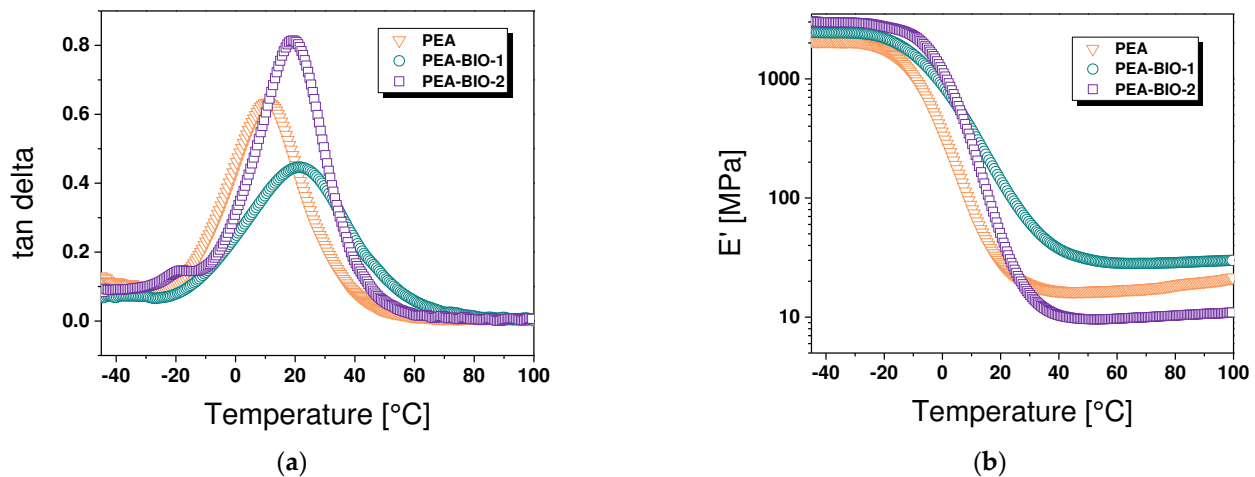
6.4.3 Mechanical and Thermomechanical Properties

To study the influence of the structure of the monomers on mechanical and thermomechanical properties of the related photopolymer networks, DMA and tensile tests were performed on DLP 3D-printed test specimens. In Table 4, the thermomechanical and mechanical properties of synthetic resin PEA are compared to bio-based resins PEA-BIO-1 and PEA-BIO-2.

Table 4. Thermomechanical and mechanical properties of photocured synthetic and bio-based resins.

Formulation	T_g (°C)	E' at 23 °C (MPa)	σ (MPa)	ε (%)
PEA	10	23.2	0.82 ± 0.07	6.59 ± 0.62
PEA-BIO-1	21	103.7	1.73 ± 0.23	6.89 ± 0.69
PEA-BIO-2	19	30.7	0.61 ± 0.03	7.60 ± 0.52

Figure 4 shows the DMA data of the cured resins. The results show that the T_g values increase from 10 to 19 and 21 °C by introducing sebacic and succinic acids, respectively. The increase in the T_g may be caused by shorter-chain dicarboxylic succinic acid, whose incorporation may lead to a more rigid polymer. Due to the higher T_g of PEA-BIO-1 compared to the synthetic counterpart PEA, its storage modulus (E') at 23 °C was significantly higher (23.2 versus 103.7 MPa). Interestingly, PEA-BIO-2 having a T_g in a similar range shows a much lower E' at 23 °C (30.7 MPa). This can be explained by an incomplete conversion of the resins during curing as an additional peak is observed in the $\tan \delta$ curve at -19 °C. The unreacted polyester resin might act as plasticizer and lowers the stiffness of the related network, which is also observed in the stress–strain curves (Figure 5).

**Figure 5.** (a) Loss factor ($\tan \delta$) and (b) storage modulus (E') versus temperature as obtained from DMA measurements of synthetic and bio-based resins.

Along with the thermomechanical properties, the mechanical performance of the 3D-printed test specimens was tested and the stress–strain curves are provided in Figure 6. The synthetic resin and the bio-based ones have a similar elongation at break ranging between 6.5 and 7.5%. The stiffer PEA-BIO-1 network yields a higher tensile strength (1.73 MPa), while PEA and PEA-BIO-2 give

comparable tensile strength values of 0.82 and 0.61 MPa, respectively. As can be seen from Figure 6, the tensile stress significantly increases after the incorporation of isosorbide into the polymer structure. Due to the rigid and symmetrical structure of isosorbide, which leads to strong intermolecular interactions and packing within the polymer matrix, properties can result in improved strength and stiffness. For the resin PEA-BIO-2, itaconic acid was introduced instead of acrylic acid. Acrylic-modified unsaturated polyester resins often show improved tensile strength due to acrylic functionalities which lead to intermolecular interactions and cross-linking within the polymer matrix, yielding materials with higher stiffness and strength. On the other hand, itaconic acid-modified unsaturated polyester resins can also cause increased tensile strength, albeit to a lesser extent than acrylic modification.^[264,280]

From the results, it can be seen that PEA-BIO-1 is an interesting alternative polyester resin for DLP 3D printing as it combines a higher content of bio-derived building blocks with decent printability and mechanical properties, which are superior to the purely petroleum-based counterpart PEA.

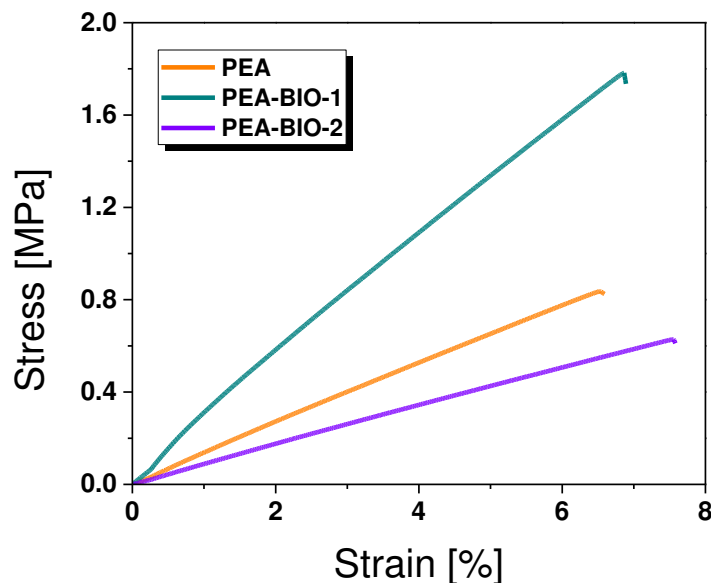


Figure 6. Stress–strain curves of photocured synthetic and bio-based polyester resins.

6.5 Conclusions

In this research, the focus was on the synthesis and characterization of DLP 3D-printable bio-based polyester resins. Using the commercially available resin PEA as a petroleum-based benchmark, monomeric building blocks were step-wise replaced with bio-based alternatives. For PEA-BIO-1,

1,6-hexanediol was substituted with bio-based 1,3-propanediol and adipic acid was replaced with bio-based succinic and sebacic acid. In the synthesis of PEA-BIO-2, the bio-based isosorbide was additionally introduced instead of cyclohexane dimethanol. Finally, for PEA-BIO-3, having the highest content of bio-based precursors, itaconic acid was additionally used instead of acrylic acid. FTIR data revealed that cure kinetics decreases with rising content of bio-based monomers. PEA-BIO-1 and BIO-2 were easily processable by DLP 3D printing, requiring a build speed of 15 to 17 s per layer (100 μm layer thickness). Due to the slow polymerization kinetics and high viscosity, PEA-BIO-3 required the addition of a bio-based reactive diluent. Although printing was carried out at a significantly higher light intensity, longer irradiation time and elevated temperature, the quality of the printed samples was inferior. Thus, no samples were printed for testing mechanical and thermomechanical properties. Synthetic resin PEA showed the lowest T_g value of 10 $^{\circ}\text{C}$, while the T_g of the two bio-based resins PEA-BIO-1 and BIO-2 amounted to 19 and 21 $^{\circ}\text{C}$, respectively. Among the studied resins, PEA-BIO-1 exhibited the highest storage modulus at 23 $^{\circ}\text{C}$ and exhibited the highest tensile strength (1.73 MPa). Based on all the results, it can be concluded that the synthesized and characterized bio-based polyester resins with reactive acrylate groups showed a great ability for additive manufacturing materials by vat photopolymerization, which was demonstrated by successful printing of tensile and DMA specimens as well as comb test structures. The presented progress enables the processing of resins with high bio-based content by using vat photopolymerization 3D printing and, thus, increases the use of sustainable and environmentally friendly materials in future applications such as soft active devices or multi-material structures.^[52,281]

6.6 Acknowledgments

The research work was performed within the COMET-Module project “Chemitecture“ (project-no.: 21647048) at the Polymer Competence Center Leoben GmbH (PCCL, Austria) within the framework of the COMET-program of the Federal Ministry for Transport, Innovation and Technology and the Federal Ministry for Digital and Economic Affairs with contributions by Montanuniversitaet Leoben, Politecnico di Torino, Helios TBLUS and bto-epoxy. Funding is provided by the Austrian Government and the State Government of Styria. The authors thank Gerald Meier (PCCL) for tensile test measurements, Walter Alabiso (PCCL) for DMA measurements and Bernhard Sölle (PCCL) for synthesizing the reactive diluent AEUG.

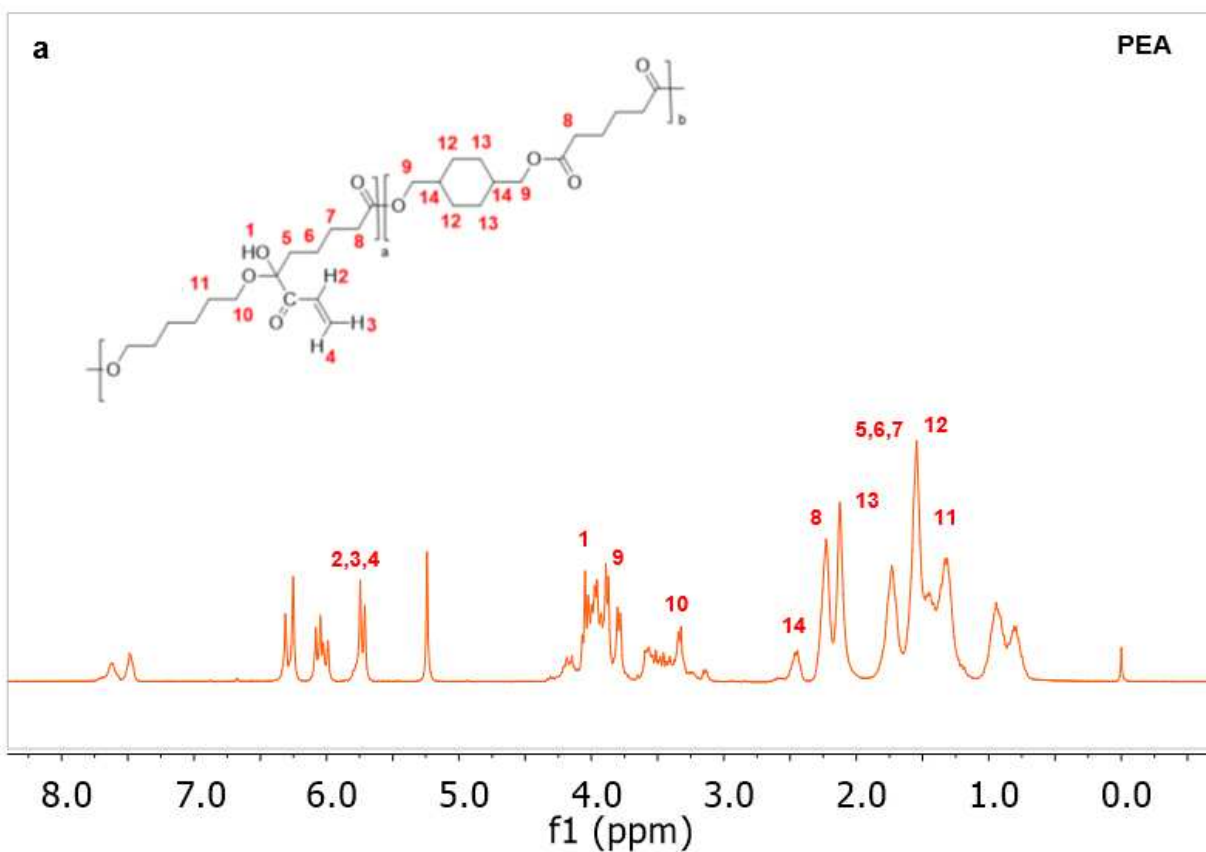
6.7 Supporting Information

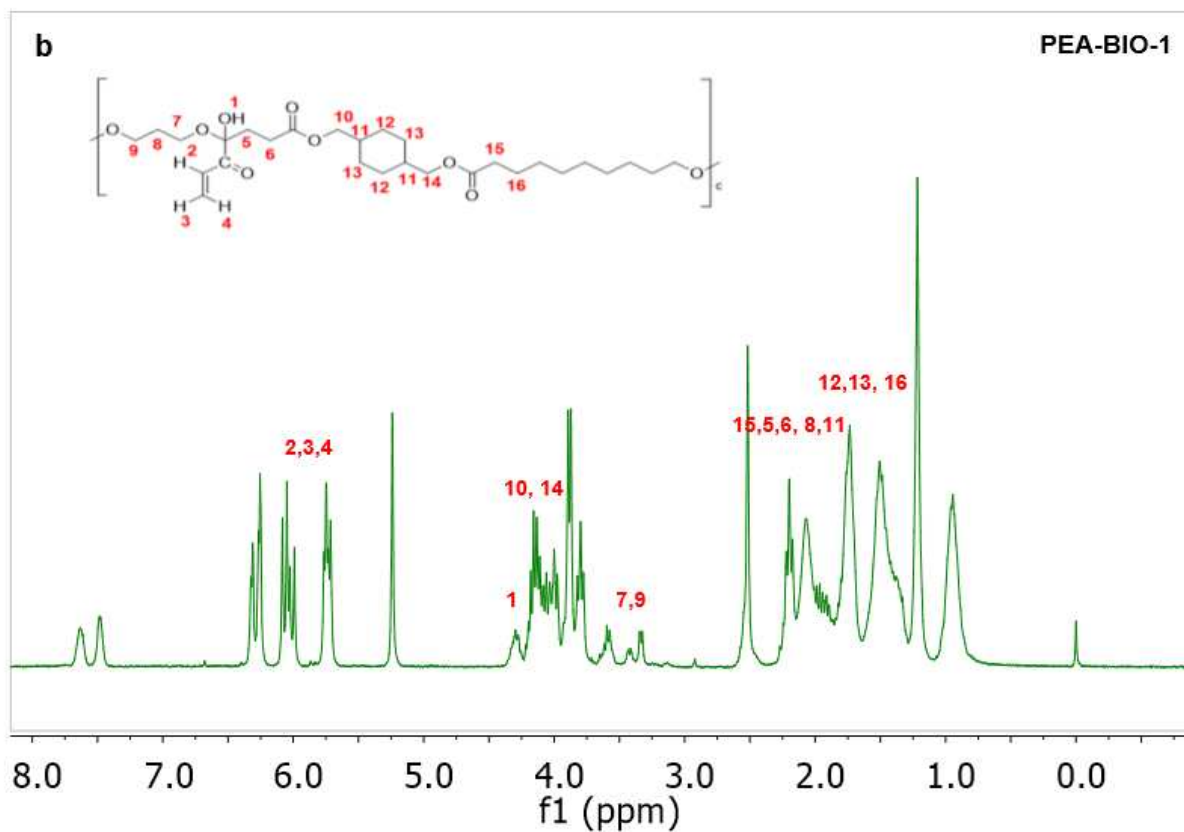
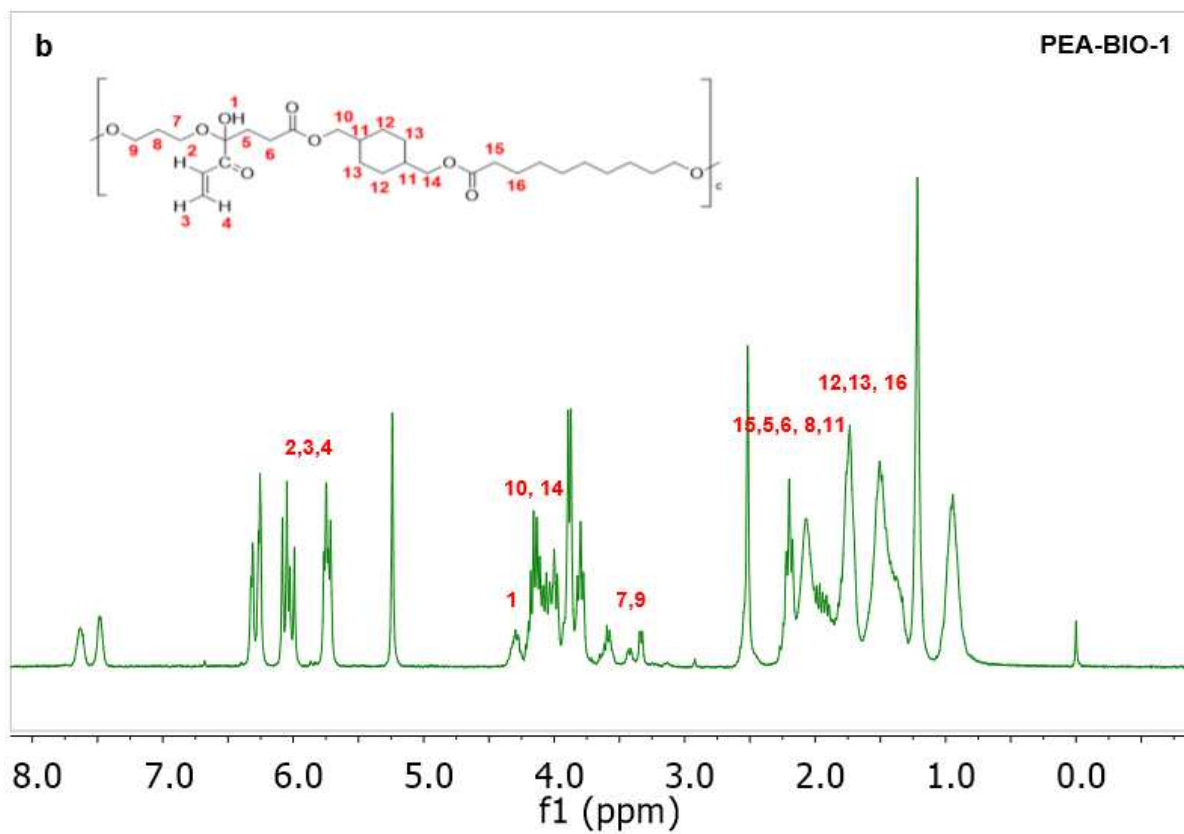
Synthesis of bio-based polyester resins for vat photopolymerization 3D printing

Ines Cazin^a, Martin Ocepek^b, Janez Kecelj^b, Aleš Stanislav Stražar^b and Sandra Schlögl^{1a*}

a. Polymer Competence Center Leoben GmbH, Sauraugasse 1, A-8700 Leoben, Austria

b. Helios Resins, Količevo 65, 1230 Domžale, Slovenia





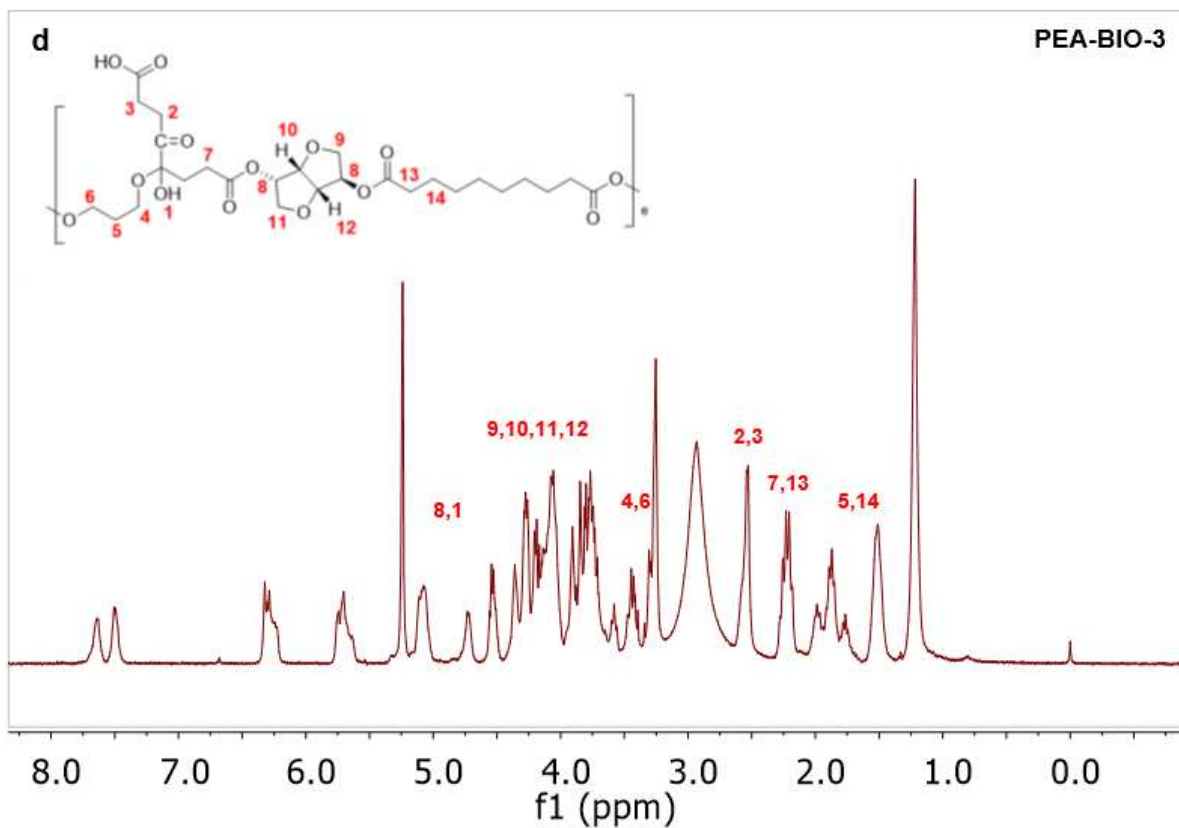


Figure S1. ¹H-NMR spectra of acrylic modified polyester resins: (a) PEA, (b) PEA-BIO-1, (c) PEA-BIO-2, (d) PEA-BIO-3.

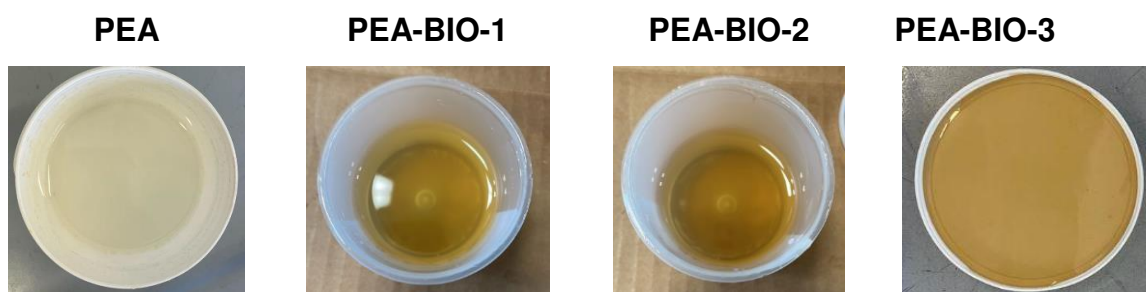


Figure S2. Appearance of synthetic and bio-based polyester – acrylates.

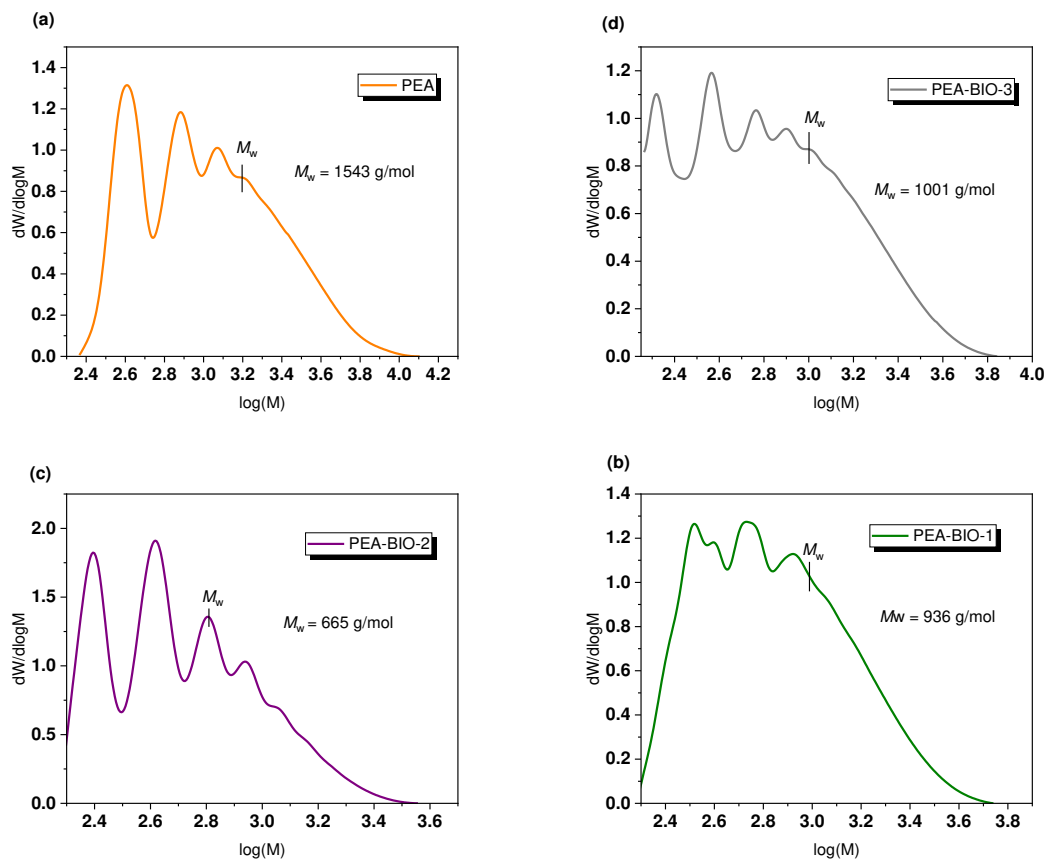


Figure S3. GPC data for (a) PEA, (b) PEA-BIO-1, (c) PEA-BIO-2 and (d) PEA-BIO-3.

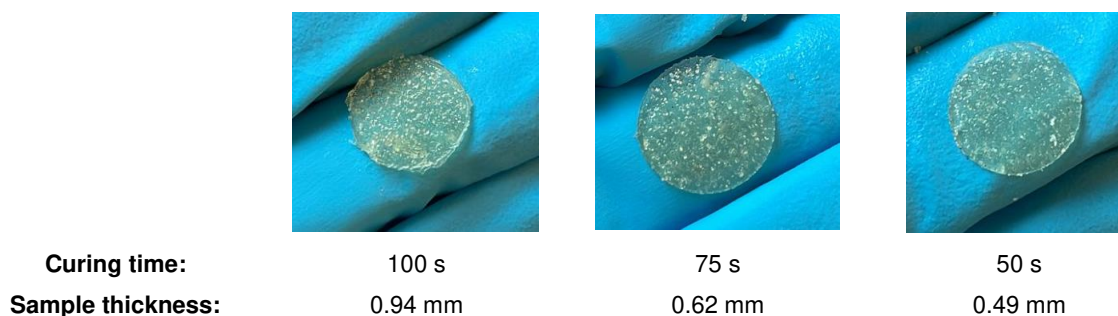


Figure S4. DLP 3D printed specimens from PEA-BIO-3 resin diluted with AEUG (mass ratio was 1:1).

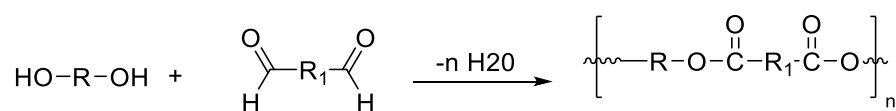


Figure S5. Schematic representation of polyester synthesis.

7 Publication IV:

*Digital Light Processing 3D Printing of Dynamic Magneto-Responsive
Thiol-Acrylate Composites*

Ines Cazin, Elisabeth Rossegger, Ignazio Roppolo, Marco Sangermano, Petra Granitzer, Klemens Rumpf, Sandra Schlögl

RSC advances **2023**, *13* (26), 17536–17544

DOI: 10.1039/D3RA02504G.

The presented manuscript in Section 6 was almost identically published in the above-mentioned paper.

Digital Light Processing 3D Printing of Dynamic Magneto-Responsive Thiol-Acrylate Composites

Ines Cazin^a, Elisabeth Rossegger^a, Ignazio Roppolo^b, Marco Sangermano^b, Petra Granitzer^c, Klemens Rumpf^c, Sandra Schlögl^{a*}

a. Polymer Competence Center Leoben GmbH, Roseggerstrasse 12, A-8700 Leoben

b. Department of Applied Science and Technology, Politecnico di Torino, Duca degli Abruzzi, 24, 10124, Torino, Italy

c. Institute of Physics, Universitätsplatz 3, 8010 Graz, Austria

7.1 Abstract

Additive manufacturing is one of the most promising processing techniques for fabricating customized 3D objects. For the 3D printing of functional and stimuli-triggered devices, the interest is steadily growing in processing materials with magnetic properties. Synthesis routes for magneto-responsive soft materials typically involve the dispersion of (nano)particles into a non-magnetic polymer matrix. Above their glass transition temperature, the shape of such composites can be conveniently adjusted by applying an external magnetic field. With their rapid response time, facile controllability, and reversible actuation, magnetically responsive soft materials can be used in the biomedical field (e.g. drug delivery, minimally invasive surgery), soft robotics or in electronic applications. Herein, we combine the magnetic response with thermo-activated healability by introducing magnetic Fe₃O₄ nanoparticles into a dynamic photopolymer network, which undergoes thermo-activated bond exchange reactions. The resin is based on a radically curable thiol-acrylate system, whose composition is optimized towards processability via digital light processing 3D printing. A mono-functional methacrylate phosphate is applied as stabilizer to increase the resins' shelf life by preventing thiol-Michael reactions. Once photocured, the organic phosphate further acts as a transesterification catalyst and activates bond exchange reactions at elevated temperature, which render the magneto-active composites mendable and malleable. The healing performance is demonstrated by recovering magnetic and mechanical properties after the thermally triggered mending of 3D-printed structures. We further demonstrate the magnetically driven movement of 3D-printed samples, which give rise to the potential use of these materials in healable soft devices activated by external magnetic fields.

7.2 Introduction

Since the beginning of the 80s, 3D printing has become a fast-emerging technology, which has been successfully implemented world-wide in academy and several industrial sectors.^[61,282–284] Multi-functional objects with complex and customized architectures are easily formed into physical objects by layer-by-layer deposition of materials directly from a computer-aided design without molds and heavy machining.^[285–288] Due to freedom in component design and production, the 3D printing technology is applied for fabricating parts used in industrial machines, consumer products (electronics), motor vehicles, aerospace or medical (dental) sector.^[53,289] However, significant progress has been achieved by introducing a shape-morphing capability into 3D-printed objects, also known as 4D printing. Initiated and termed by researchers from MIT^[290] in collaboration with Stratasys, Inc., the fourth dimension of 3D printed objects offers the ability to switch their geometric configuration in response of variations of the surrounding environment. This unlocks a new toolbox of application areas in 3D printing.^[291–293] Numerous external stimuli can be applied such as light^[294,295], heat^[294,296], temperature^[297,298], solvent^[132,299–301], pH value^[302], electric field^[303–305], magnetic field^[306–311] or humidity^[312]. Due to their multi-functional behavior (e.g. reconfigurable structure, shape memory effect, actuation, sensing), these composites can be used in a broad variety of applications^[313] including soft robotics^[314–316], shape memory structures^[317], sensors and actuators.^[318–321]

In this context, great effort has been devoted to develop magneto-active materials for functional composites.^[322–325] By exposure to an external magnetic field, these materials undergo mechanical and rheological changes (e.g. damping, elasticity), and shape. Magneto-responsive materials are found in the form of a fluid, a gel or a solid.^[326,327] Solid magneto-active materials consist of a soft polymeric matrix, in which inorganic magnetic particles (e.g. ferrite particles Fe_3O_4 , maghemite $\gamma\text{-Fe}_2\text{O}_3$ or neodymium-iron-boron particles NdFeB)^[328–333] are dispersed. Prominent examples of polymers are elastomers^[334–336], plastomers^[337,338] and foams.^[339,340] A typical behavior of magneto-responsive elastomers (MREs) under the application of a magnetic field is their change of modulus. However, the range of applications is limited due to small magnetically induced actuation strain. Various additive manufacturing techniques, such as direct ink writing (DIW) and fused filament fabrication (FFF) have been employed to fabricate polymers containing high loads of magnetic fillers.^[341–343] Colorado and Restrepo demonstrated the printing of an epoxy resin loaded with magnetite particles up to 41 wt% via DIW. Results on compressive strength and ductility of tested printed composites showed its applicability in structural components.^[344] In

2018, Zhao *et al.* reported the 3D printing of elastomer composites filled with ferromagnetic microparticles prepared by direct ink writing. More precisely, they were able to program ferromagnetic domains in complexly designed 3D-printed materials by applying a magnetic field directly to the dispensing nozzle during the printing process.^[345]

Recently, Rodionova *et al.* incorporated magnetic ferrite particles into polylactic acid and produced objects with tunable magnetic properties via FFF. Results set up the stage for the additive manufacturing of composites with controlled magnetic anisotropy, as well as, for achieving a spatial distribution of nanofillers in a non-magnetic polymeric matrix.^[346] One of the salient feature of DIW is that inks with high loads of magnetic fillers are applicable.^[341] Moreover, previous research showed that both DIW and FFF can be used to produce fast responding actuators^[347–349] as well as permanent magnets.^[350,351] Despite the mentioned advantages, objects printed by these techniques suffer from poor resolution. In addition, fillers may be not homogeneously dispersed, which leads to inhomogeneous magnetic response. In addition, high temperatures required during the FFF process may affect the fillers negatively.^[352,353]

Another promising printing approach is based on vat photopolymerization, in which the liquid photo-reactive resin is mixed with magnetic fillers. The method known as digital light processing (DLP) 3D printing is based on a layer-by-layer curing of the resin upon irradiation with a suitable light source. Compared to DIW and FFF, DLP offers several advantages, as it provides higher resolution and build speed, and it operates at room temperature. However, vat photopolymerization presents some drawbacks in terms of the maximum load of fillers in the resin. The photopolymerization process may be negatively affected by an increase in the content of fillers, which compromise on the optical properties of the resin. In addition, the stability and sedimentation of dispersed fillers in the liquid resin plays a vital role in achieving 3D-printed objects with a homogeneous magnetic response. In 2019, Lantean *et al.* developed magneto-responsive photopolymers based on a urethane-acrylate resin filled with Fe₃O₄ nanoparticles. Mechanical properties were tuned by adding butyl acrylate, which reduced the resin's viscosity, and magnetic properties were tailored by loading magnetic filler up to 6 wt%.^[354] In subsequent work, the authors studied the magnetically driven self-assembly of Fe₃O₄ nanoparticles into chain-like structures within the vat. The rotation and kinetics of chain formation depended on the viscosity, weight percentage of nanofillers, the intensity of the external magnetic field, and its application time. By applying magnetic fields of varying direction and intensity during the printing process, the authors

could control the orientation and the length of the magnetic chains in each printed layer, which was exploited for the fabrication of magnetically driven devices.^[355,356]

Recently, our group demonstrated the possibility to print soft magneto-active objects using thiol-click photopolymers as matrix. In particular, by advancing from pure acrylate to thiol-acrylate systems, we overcome shrinkage stress, oxygen inhibition and low monomer conversion of the filled photopolymers. Soft and flexible polymer composites were obtained by DLP 3D printing with 6 wt% of Fe₃O₄ nanoparticles at a reasonable build time.^[357]

Herein, we extended the functionality of 3D printable magneto-responsive thiol-acrylate composites by introducing an additional healing and re-shaping function. In particular, we exploited thermo-activated bond exchange reactions following catalyzed transesterification to induce a material flow above the networks topological freezing temperature. We optimized the composition of the photocurable formulation in terms of viscosity and stability and were able to 3D print objects with a Fe₃O₄ loading of up to 6 wt%. As a proof of concept, magneto-responsive structures were DLP 3D printed, which were thermally healed and could be conveniently reshaped and activated by applying an external magnetic field.

7.3 Results and discussion

7.3.1 Network design and optimization of the photocurable resin containing Fe₃O₄ nanofillers

To prepare magnetically responsive dynamic photopolymers, we used our recently reported thiol-acrylate system, which has been loaded with magnetic Fe₃O₄ nanoparticles ($d_{50} = 50$ nm) as a basis.^[358]

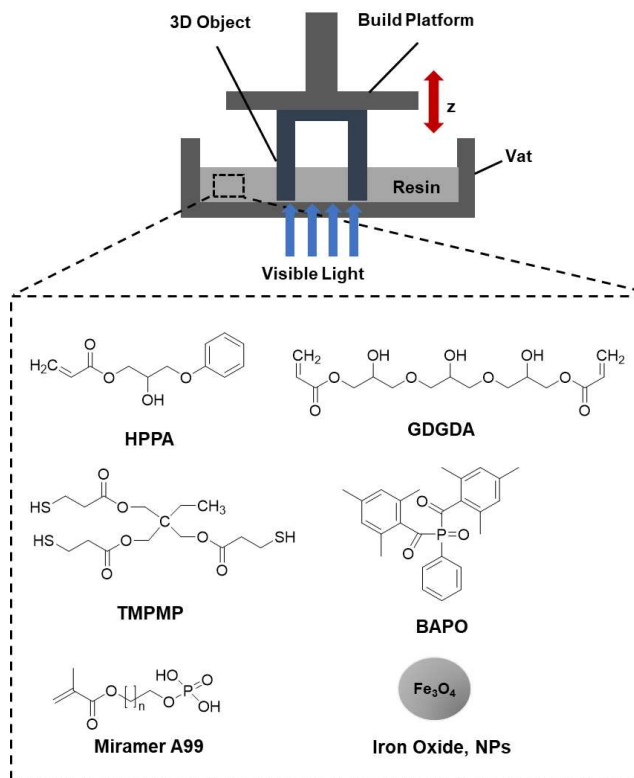


Figure 1. Monomers, transesterification catalyst, photoinitiator and iron oxide nanoparticles (NPs) used in magneto-responsive resins processed via DLP 3D printing.

The system was composed of hydroxy-2-phenoxypropyl acrylate (HPPA) and glycerol 1,3-diglycerolate diacrylate (GDGDA) and provided ample -OH groups for the thermo-activated transesterification reaction (Figure 1).

Trimethylolpropane tri(3-mercaptopropionate) (TMPMP) was added as a thiol cross-linker to switch the curing mechanism of pure acrylates following a chain-growth mechanism to a mixed mode one including chain-growth and step-growth reactions. In previous work, we further employed a mono-functional methacrylate phosphate as stabilizer to prevent thiol-Michael reactions and to increase the stability of the photo-curable resins during storage and printing. In another study we showed that this stabilizer is also able to catalyze transesterification reactions due to its Brønsted acidity.^[357] Herein, we exploited this feature to print magneto-active composites with additional functions such as thermo-activated mendability.

We varied the filler loading between 0 and 6 wt%, as previous work revealed that filler loadings > 6 wt% negatively affect the cure kinetics and stability of the photocurable thiol-acrylate resins. In

the present study, we additionally varied the content of the low viscous HPPA and the thiol cross-linker to reduce the viscosity of the formulations and increase the resins' stability, respectively (Table 1).

Table 1. Molar composition of the thiol-acrylate formulations under investigation

Compound	Resin-1 ^[358]	Resin-2
HPPA	50 mol%	65 mol%
GDGDA	25 mol%	25 mol%
TMPMP	25 mol%	10 mol%
BAPO	2 wt%	5 wt%
Miramer A99	5 wt%	5 wt%

As viscosity and shelf life of the resin are crucial parameters in vat photopolymerization 3D printing, we determined the viscosity of the new resin formulation (resin-2) with varying content of magnetic nanofillers (0 – 6 wt%) (Figure 2b) and compared it with our previously published system (Figure 2a). The measurements were performed over a prolonged time (15 min) to further get an idea of the resins' stability. Rheological data reveal that the viscosity increases with rising filler concentration but does not exceed 1,000 mPa·s, which is still within the range (250 and 5,000 mPa·s) of 3D DLP printable resins.^[359]

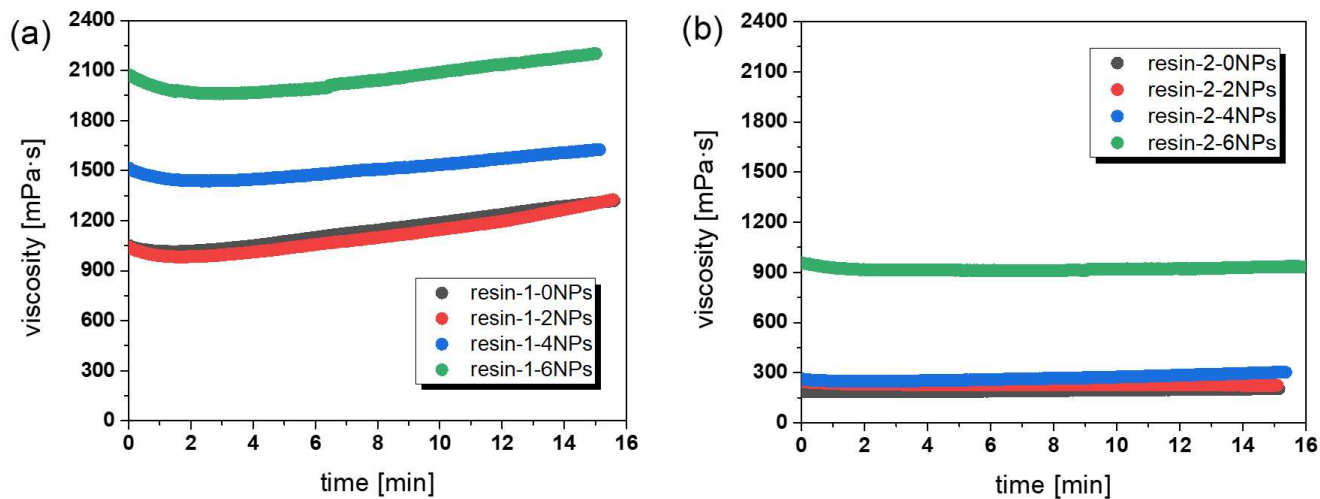


Figure 2. Stability of the resins filled with up to 6 wt% of nanofiller at a constant shear of 300 s⁻¹ (a) published thiol-acrylate vitrimer system (resin-1)³⁶ and (b) modified thiol-acrylate vitrimer system (resin-2).

By increasing the HPPA content from 50 mol% to 65 mol% and by decreasing the thiol content from 25 mol% to 10 mol%, the viscosity of the filled and unfilled resins could be significantly

reduced. In particular, for the unfilled resin, a decrease in the viscosity from 1,320 to 203 mPa·s was observed. Interestingly, the addition of up to 4 wt% of nanofillers did not significantly affect the viscosity compared to the unfilled system (302 versus 203 mPa·s). In contrast, the presence of 6 wt% of nanofillers resulted in a rapid increase in viscosity (934 mPa·s) which is also reported for other systems.^[360] Due to the reduction of the thiol content in resin-2, the stability of the filled and unfilled compounds could be significantly improved compared to the previously studied resin systems.

We studied the cure kinetics by Fourier-transform infrared (FTIR) spectroscopy, in which the C=C-H stretching band of the acrylate groups was monitored at 1616 and 1634 cm^{-1} upon exposure at 405 nm. It should be pointed out that the IR signal at 2575 cm^{-1} , which belongs to the mercapto groups, was too weak to consider for quantitative evaluation. The IR spectrum of resin-2-0NPs (prior to and after light exposure) is provided in Figure S1 in ESI. We studied the acrylate conversion versus the filler content as Fe_3O_4 nanoparticles absorb light in the UV and visible region (internal filter effect). The results clearly show that the presence of the nanofillers slows down the reaction kinetics, albeit at a lower extent as expected (Figure 3). For the unfilled resin, the monomer conversion amounted to 85% after 64 s of light exposure, whilst it decreased to 76% for the system containing 6 wt% filler.

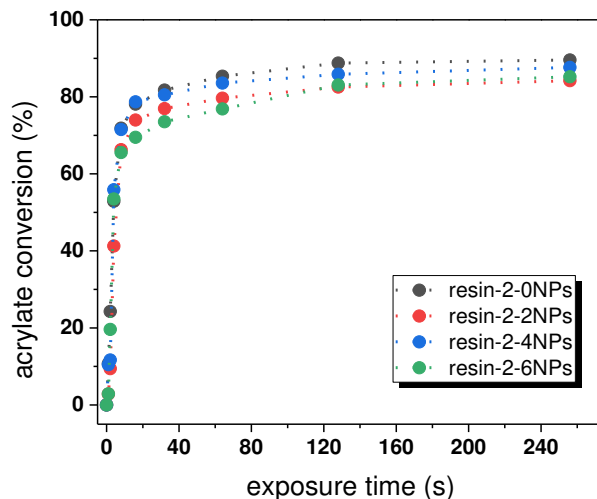


Figure 3. Monitoring the acrylate conversion of resin-2 as a function of the concentration of Fe_3O_4 nanoparticles. The lines are a guide for the eye.

7.3.2 Printing and material characterization

Due to the decent cure rates, it was possible to DLP 3D print test specimen for dynamic mechanical thermal analysis (DMTA) and stress relaxation studies. DMTA was used to study the thermo-mechanical properties of the 3D-printed samples filled with nanofillers in the range of 0 to 6 wt% (Figure 4). When nanoparticles were added to the photocurable formulation, the T_g of the printed composites increased from 45 °C (resin-2-0NPs) to 51 °C (resin-2-6NPs). In previous works, a reduction of the T_g for magneto-responsive nanocomposites based on urethane-acrylate resins was observed and explained by the decrease of the monomer conversion due to competition between the photoinitiator and nanofiller in absorbing radiation during the printing process.^[354]

Interestingly, here we observed a slight increase in the T_g value by introducing nanofillers into the system. On the one hand, this can be explained by the presence of the thiol cross-linkers, which lead to higher carbon double bond conversion due to the mixed mode curing mechanism. Thiols act as chain-transfer agents for the chain-growth polymerization of acrylates and reduce the kinetic chain length. This results in lower diffusion limitations of the reacting monomers and a shift of the gel point to higher conversions.^[361,362]

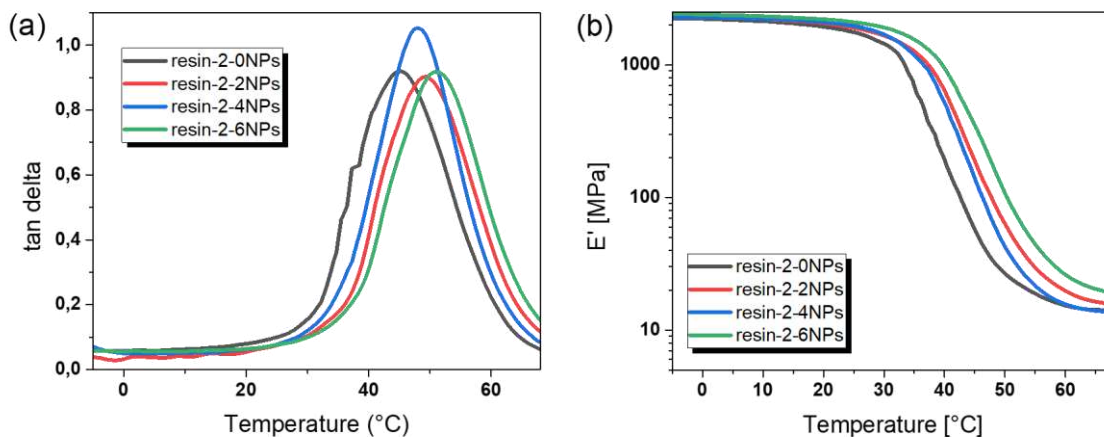


Figure 4. (a) Loss factor ($\tan \delta$) and (b) storage modulus (E') versus temperature as obtained from DMA measurements of resin-2 filled with nanofillers up to 6 wt%.

On the other hand, coordinative bonds might be formed between the Fe_3O_4 nanoparticles and the unreacted thiol groups, which anchor the filler to the photopolymer matrix.^[357] In the presence of the organic phosphate, the photopolymer composites are able to undergo thermo-activated dynamic

bond exchange reactions across the functional -OH and ester groups (transesterification). The change in the viscoelastic properties was studied by rheometer experiments.

Figure 5 provides the time-dependent evolution of the relaxation modulus for resin-2 with varying concentration of nanofillers at 180 °C. While temperature and catalyst in the thiol-acrylate systems have an impact on the stress relaxation kinetics^[358], the results clearly indicate that the addition of nanofillers (and the related slight shift to higher T_g values) does not significantly affect the bond exchange rate within the investigated range of filler concentration.

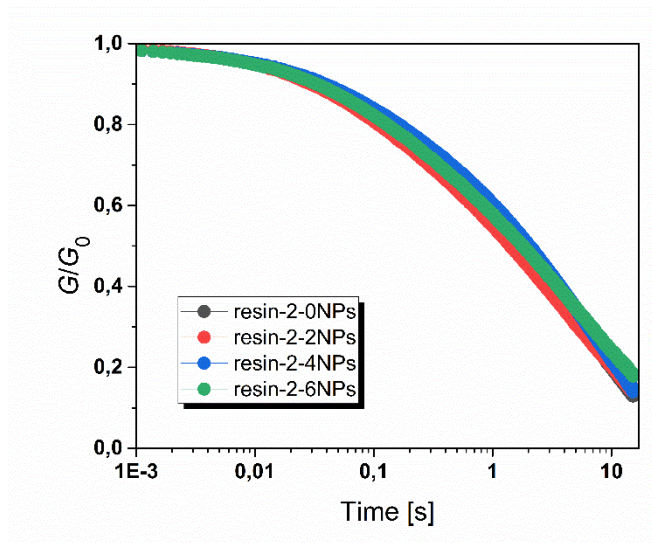


Figure 5. Normalized stress-relaxation curves (obtained at 180 °C) of resin-2 with varying filler concentration.

7.3.3 Thermal healing and magnetic properties

Although resin-2 was printed with up to 6 wt% of nanofillers, we performed further printing studies with resin-2-4NPs to avoid premature gelation during the printing process. To demonstrate the magnetic response of the filled thiol-acrylate vitrimer network, a printed stripe was fixed on one side with tweezers. As is shown in Figure 6a, by applying an external magnetic field (1.24 T), the stick containing 4 wt% of nanofillers could be activated even without physical contact between the magnet and the stick. Moreover, we printed a stickman where every single part was activated separately. It should be noted that we were not able to print more complex structures as premature gelation occurred at a filler concentration of 4 wt% upon prolonged printing time. In addition, the viscosity of the filled resin was too high to print objects with feature sizes lower than 1 mm.

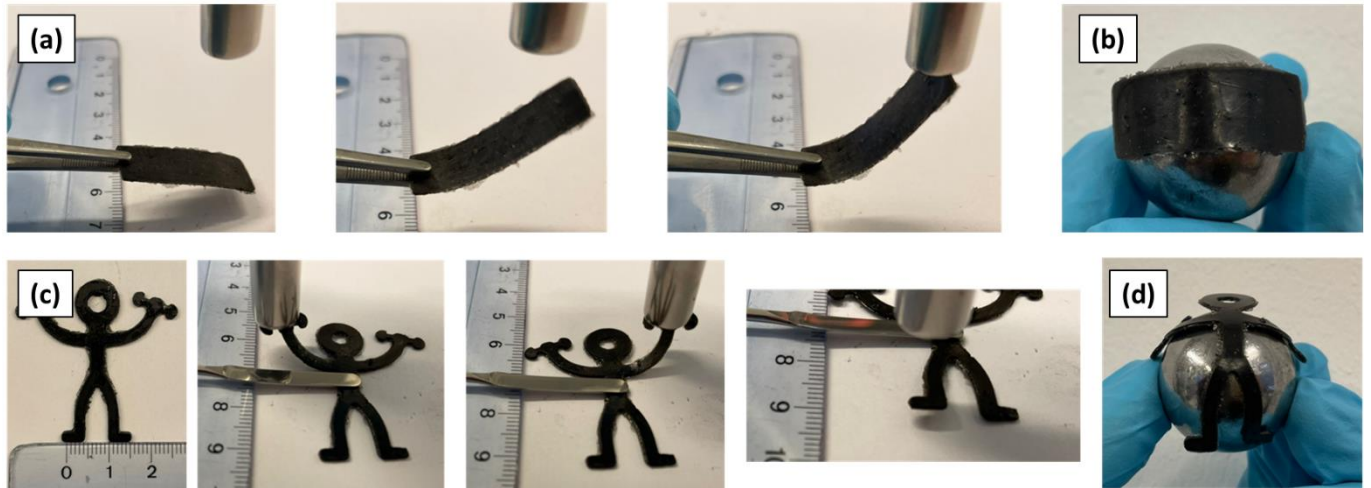


Figure 6. Activation of objects DLP 3D-printed with resin-2 containing 4 wt% of Fe_3O_4 nanoparticles.

Thermal healing of magneto-responsive photopolymers was demonstrated on 3D-printed dumbbell test specimens. An appropriate aligning of thin broken test bars is challenging and thus, test bars with a circular-shaped hole in the center were printed together with the circular-shaped counterpart (Figure 7b).

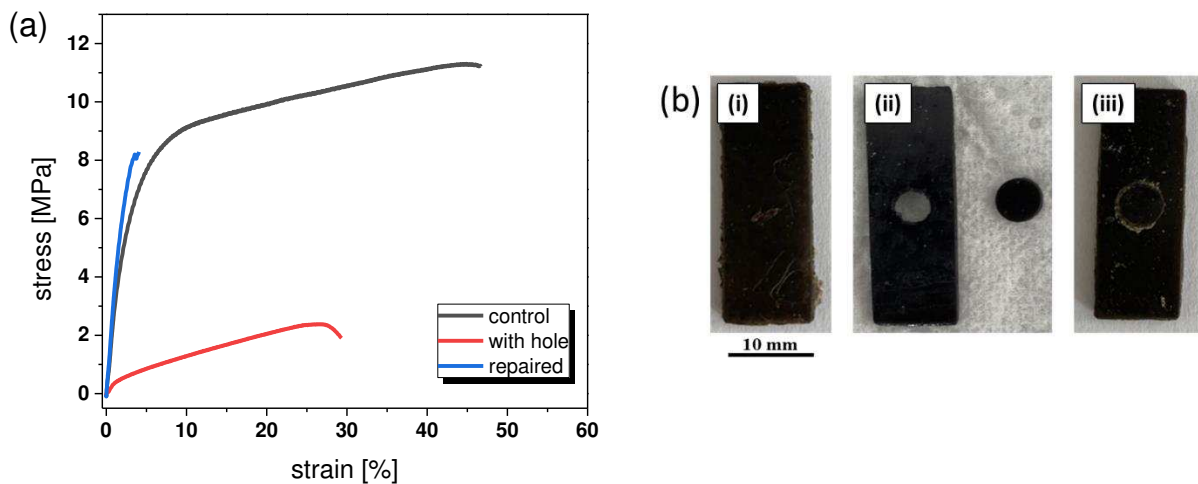


Figure 7. (a) Stress-strain curves of test specimens DLP printed with resin-2 containing 4 wt% of Fe_3O_4 nanoparticles prior to and after a thermal healing at $180\text{ }^\circ\text{C}$ for 4 h, (b) DLP 3D printed test specimen used for thermal healing experiments: (i) DLP printed control sample. (ii) DLP printed test specimen with a circular-shaped hole in the center and DLP printed circular shaped counterpart. (iii) Test specimen after fitting the circular-shaped counterpart in the hole and subsequent thermal treatment.

For the healing step, the disc was fitted in the hole and a thermal healing/welding at 180 °C for 4 h was carried out. Due to the macroscopic reflow, the boundaries between the two parts efficiently welded together and the original tensile strength (defect-free bar) could be partly recovered. The defect-free control samples (Figure 7b) resulted in a tensile strength of 11.2 MPa and an ultimate elongation of 46 %. In contrast, the tensile strength of the sample, which contained the hole, was drastically reduced to 2.3 MPa with an elongation of 27.9 %.

Due to the thermally triggered repair process, the tensile strength could be regained to a large extent (8.1 MPa), whilst the elongation (3.9 %) was even lower than the value measured for the sample containing the hole. Whilst the test bars were breaking nearly in the center (Figure S2 in ESI), the fracture behavior changed. Since this behavior was not observed in our previous studies on the healing of unfilled dynamic photopolymer networks, we assume that this change in damage behavior is mainly related to the fillers present in the dynamic thiol-acrylate composite.

Along with mechanical performance, the magnetic properties were determined prior to and after thermally induced welding. Room-temperature hysteresis loops of 3D-printed control and welded samples are shown in Figure 8. The hysteresis curves and the magnetic characteristics of both types of samples (control and welded) are comparable. The coercivities are around 80 Oe (control sample) and 75 Oe (welded sample). Due to the low coercivity at room temperature, one can assume a superparamagnetic behavior, which does not change due to the thermo-activated healing process. The results indicate that the magnetic properties are not affected by the thermal healing step, which has been carried out at 180 °C for 4 h.

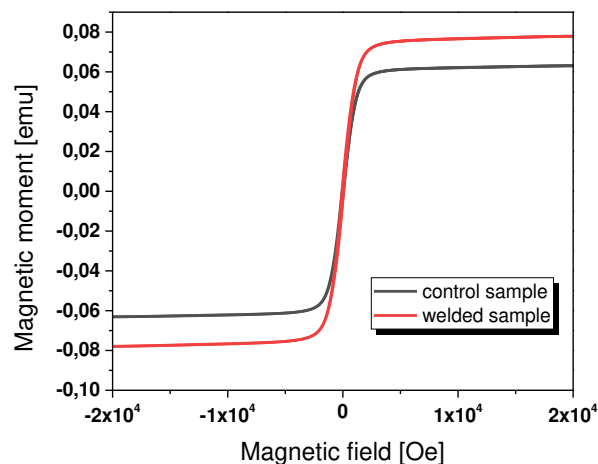


Figure 8. Room temperature hysteresis loops of 3D-printed magnetic composites from resin-2-4NPs prior to and after welding at 180 °C for 4 h.

7.4 Experimental

7.4.1 Materials and chemicals

2-Hydroxy-2-phenoxypropyl acrylate (HPPA), glycerol 1,3-diglycerolate diacrylate (GDGDA), trimethylolpropane tri(3-mercaptopropionate) (TMPMP), Fe(II,III) oxide nanoparticles ($d_{50} = 50$ nm), and phenylbis(2,4,6-trimethylbenzoyl) phosphine oxide (BAPO) were purchased from Sigma-Aldrich. Miramer A99 was used as stabilizer and transesterification catalyst, and was received from Miwon Speciality Chemical (Korea). All chemicals were used without further purification.

7.4.2 Preparation of resins

Preparation of resin-1: HPPA (50 mol%) was mixed with GDGDA (25 mol%) and 5 wt% Miramer A99. 0.05 wt% Sudan II was added and the formulation was ultra-sonicated until the photoabsorber was dissolved. 3 wt% phenylbis(2,4,6-trimethylbenzoyl)phosphine oxide and TMPMP (25 mol%) were added and dissolved by stirring the formulation at room temperature for 30 min.

Preparation of resin-2: HPPA (65 mol%) was mixed with GDGDA (25 mol%) by means of a magnetic stirrer at room temperature. Subsequently, 5 wt% of phenylbis(2,4,6-trimethylbenzoyl) phosphine oxide and 5 wt% Miramer A99 were added and the formulations were ultra-sonicated at 40 °C until all components were dissolved. After cooling to room temperature, TMPMP (10 mol%) and Fe₃O₄ nanoparticles were added. The prepared formulation was manually stirred with a spatula and sonicated for 1 min at room temperature.

7.4.3 Characterization

Fourier transform infrared spectroscopy was studied on a Vertex 70 spectrometer (Bruker, USA). Spectra were taken in transmittance mode over a wavenumber range from 4000 to 700 cm⁻¹. All spectra were accumulated from 16 scans at a resolution of 4 cm⁻¹ and the absorption peak areas were calculated with OPUS software. For sample preparation, 1.5 μL of resin was drop cast between two CaF₂ discs. Samples were irradiated with a light emitting diode lamp (zgood® wireless LED curing lamp) with a power density of 3.3 mWcm⁻² ($\lambda = 420 - 450$ nm). The conversion at corresponding exposure times were calculated with OPUS software by evaluating the decrease of the characteristic acrylate infrared absorption band at 1620 - 1636 cm⁻¹.

The viscosity of the formulations was determined with a modular compact rheometer MCR 102 from Anton Paar (Austria) in a parallel plate set up with a 25 mm diameter. Each measurement was carried out with 0.5 mL formulation at room temperature and a shear rate ranging between 0.1 and 300 s⁻¹. The same measuring setup was utilized to determine the stability of the resins by applying a shear rate of 300 s⁻¹ over 14 min.

Dynamic mechanical analysis (DMA) was carried out on a Mettler Toledo DMA/SDTA861e analyzer. Mechanical loss factors ($\tan \delta$) and storage moduli (E') were monitored over a temperature range from -25 to 70 °C at a heating rate of 3 °C/min, with a frequency of 1 Hz, in a displacement-controlled mode with maximum amplitude 10 μm and maximum force of 5 N. The glass transition temperature (T_g) was determined by the temperature at the maximum of the loss factor. For sample preparation, test specimen (30 mm × 4 mm × 1 mm) were 3D printed with resin-**2** using a commercial printer from Anycubic (China).

Mechanical properties were characterized by a ZwickRoell (Germany) Z1.0 static materials testing machine with a crosshead speed of 250 mm min⁻¹. Tensile tests were performed on 3D printed dumbbell specimens (resin-**2** filled with 4 wt% nanoparticles) with the dimensions of 2 x 12.5 x 75 mm.

Stress relaxation experiments were carried out at 180 °C on an Anton Paar Physica MCR 501 rheometer (Austria) with parallel plate geometry. Printed samples (10 x 1 mm) of resin-**2** were equilibrated to the set temperature and a specified constant normal force of 20 N was applied for 15 min. Subsequently, 3% step strain was applied and the decreasing stress was recorded over time.

7.4.4 DLP 3D printing

3D printing was performed on an Anycubic Photo Mono printer (China) with a LED 405 m light source. Two bottom layers were exposed for 24 s, whereas the other layers were illuminated for 5 s. The layer height was set to 50 μm with a building speed of 6 mm s⁻¹ and a retracting speed of 1 mm s⁻¹.

7.4.5 Thermo-activated healing

Both, the control sample and the defect sample with a hole had dimensions of 30 × 10 × 1.5 mm and were printed together with the corresponding disc (d = 5 mm) *via* DLP 3D printing using resin-**2** filled with 4 wt% of nanofillers. For the thermal healing, the printed disc was fitted inside the hole and the samples were heated to 180 °C for 4 h.

7.4.6 Welding experiments and magnetic properties

Three discs (10 x 1 mm) were printed with resin-2 containing 4 wt% of nanofillers. Welding of two discs was achieved by pressing the discs over each other and heating at 180 °C for 4 h. Magnetic properties of control and welded samples were measured with a vibrating sample magnetometer (8600 Series VSM System, Lake Shore) at room temperature. The magnetic field was applied perpendicular to the sample surface in a range between +/- 1 T.

7.5 Conclusions

In summary, we have prepared DLP 3D printable thiol-acrylate resins containing magneto-active fillers and dynamic covalent bonds, which rendered the cured photopolymers malleable and thermally mendable. Whilst viscosity and T_g increased with rising filler content, the cure kinetics decreased due to the competition between the nanofiller and the photoinitiator resulting in a slight delay in the photopolymerization process. At a concentration of 4 wt% nanofillers, objects with a simple geometry could be DLP 3D printed and their activation by an external magnetic field was demonstrated. Due to thermo-activated transesterifications, the photopolymers were weldable and thermally healable. Both control and welded samples showed supermagnetic behavior after thermal treatment at 180 °C for 4 hours and the magnetic properties did not significantly change during the welding step. In addition, thermal healing of printed test bars was demonstrated giving rise to the versatility and functionality of the developed resin system.

7.6 Acknowledgements

The research work was performed within the COMET-Module project “Chemitecture” (project-no. 21647048) at the Polymer Competence Center Leoben GmbH (PCCL, Austria) within the framework of the COMET-program of the Federal Ministry for Transport, Innovation and Technology and the Federal Ministry for Digital and Economic Affairs with contributions by Montanuniversitaet Leoben, Politecnico di Torino, Helios TBLUS and bto-epoxy. Funding is provided by the Austrian Government and the State Government of Styria. In addition, the authors thank David Reisinger (PCCL) for performing stress-relaxation experiments and Walter Alabiso (PCCL) for carrying out the DMA measurements.

7.7 Supporting Information

Digital Light Processing 3D Printing of Dynamic Magneto-Responsive Thiol-Acrylate Composites

Ines Cazin^a, Elisabeth Rossegger^a, Ignazio Roppolo^b, Marco Sangermano^b, Petra Granitzer^c, Klemens Rumpf^c, Sandra Schlögl^{a*}

a. Polymer Competence Center Leoben GmbH, Roseggerstrasse 12, A-8700 Leoben

b. Department of Applied Science and Technology, Politecnico di Torino, Duca degli Abruzzi, 24, 10124, Torino, Italy

c. Institute of Physics, Universitätsplatz 3, 8010 Graz, Austria

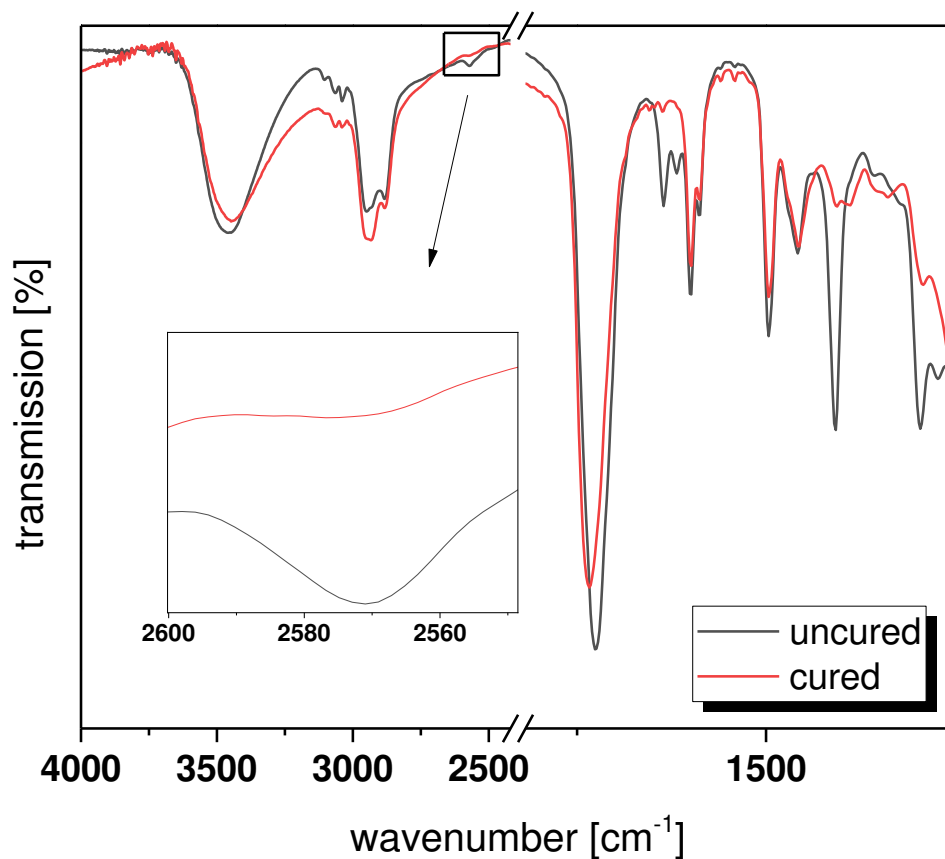


Figure S1. FTIR spectrum of resin-2-ONPs prior to and after photocuring.

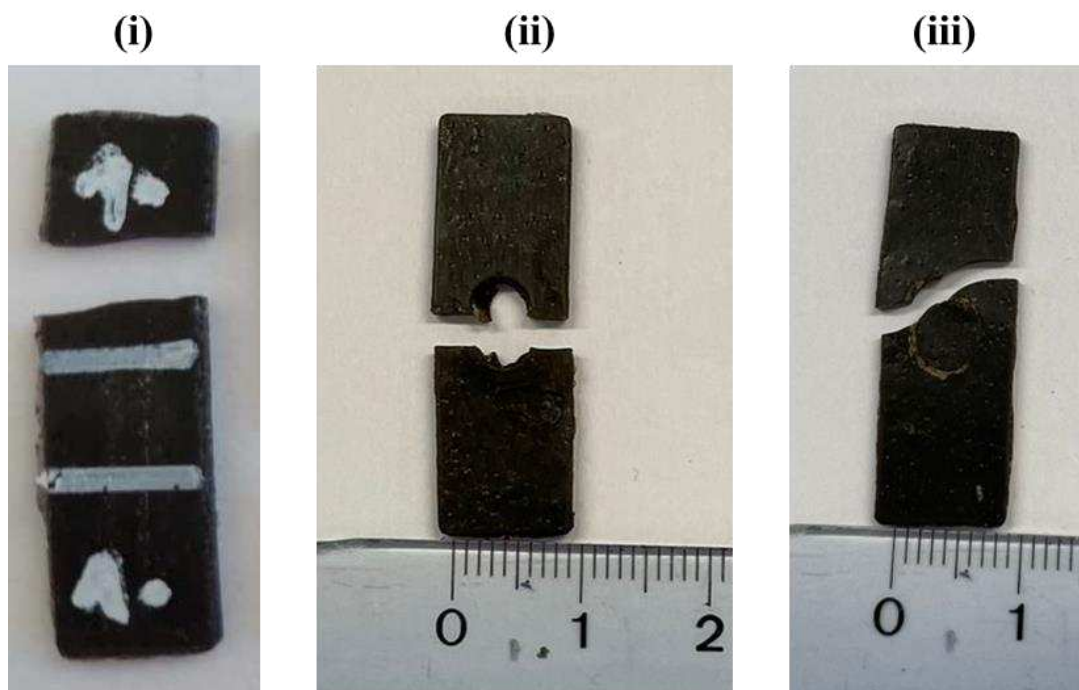


Figure S2. DLP printed test specimens containing 4 wt% of Fe_3O_4 nanoparticles after tensile testing. (i) DLP printed control sample. (ii) DLP printed test specimen with a circular-shaped hole in the center. (iii) Self-healed tensile specimen.

8 Conclusions and outlook

In conclusion, the first part of this dissertation presents a developed resin for multi-material additive manufacturing by vat photopolymerization. The research field is new, and only a few publications are published on this topic to date. Developed and optimized dual curable resin consisted of 50 wt% of mono-functional acrylates and 50 wt% of bi-functional epoxy monomers (dual resin-D50:E50). The wavelength-selective network formation was confirmed by FT-IR experiments, where acrylate groups showed fast conversion, whilst epoxy monomers required an additional thermal post-baking step for 2 hours at 120 °C to obtain a higher degree of conversion. Furthermore, tensile tests and dynamic mechanical analysis showed distinctive differences in the related mechanical properties. The printing experiments were carried out with a dual-wavelength DLP printer prototype, operating at 405 and 365 nm. The optimized printing conditions enabled fast printing (with a layer cure time within seconds) of multi-material objects. It is interesting to note that by simply switching the wavelength of the light source, the mechanical properties (e.g. Young's modulus) of the printed objects could be locally adjusted over two orders of magnitude. By using commercially available resins and photoinitiators, 3D objects with heterogeneous properties in the mm-range and good interfacial adhesion between soft and stiff areas were fabricated. Possible application fields of the developed materials include soft robotics and soft actuators (e.g. soft robotic locomotion, grippers). In the field of shape memory polymers, the functionality can be tuned by locally controlling the glass transition temperature in the mm-range. The presented system has the potential for application in macroscopic composite structures, e.g. functional orthoses and prosthetics, comprising soft areas, which are in contact with the human body, and stiff regions that ensure the structural robustness of the devices. The tested heterogeneous specimens showed good interlayer adhesion which can be explained by the diffusion of the cationic initiating species from an area illuminated with 365 nm to an area illuminated with 405 nm during the printing process and thermal post-baking step. Therefore, no sharp interface properties were obtained between soft and rigid domains. Further studies should explore a blocking of the diffusion of cationic initiating species from rigid to soft domains. One way to overcome this is the covalent attachment of the photolabile acid within the polymer matrix during the visible curing process at 405 nm.

The orthogonal chemistry approach to spatially control layer-by-layer network formation shows the advantage of using a single resin formulation where the potential for contamination with a

second monomer is minimized. This method, however, has a limitation on the selection of functional monomers available commercially, and most importantly orthogonal chemistry precursors must be miscible. Integration of additional light sources is necessary, with hardware and software to change the different light sources during the manufacturing of 3D multi-material objects.

Furthermore, the influence of resin composition and light source on the microscopic film morphology and macroscopic thermomechanical and mechanical properties of dual wavelength 3D printed objects were investigated. In particular, dual curable acrylate-epoxy resins with varying monomer ratios (dual resin-D75:E25, dual resin-D50:E50, and dual resin-D25:E75) were used. Generally, tensile strength, stiffness, and glass transition temperature increased with a higher amount of epoxy monomer. It is important to note that a higher amount of epoxy monomer in combination with a higher epoxy concentration had a negative effect on the system orthogonality. This can be explained by a higher amount of photoacid generator (weight was calculated according to the weight of ECC) and its higher reduction potential and susceptibility to sensitization through Irgacure 819's free radical oxidation. Moreover, as a function of the resin composition and applied wavelength, the phase distribution images obtained by AFM did show significant differences in the film morphology. Interpenetrating networks with a homogeneous morphology as well as heterogeneous networks with distinct phase separation (visible-light-cured dual resin-D50:E50) were formed, depending on the degree of cure and the presence of uncured monomer. The rising content of epoxy monomers cured by UV light exposure significantly affected thermomechanical and mechanical properties.

Future studies should be focused on investigating the loss in the orthogonality between two photoreactions by changing the monomer compositions, therefore optimization of radical and cationic photoinitiators is necessary. Moreover, further tests should be focused on unreacted monomers in printed materials since they can affect mechanical properties by migration under higher temperatures due to post-polymerization reactions.

The second part of the thesis was focused on the synthesis and characterization of DLP 3D-printable bio-based polyester resins. Herein, a commercially available petroleum-based benchmark resin (PEA) was step-wise replaced with monomer building blocks based on bio-based alternatives. For PEA-BIO-1, 1,6-hexanediol was substituted with bio-based 1,3-propanediol, and adipic acid was replaced with bio-based succinic and sebacic acid. In the synthesis of PEA-BIO-2, the bio-

based isosorbide was additionally introduced instead of cyclohexane dimethanol. Finally, for PEA-BIO-3, having the highest content of bio-based precursors, itaconic acid was additionally used instead of acrylic acid. Although cure kinetics decreases with increasing the content of bio-based alternatives, the first two synthesized resins (PEA-BIO-1 and PEA-BIO-2) were printed with a build speed of 15 to 17 seconds per layer (100 μm layer thickness). Therefore, the first two resins increase the usage of environmentally friendly and sustainable materials in the future vat photopolymerization printing and applications (e.g. multi-material structures and soft active devices). Further study should explore the improvement of polymerization kinetics and viscosity reduction of PEA-BIO-3 resin.

The usage of bio-based resins in DLP 3D printing is a promising technology due to a growing market demand for sustainable materials with biodegradability and reduced toxicity. Moreover, bio-based resins can enhance mechanical properties, such as improved mechanical strength, flexibility, and biocompatibility. In the present work, the process for printing resins with high bio-based content was successfully developed. The resins can be used in the printing of multi-material structures or future applications such as soft active devices. Future work should be focused on developing resins with the highest amount of bio-based content with sufficient properties for processing with vat photopolymerization. For this, the viscosity and reactivity should be adjusted.

In the third part of the thesis, DLP 3D-printed thiol-acrylate resins containing magneto-active fillers and dynamic covalent bonds were presented. The photocurable resin was filled only up to 4 wt% of nanofillers due to a delay in the photopolymerization process with an increasing amount of nanofillers. The crucial parameters in vat photopolymerization 3D printing are the viscosity and shelf life of the resin. The photocurable resin was tested with varying content of magnetic nanofillers up to 6%. According to rheological data, the viscosity increases with the increase of nanofiller concentration in the resin and remains stable over 15 minutes. However, it is still below the range of 1000 mPa s, which is still within the range (250 and 5000 mPa s) of 3D DLP printable resins. FTIR spectroscopy confirms slower reaction kinetics in the presence of the nanofillers. After the addition of nanofillers, T_g of the printed composites increased from 45 °C (non-filled resin) to 51 °C (resin with 6% of nanofillers). Due to thermo-activated transesterifications, the 3D-printed photopolymers were weldable and thermally healable. Moreover, the healing performance was demonstrated by recovering mechanical and magnetic properties after the thermally triggered mending of 3D-printed structures. The magnetically driven movement of 3D-printed samples was

additionally demonstrated, which materials give potential to use in healable soft devices activated by external magnetic fields.

The current doctoral thesis opens up new horizons in the vat photopolymerization 3D printing based on orthogonal chemistry mechanisms and a dual-wavelength approach. The developed method offers not only a promising solution for manufacturing multi-material objects with significant differences in soft and stiff polymer networks but also explains and clarifies the orthogonal mechanism dependent on the light source, resin composition, and amounts of photoinitiators. Moreover, applications of the technology in the fabrication of macroscopic composites are highly promising. Examples are functional orthoses and prostheses, which have stiff sections that guarantee the devices' structural integrity, and soft sections that come into contact with the human body. Printed objects with multi-material domains in the mm-range and good interface properties (confirmed by testing heterogeneous specimens) can be used in soft robotic systems (e.g. grippers, soft robotic locomotion) and macroscopic soft actuators. The thesis also covers the development of bio-based resins that can be processed by vat photopolymerization 3D printing. The implementation of bio-based resins in additive manufacturing is crucial for both scientific community and the industry sector due to environmental sustainability by reducing the usage of fossil fuels. To date, they are the driving force in developing innovative and biodegradable materials.

9 References

- [1] Z. Li, X. Zou, G. Zhu, X. Liu, R. Liu, *ACS applied materials & interfaces* **2018**, *10*, 16113.
- [2] H. Pan, S. Chen, M. Jin, J.-P. Malval, D. Wan, F. Morlet-Savary, *Polym. Chem.* **2019**, *10*, 1599.
- [3] E. Hola, J. Ortyl, M. Jankowska, M. Pilch, M. Galek, F. Morlet-Savary, B. Graff, C. Dietlin, J. Lalevée, *Polym. Chem.* **2020**, *11*, 922.
- [4] Q. Jiang, M. Zhang, A. S. Mujumdar, *Trends in food science & technology* **2020**, *105*, 200.
- [5] S. Cuadros, J. Paut, E. Anselmi, G. Dagousset, E. Magnier, L. Dell'Amico, *Angewandte Chemie (International ed. in English)* **2024**, *63*, e202317333.
- [6] C. Sattler, F.-J. Müller, K.-J. Riffelmann, J. Ortner, K.-H. Funken, *J. Phys. IV France* **1999**, *09*, Pr3-723-Pr3-727.
- [7] J. P. Fouassier, J. F. Rabek, *Radiation curing in polymer science and technology*, Elsevier Applied Sci, London **1993**.
- [8] X. He, L. Zang, Y. Xin, Y. Zou, *Applied Research* **2023**, *2*.
- [9] S. Chatani, C. J. Kloxin, C. N. Bowman, *Polym. Chem.* **2014**, *5*, 2187.
- [10] S. Aubert, M. Bezagu, A. C. Spivey, S. Arseniyadis, *Nat Rev Chem* **2019**, *3*, 706.
- [11] H. Frisch, D. E. Marschner, A. S. Goldmann, C. Barner-Kowollik, *Angewandte Chemie (International ed. in English)* **2018**, *57*, 2036.
- [12] M. M. Lerch, M. J. Hansen, W. A. Velema, W. Szymanski, B. L. Feringa, *Nature communications* **2016**, *7*, 12054.
- [13] W. Szymański, J. M. Beierle, H. A. V. Kistemaker, W. A. Velema, B. L. Feringa, *Chemical reviews* **2013**, *113*, 6114.
- [14] G. Ciamician, *Science (New York, N.Y.)* **1912**, *36*, 385.
- [15] D. H. R. Barton, P. de Mayo, M. Shafiq, *J. Chem. Soc.* **1958**.
- [16] HERBERT A. J., *Jour Appl Photo Eng* **1982**,
<https://cir.nii.ac.jp/crid/1570291224116690304>.

- [17] C. W. Hull, *Apparatus for production of three-dimensional objects by stereolithography*, Google Patents **1986**.
- [18] J. C. André, A. Le Mehaute, O. de Witte, *French Patent FR* **1984**, 2, 567.
- [19] K. L. Sampson, B. Deore, A. Go, M. A. Nayak, A. Orth, M. Gallerneault, P. R. L. Malenfant, C. Paquet, *ACS Appl. Polym. Mater.* **2021**, 3, 4304.
- [20] A. Albini, M. Fagnoni, *Green Chem.* **2004**, 6, 1.
- [21] R. Bongiovanni, S. D. Vacche, A. Vitale, *Polymers* **2021**, 13.
- [22] A. Albini, M. Fagnoni, M. Mella, *Pure and Applied Chemistry* **2000**, 72, 1321.
- [23] B. Wardle, *Principles and Applications of Photochemistry*, John Wiley & Sons, Incorporated, Newark **2010**.
- [24] W. Mäntele, E. Deniz, *Spectrochimica acta. Part A, Molecular and biomolecular spectroscopy* **2017**, 173, 965.
- [25] D. Frackowiak, *Journal of Photochemistry and Photobiology B: Biology* **1988**, 2, 399.
- [26] J. Zimmermann, A. Zeug, B. Röder, *Phys. Chem. Chem. Phys.* **2003**, 5, 2964.
- [27] M. Nocita, A. Stevens, C. Noon, B. van Wesemael, *Geoderma* **2013**, 199, 37.
- [28] J. Zwinkels, in *Encyclopedia of Color Science and Technology* (Ed.: R. Luo), Springer Berlin Heidelberg. Berlin, Heidelberg **2014**, p. 1.
- [29] C. Dietlin, T. T. Trinh, S. Schweizer, B. Graff, F. Morlet-Savary, P.-A. Noirot, J. Lalevée, *Molecules (Basel, Switzerland)* **2020**, 25.
- [30] X. He, Y. Gao, J. Nie, F. Sun, *Macromolecules* **2021**, 54, 3854.
- [31] F. Petko, M. Galek, E. Hola, R. Popielarz, J. Ortyl, *Macromolecules* **2021**, 54, 7070.
- [32] M. Topa, E. Hola, M. Galek, F. Petko, M. Pilch, R. Popielarz, F. Morlet-Savary, B. Graff, J. Lalevée, J. Ortyl, *Polym. Chem.* **2020**, 11, 5261.
- [33] M. Jin, R. Zhou, M. Yu, H. Pan, D. Wan, *J. Polym. Sci. A Polym. Chem.* **2018**, 56, 1146.
- [34] H. Salmi, X. Allonas, C. Ley, A. Defoin, A. Ak, *Polym. Chem.* **2014**, 5, 6577.
- [35] H. Salmi, X. Allonas, C. Ley, *Progress in Organic Coatings* **2016**, 100, 81.

- [36] X. Dong, P. Hu, G. Zhu, Z. Li, R. Liu, X. Liu, *RSC Adv.* **2015**, *5*, 53342.
- [37] C. N. Bowman, C. J. Kloxin, *AIChE Journal* **2008**, *54*, 2775.
- [38] U. Shaukat, E. Rossegger, S. Schlögl, *Polymers* **2022**, *14*.
- [39] X. Ma, R. Gu, L. Yu, W. Han, J. Li, X. Li, T. Wang, *Polym. Chem.* **2017**, *8*, 6134.
- [40] E. Paruli, III, O. Soppera, K. Haupt, C. Gonzato, *ACS Appl. Polym. Mater.* **2021**, *3*, 4769.
- [41] J. Zhou, X. Allonas, A. Ibrahim, X. Liu, *Progress in Polymer Science* **2019**, *99*, 101165.
- [42] X. Allonas, J. P. Fouassier, M. Kaji, M. Miyasaka, T. Hidaka, *Polymer* **2001**, *42*, 7627.
- [43] J. Kabatc, J. Paćzkowski, *Dyes and Pigments* **2010**, *86*, 133.
- [44] J. V. Crivello, J. H. W. Lam, *Macromolecules* **1977**, *10*, 1307.
- [45] J. V. Crivello, J. H. W. Lam, *J. Polym. Sci. Polym. Chem. Ed.* **1979**, *17*, 977.
- [46] F. Zhang, L. Zhu, Z. Li, S. Wang, J. Shi, W. Tang, N. Li, J. Yang, *Additive Manufacturing* **2021**, *48*, 102423.
- [47] L. Zhang, L. Li, Y. Chen, J. Pi, R. Liu, Y. Zhu, *Polymers* **2023**, *15*.
- [48] J. V. Crivello, S. Liu, *J. Polym. Sci. A Polym. Chem.* **2000**, *38*, 389.
- [49] N. Klikovits, P. Knaack, D. Bomze, I. Krossing, R. Liska, *Polym. Chem.* **2017**, *8*, 4414.
- [50] Q. Michaudel, V. Kottisch, B. P. Fors, *Angewandte Chemie (International ed. in English)* **2017**, *56*, 9670.
- [51] I. Cazin, M. O. Gleirscher, M. Fleisch, M. Berer, M. Sangermano, S. Schlögl, *Additive Manufacturing* **2022**, *57*, 102977.
- [52] I. Cazin, K. Plevová, W. Alabiso, E. Vidović, S. Schlögl, *Adv Eng Mater* **2024**.
- [53] N. Shahrubudin, T. C. Lee, R. Ramlan, *Procedia Manufacturing* **2019**, *35*, 1286.
- [54] X. Cheng, L. J. Guo, P.-F. Fu, *Advanced materials (Deerfield Beach, Fla.)* **2005**, *17*, 1419.
- [55] L. J. Guo, *Advanced Materials* **2007**, *19*, 495.
- [56] M. Tsunooka, K. Suyama, H. Okumura, M. Shirai, *J. Photopol. Sci. Technol.* **2006**, *19*, 65.
- [57] C. J. Martin, G. Rapenne, T. Nakashima, T. Kawai, *Journal of Photochemistry and Photobiology C: Photochemistry Reviews* **2018**, *34*, 41.

- [58] N. Zivic, P. K. Kuroishi, F. Dumur, D. Gigmes, A. P. Dove, H. Sardon, *Angewandte Chemie* **2019**, *131*, 10518.
- [59] H.-W. Pei, K. Ye, Y. Shao, D. Chen, Z.-Y. Sun, T. Gong, D. Liu, K. Sun, *Polym. Chem.* **2024**, *15*, 248.
- [60] M. Ahmadi, K. Ehrmann, T. Koch, R. Liska, J. Stampfl, *Chemical reviews* **2024**, *124*, 3978.
- [61] S. C. Ligon, R. Liska, J. Stampfl, M. Gurr, R. Mülhaupt, *Chemical reviews* **2017**, *117*, 10212.
- [62] S. Saleh Alghamdi, S. John, N. Roy Choudhury, N. K. Dutta, *Polymers* **2021**, *13*.
- [63] N. T. Tuli, S. Khatun, A. B. Rashid, *Heliyon* **2024**, *10*, e27328.
- [64] K. V. Wong, A. Hernandez, *ISRN Mechanical Engineering* **2012**, *2012*, 1.
- [65] A. Bagheri, J. Jin, *ACS Appl. Polym. Mater.* **2019**, *1*, 593.
- [66] B. Steyrer, P. Neubauer, R. Liska, J. Stampfl, *Materials (Basel, Switzerland)* **2017**, *10*.
- [67] F. Ning, W. Cong, J. Qiu, J. Wei, S. Wang, *Composites Part B: Engineering* **2015**, *80*, 369.
- [68] X. Tian, T. Liu, C. Yang, Q. Wang, D. Li, *Composites Part A: Applied Science and Manufacturing* **2016**, *88*, 198.
- [69] N. Fomina, J. Sankaranarayanan, A. Almutairi, *Advanced drug delivery reviews* **2012**, *64*, 1005.
- [70] M. Pape, *Pure and Applied Chemistry* **1975**, *41*, 535.
- [71] C.-H. Lin, Y.-M. Lin, Y.-L. Lai, S.-Y. Lee, *The Journal of prosthetic dentistry* **2020**, *123*, 349.
- [72] G. Gomez-Gras, R. Jerez-Mesa, J. A. Travieso-Rodriguez, J. Lluma-Fuentes, *Materials & Design* **2018**, *140*, 278.
- [73] F. Zhao, D. Li, Z. Jin, *Materials (Basel, Switzerland)* **2018**, *11*.
- [74] T. J. Wallin, J. Pikul, R. F. Shepherd, *Nat Rev Mater* **2018**, *3*, 84.
- [75] V. G. Rocha, E. Saiz, I. S. Tirichenko, E. García-Tuñón, *J. Mater. Chem. A* **2020**, *8*, 15646.
- [76] S. V. Murphy, A. Atala, *Nature biotechnology* **2014**, *32*, 773.

- [77] S. A. Khan, I. Lazoglu, *Prog Addit Manuf* **2020**, *5*, 153.
- [78] A. Mazzoli, *Medical & biological engineering & computing* **2013**, *51*, 245.
- [79] I. Gibson, D. Shi, *Rapid Prototyping Journal* **1997**, *3*, 129.
- [80] K.-F. Leong, D. Liu, C.-K. Chua, in *Comprehensive Materials Processing*, Elsevier **2014**, p. 251.
- [81] H. Quan, T. Zhang, H. Xu, S. Luo, J. Nie, X. Zhu, *Bioactive materials* **2020**, *5*, 110.
- [82] Z. Zhu, *IEEE Photonics J.* **2023**, *15*, 1.
- [83] M. Pfaffinger, *Laser Technik Journal* **2018**, *15*, 45.
- [84] C. Dall'Argine, A. Hochwallner, N. Klikovits, R. Liska, J. Stampf, M. Sangermano, *Macro Materials & Eng* **2020**, 305.
- [85] F. Sameni, B. Ozkan, H. Zarezadeh, S. Karmel, D. S. Engstrøm, E. Sabet, *Polymers* **2022**, *14*.
- [86] B. Steyrer, B. Buseti, G. Harakály, R. Liska, J. Stampfl, *Additive Manufacturing* **2018**, *21*, 209.
- [87] S. Wu, J. Serbin, M. Gu, *Journal of Photochemistry and Photobiology A: Chemistry* **2006**, *181*, 1.
- [88] H. B. Sun, S. Kawatal, *TwoPhoton Photopolymerization and 3D Lithographic Micro fabrication. APS*, *170*, 169-273 **2004**.
- [89] T. Tanaka, H.-B. Sun, S. Kawata, *Applied Physics Letters* **2002**, *80*, 312.
- [90] Z. Faraji Rad, P. D. Prewett, G. J. Davies, *Microsystems & nanoengineering* **2021**, *7*, 71.
- [91] Y. Shou, *MRS Bulletin* **2021**, *46*, 12.
- [92] P. N. Bernal, P. Delrot, D. Loterie, Y. Li, J. Malda, C. Moser, R. Levato, *Advanced Materials* **2019**, *31*, e1904209.
- [93] B. E. Kelly, I. Bhattacharya, H. Heidari, M. Shusteff, C. M. Spadaccini, H. K. Taylor, *Science (New York, N.Y.)* **2019**, *363*, 1075.
- [94] J.-W. Choi, H.-C. Kim, R. Wicker, *Journal of Materials Processing Technology* **2011**, *211*, 318.

- [95] T. J. Wallin, J. H. Pikul, S. Bodkhe, B. N. Peele, B. C. Mac Murray, D. Therriault, B. W. McEnerney, R. P. Dillon, E. P. Giannelis, R. F. Shepherd, *Journal of materials chemistry. B* **2017**, *5*, 6249.
- [96] V. M. Vaz, L. Kumar, *AAPS PharmSciTech* **2021**, *22*, 49.
- [97] X. Wang, M. Jiang, Z. Zhou, J. Gou, D. Hui, *Composites Part B: Engineering* **2017**, *110*, 442.
- [98] V. Truxova, J. Safka, M. Seidl, I. Kovalenko, L. Volensky, M. Ackermann, *MM SJ* **2020**, *2020*, 3905.
- [99] D. E. Mouzakis, in *Lamination - Theory and Application* (Ed.: C. A. Osheku), InTech **2018**.
- [100] A. Luongo, V. Falster, M. B. Doest, M. M. Ribo, E. R. Eiriksson, D. B. Pedersen, J. R. Frisvad, *Computer Graphics Forum* **2020**, *39*, 347.
- [101] J. Zhang, P. Xiao, *Polym. Chem.* **2018**, *9*, 1530.
- [102] S. C. Ligon-Auer, M. Schwentenwein, C. Gorsche, J. Stampfl, R. Liska, *Polym. Chem.* **2016**, *7*, 257.
- [103] C. E. Hoyle, C. N. Bowman, *Angewandte Chemie (International ed. in English)* **2010**, *49*, 1540.
- [104] J. V. Crivello, E. Reichmanis, *Chem. Mater.* **2014**, *26*, 533.
- [105] D. G. Moore, L. Barbera, K. Masania, A. R. Studart, *Nature materials* **2020**, *19*, 212.
- [106] P. Robles-Martinez, X. Xu, S. J. Trenfield, A. Awad, A. Goyanes, R. Telford, A. W. Basit, S. Gaisford, *Pharmaceutics* **2019**, *11*.
- [107] Y. Lu, S. N. Mantha, D. C. Crowder, S. Chinchilla, K. N. Shah, Y. H. Yun, R. B. Wicker, J.-W. Choi, *Biofabrication* **2015**, *7*, 45001.
- [108] K. Arcaute, B. Mann, R. Wicker, *Acta biomaterialia* **2010**, *6*, 1047.
- [109] H. Xing, B. Zou, X. Liu, X. Wang, C. Huang, Y. Hu, *Journal of the European Ceramic Society* **2020**, *40*, 5797.
- [110] R. Raman, B. Bhaduri, M. Mir, A. Shkumatov, M. K. Lee, G. Popescu, H. Kong, R. Bashir, *Advanced healthcare materials* **2016**, *5*, 610.

- [111] V. Chan, P. Zorlutuna, J. H. Jeong, H. Kong, R. Bashir, *Lab on a chip* **2010**, *10*, 2062.
- [112] V. Chan, J. H. Jeong, P. Bajaj, M. Collens, T. Saif, H. Kong, R. Bashir, *Lab on a chip* **2012**, *12*, 88.
- [113] P. Zorlutuna, J. H. Jeong, H. Kong, R. Bashir, *Adv Funct Materials* **2011**, *21*, 3642.
- [114] K. Arcaute, B. K. Mann, R. B. Wicker, *Annals of biomedical engineering* **2006**, *34*, 1429.
- [115] K. Arcaute, B. K. Mann, R. B. Wicker, *Tissue engineering. Part C, Methods* **2011**, *17*, 27.
- [116] G. Mapili, Y. Lu, S. Chen, K. Roy, *Journal of biomedical materials research. Part B, Applied biomaterials* **2005**, *75*, 414.
- [117] Y. Lu, G. Mapili, G. Suhali, S. Chen, K. Roy, *Journal of biomedical materials research. Part A* **2006**, *77*, 396.
- [118] A. K. Mishra, T. J. Wallin, W. Pan, A. Xu, K. Wang, E. P. Giannelis, B. Mazzolai, R. F. Shepherd, *Science robotics* **2020**, *5*.
- [119] *Multi-polymer microstereolithography for hybrid opto-MEMS*, IEEE **2001**.
- [120] R. Wicker, F. Medina, C. Elkins **2004**.
- [121] C. Xia, N. Fang, *J. Micromech. Microeng.* **2009**, *19*, 115029.
- [122] X. Kuang, J. Wu, K. Chen, Z. Zhao, Z. Ding, F. Hu, D. Fang, H. J. Qi, *Science advances* **2019**, *5*, eaav5790.
- [123] G. I. Peterson, J. J. Schwartz, Di Zhang, B. M. Weiss, M. A. Ganter, D. W. Storti, A. J. Boydston, *ACS applied materials & interfaces* **2016**, *8*, 29037.
- [124] Z. Zhao, J. Wu, X. Mu, H. Chen, H. J. Qi, D. Fang, *Macromolecular rapid communications* **2017**, *38*.
- [125] Z. Zhao, J. Wu, X. Mu, H. Chen, H. J. Qi, D. Fang, *Science advances* **2017**, *3*, e1602326.
- [126] J. Hobich, E. Blasco, M. Wegener, H. Mutlu, C. Barner-Kowollik, *Macro Chemistry & Physics* **2023**, *224*.
- [127] G. Barany, R. B. Merrifield, *Journal of the American Chemical Society* **1977**, *99*, 7363.
- [128] F. A. Leibfarth, K. M. Mattson, B. P. Fors, H. A. Collins, C. J. Hawker, *Angewandte Chemie (International ed. in English)* **2013**, *52*, 199.

- [129] A. J. Teator, D. N. Lastovickova, C. W. Bielawski, *Chemical reviews* **2016**, *116*, 1969.
- [130] N. D. Dolinski, Z. A. Page, E. B. Callaway, F. Eisenreich, R. V. Garcia, R. Chavez, D. P. Bothman, S. Hecht, F. W. Zok, C. J. Hawker, *Advanced Materials* **2018**, *30*, e1800364.
- [131] N. D. Dolinski, E. B. Callaway, C. S. Sample, L. F. Gockowski, R. Chavez, Z. A. Page, F. Eisenreich, S. Hecht, M. T. Valentine, F. W. Zok, C. J. Hawker, *ACS applied materials & interfaces* **2021**, *13*, 22065.
- [132] J. J. Schwartz, A. J. Boydston, *Nature communications* **2019**, *10*, 791.
- [133] E. Rossegger, K. Moazzen, M. Fleisch, S. Schlögl, *Polym. Chem.* **2021**, *12*, 3077.
- [134] L. Brunsveld, B. J. Folmer, E. W. Meijer, R. P. Sijbesma, *Chemical reviews* **2001**, *101*, 4071.
- [135] C. Fouquey, J.-M. Lehn, A.-M. Levelut, *Advanced Materials* **1990**, *2*, 254.
- [136] Y. Amamoto, H. Otsuka, A. Takahara, K. Matyjaszewski, *Advanced Materials* **2012**, *24*, 3975.
- [137] B. T. Michal, C. A. Jaye, E. J. Spencer, S. J. Rowan, *ACS macro letters* **2013**, *2*, 694.
- [138] P. Chakma, D. Konkolewicz, *Angewandte Chemie (International ed. in English)* **2019**, *58*, 9682.
- [139] W. Zou, J. Dong, Y. Luo, Q. Zhao, T. Xie, *Advanced Materials* **2017**, *29*.
- [140] J. M. Winne, L. Leibler, F. E. Du Prez, *Polym. Chem.* **2019**, *10*, 6091.
- [141] W. Denissen, J. M. Winne, F. E. Du Prez, *Chemical science* **2016**, *7*, 30.
- [142] W. Alabiso, S. Schlögl, *Polymers* **2020**, *12*.
- [143] O. Konuray, F. Di Donato, M. Sangermano, J. Bonada, A. Tercjak, X. Fernandez-Francos, A. Serra, X. Ramis, *Express Polym. Lett.* **2020**, *14*, 881.
- [144] M. S. Silverstein, *Polymer* **2020**, *207*, 122929.
- [145] C. R. Szczepanski, J. W. Stansbury, *European polymer journal* **2015**, *67*, 314.
- [146] B. Peng, Y. Yang, K. Gu, E. J. Amis, K. A. Cavicchi, *ACS Materials Lett.* **2019**, *1*, 410.
- [147] Y. Wang, J. Wang, *Micromachines* **2018**, *9*.

- [148] B. Cappella, G. Dietler, *Surface Science Reports* **1999**, *34*, 1.
- [149] E. Hasa, J. W. Stansbury, C. A. Guymon, *Polymer* **2020**, *202*, 122699.
- [150] F. Zareanshahraki, A. Jannesari, S. Rastegar, *Polymer Testing* **2020**, *85*, 106412.
- [151] C. Rocco, F. Karasu, C. Croutxé-Barghorn, X. Allonas, M. Lecompère, G. Riess, Y. Zhang, A. Esteves, L. van der Ven, R. van Benthem, G. de With, *Materials Today Communications* **2016**, *6*, 17.
- [152] F. Wu, M. Misra, A. K. Mohanty, *Polymer Degradation and Stability* **2020**, *173*, 109066.
- [153] E. Hasa, J. P. Scholte, J. L. P. Jessop, J. W. Stansbury, C. A. Guymon, *Macromolecules* **2019**, *52*, 2975.
- [154] J. Bachmann, S. Schmolzer, M. A. Ruderer, G. Fruhmann, O. Hinrichsen, *SPE Polymers* **2022**, *3*, 41.
- [155] F. Jiang, D. Drummer, *Polymers* **2020**, *12*.
- [156] J. H. Martin, B. D. Yahata, J. M. Hundley, J. A. Mayer, T. A. Schaedler, T. M. Pollock, *Nature* **2017**, *549*, 365.
- [157] M. Hofmann, *ACS Macro Lett.* **2014**, *3*, 382.
- [158] M. Nadgorny, A. Ameli, *ACS applied materials & interfaces* **2018**, *10*, 17489.
- [159] R. L. Truby, J. A. Lewis, *Nature* **2016**, *540*, 371.
- [160] P. Fiedor, J. Ortyl, *Materials (Basel, Switzerland)* **2020**, *13*.
- [161] T. D. Ngo, A. Kashani, G. Imbalzano, K. T. Nguyen, D. Hui, *Composites Part B: Engineering* **2018**, *143*, 172.
- [162] M. Shusteff, A. E. M. Browar, B. E. Kelly, J. Henriksson, T. H. Weisgraber, R. M. Panas, N. X. Fang, C. M. Spadaccini, *Science advances* **2017**, *3*, eaao5496.
- [163] B. Cao, N. Boechler, A. J. Boydston, *Polymer* **2018**, *152*, 4.
- [164] D. Ahn, L. M. Stevens, K. Zhou, Z. A. Page, *ACS central science* **2020**, *6*, 1555.
- [165] M. S. Mannoor, Z. Jiang, T. James, Y. L. Kong, K. A. Malatesta, W. O. Soboyejo, N. Verma, D. H. Gracias, M. C. McAlpine, *Nano letters* **2013**, *13*, 2634.
- [166] Y. L. Yap, S. L. Sing, W. Y. Yeong, *RPJ* **2020**, *26*, 1345.

- [167] A. Zolfagharian, A. Kaynak, A. Kouzani, *Materials & Design* **2020**, 188, 108411.
- [168] J. Z. Gul, M. Sajid, M. M. Rehman, G. U. Siddiqui, I. Shah, K.-H. Kim, J.-W. Lee, K. H. Choi, *Science and technology of advanced materials* **2018**, 19, 243.
- [169] F. P. W. Melchels, J. Feijen, D. W. Grijpma, *Biomaterials* **2010**, 31, 6121.
- [170] P. Ahangar, M. E. Cooke, M. H. Weber, D. H. Rosenzweig, *Applied Sciences* **2019**, 9, 1713.
- [171] W. Zhu, X. Ma, M. Gou, D. Mei, K. Zhang, S. Chen, *Current opinion in biotechnology* **2016**, 40, 103.
- [172] Y. BOZKURT, E. KARAYEL, *Journal of Materials Research and Technology* **2021**, 32, 987.
- [173] A. H. Espera, J. R. C. Dizon, Q. Chen, R. C. Advincula, *Progress in Additive Manufacturing* **2019**, 4, 245.
- [174] D. V. Baker, C. Bao, W. S. Kim, *ACS Appl. Electron. Mater.* **2021**, 3, 2423.
- [175] E. Sachyani Keneth, A. Kamyshny, M. Totaro, L. Beccai, S. Magdassi, *Advanced materials (Deerfield Beach, Fla.)* **2021**, 33, e2003387.
- [176] K. Jung, N. Corrigan, M. Ciftci, J. Xu, S. E. Seo, C. J. Hawker, C. Boyer, *Advanced materials (Deerfield Beach, Fla.)* **2020**, 32, e1903850.
- [177] D. Joung, V. Truong, C. C. Neitzke, S.-Z. Guo, P. J. Walsh, J. R. Monat, F. Meng, S. H. Park, J. R. Dutton, A. M. Parr, M. C. McAlpine, *Advanced functional materials* **2018**, 28.
- [178] *2017 IEEE International Conference on Industrial Engineering and Engineering Management (IEEM)*, IEEE **2017 - 2017**.
- [179] G. Coelho, T. M. F. Chaves, A. F. Goes, E. C. Del Massa, O. Moraes, M. Yoshida, *Child's nervous system ChNS official journal of the International Society for Pediatric Neurosurgery* **2018**, 34, 749.
- [180] A. J. Cresswell-Boyes, A. H. Barber, D. Mills, A. Tatla, G. R. Davis, *Journal of microscopy* **2018**, 272, 207.
- [181] M. Schaffner, J. A. Faber, L. Pianegonda, P. A. Rühls, F. Coulter, A. R. Studart, *Nature communications* **2018**, 9, 878.

- [182] C. Yuan, D. J. Roach, C. K. Dunn, Q. Mu, X. Kuang, C. M. Yakacki, T. J. Wang, K. Yu, H. J. Qi, *Soft matter* **2017**, *13*, 5558.
- [183] Y.-F. Zhang, N. Zhang, H. Hingorani, N. Ding, D. Wang, C. Yuan, B. Zhang, G. Gu, Q. Ge, *Adv. Funct. Mater.* **2019**, *29*, 1806698.
- [184] A. D. Valentine, T. A. Busbee, J. W. Boley, J. R. Raney, A. Chortos, A. Kotikian, J. D. Berrigan, M. F. Durstock, J. A. Lewis, *Advanced materials (Deerfield Beach, Fla.)* **2017**, *29*.
- [185] V. A. Bobrin, K. Lee, J. Zhang, N. Corrigan, C. Boyer, *Advanced materials (Deerfield Beach, Fla.)* **2022**, *34*, e2107643.
- [186] Q. Ge, A. H. Sakhaei, H. Lee, C. K. Dunn, N. X. Fang, M. L. Dunn, *Scientific reports* **2016**, *6*, 31110.
- [187] C. Zhou, Y. Chen, Z. Yang, B. Khoshnevis, *RPJ* **2013**, *19*, 153.
- [188] D. Chen, X. Zheng, *Scientific reports* **2018**, *8*, 9139.
- [189] J. Odent, S. Vanderstappen, A. Toncheva, E. Pichon, T. J. Wallin, K. Wang, R. F. Shepherd, P. Dubois, J.-M. Raquez, *J. Mater. Chem. A* **2019**, *7*, 15395.
- [190] H. Kim, J.-W. Choi, R. Wicker, *RPJ* **2010**, *16*, 232.
- [191] K. Ikemura, K. Ichizawa, M. Yoshida, S. Ito, T. Endo, *Dental materials journal* **2008**, *27*, 765.
- [192] A. Huber, A. Kuschel, T. Ott, G. Santiso-Quinones, D. Stein, J. Bräuer, R. Kissner, F. Krumeich, H. Schönberg, J. Levalois-Grützmacher, H. Grützmacher, *Angewandte Chemie (International ed. in English)* **2012**, *51*, 4648.
- [193] M. Sangermano, W. Carbonaro, G. Malucelli, A. Priola, *Macromol. Mater. Eng.* **2008**, *293*, 515.
- [194] E. Rossegger, R. Höller, D. Reisinger, J. Strasser, M. Fleisch, T. Griesser, S. Schlögl, *Polym. Chem.* **2021**, *12*, 639.
- [195] E. Rossegger, D. Nees, S. Turisser, S. Radl, T. Griesser, S. Schlögl, *Polym. Chem.* **2020**, *11*, 3125.
- [196] A. Oesterreicher, C. Gorsche, S. Ayalur-Karunakaran, A. Moser, M. Edler, G. Pinter, S. Schlögl, R. Liska, T. Griesser, *Macromolecular rapid communications* **2016**, *37*, 1701.

- [197] J. V. Crivello, J. H. W. Lam, *Journal of Polymer Science: Polymer Chemistry Edition* **1979**, *17*, 977.
- [198] J.-P. Fouassier, J. Lalevée, J. Laleve, *Photoinitiators for Polymer Synthesis Scope, Reactivity, and Efficiency*, John Wiley & Sons, Incorporated, Weinheim, GERMANY **2012**.
- [199] M. Fleisch, A. Thalhamer, G. Meier, I. Raguž, P. F. Fuchs, G. Pinter, S. Schlögl, M. Berer, *Materials Today Advances* **2021**, *11*, 100155.
- [200] E. Rossegger, R. Höller, D. Reisinger, M. Fleisch, J. Strasser, V. Wieser, T. Griesser, S. Schlögl, *Polymer* **2021**, *221*, 123631.
- [201] M. Paggi, A. Carpinteri, *Appl. Mech. Rev.* **2008**, *61*, 20801.
- [202] B. Blakey-Milner, P. Gradl, G. Snedden, M. Brooks, J. Pitot, E. Lopez, M. Leary, F. Berto, A. Du Plessis, *Materials & Design* **2021**, *209*, 110008.
- [203] A. Vafadar, F. Guzzomi, A. Rassau, K. Hayward, *Applied Sciences* **2021**, *11*, 1213.
- [204] S. Hasanov, S. Alkunte, M. Rajeshirke, A. Gupta, O. Huseynov, I. Fidan, F. Alifui-Segbaya, A. Rennie, *JMMP* **2022**, *6*, 4.
- [205] D. Han, H. Lee, *Current Opinion in Chemical Engineering* **2020**, *28*, 158.
- [206] E. Roels, S. Terry, F. Iida, A. W. Bosman, S. Norvez, F. Clemens, G. van Assche, B. Vanderborght, J. Brancart, *Advanced materials (Deerfield Beach, Fla.)* **2022**, *34*, e2104798.
- [207] T. D. Ngo, A. Kashani, G. Imbalzano, K. T. Nguyen, D. Hui, *Composites Part B: Engineering* **2018**, *143*, 172.
- [208] X. Zheng, H. Lee, T. H. Weisgraber, M. Shusteff, J. DeOtte, E. B. Duoss, J. D. Kuntz, M. M. Biener, Q. Ge, J. A. Jackson, S. O. Kucheyev, N. X. Fang, C. M. Spadaccini, *Science (New York, N.Y.)* **2014**, *344*, 1373.
- [209] J. Huang, Q. Qin, J. Wang, *Processes* **2020**, *8*, 1138.
- [210] R. Chaudhary, P. Fabbri, E. Leoni, F. Mazzanti, R. Akbari, C. Antonini, *Prog Addit Manuf* **2023**, *8*, 331.
- [211] J. W. Halloran, *Annu. Rev. Mater. Res.* **2016**, *46*, 19.
- [212] B. Tiller, A. Reid, B. Zhu, J. Guerreiro, R. Domingo-Roca, J. Curt Jackson, J. Windmill, *Materials & Design* **2019**, *165*, 107593.

- [213] M. M. Zieger, P. Mueller, A. S. Quick, M. Wegener, C. Barner-Kowollik, *Angewandte Chemie (International ed. in English)* **2017**, *56*, 5625.
- [214] M. Schmid, S. Thiele, A. Herkommer, H. Giessen, *Optics letters* **2018**, *43*, 5837.
- [215] D. Han, Z. Lu, S. A. Chester, H. Lee, *Scientific reports* **2018**, *8*, 1963.
- [216] E. Rossegger, J. Strasser, R. Höller, M. Fleisch, M. Berer, S. Schlögl, *Macromolecular rapid communications* **2023**, *44*, e2200586.
- [217] F. Chambon, H. H. Winter, *Journal of Rheology* **1987**, *31*, 683.
- [218] A. Balcerak, J. Kabatc, *RSC advances* **2019**, *9*, 28490.
- [219] I. Calvez, C. R. Szczepanski, V. Landry, *Macromolecules* **2022**, *55*, 3129.
- [220] H. Sasaki, *Progress in Organic Coatings* **2007**, *58*, 227.
- [221] T. Zandrini, N. Liaros, L. J. Jiang, Y. F. Lu, J. T. Fourkas, R. Osellame, T. Baldacchini, *Opt. Mater. Express* **2019**, *9*, 2601.
- [222] J. R. Nowers, B. Narasimhan, *Polymer* **2006**, *47*, 1108.
- [223] A. A. Baidak, J. M. Ligeois, L. H. Sperling, *J. Polym. Sci. B Polym. Phys.* **1997**, *35*, 1973.
- [224] K. Dean, W. D. Cook, *Macromolecules* **2002**, *35*, 7942.
- [225] M. Gastaldi, F. Cardano, M. Zanetti, G. Viscardi, C. Barolo, S. Bordiga, S. Magdassi, A. Fin, I. Roppolo, *ACS Materials Lett.* **2021**, *3*, 1.
- [226] M. Aoki, A. Shundo, S. Yamamoto, K. Tanaka, *Soft matter* **2020**, *16*, 7470.
- [227] V. S. D. Voet, G. H. M. Schnelting, J. Xu, K. Loos, R. Folkersma, J. Jager, *Journal of visualized experiments JoVE* **2018**.
- [228] E. M. Maines, M. K. Porwal, C. J. Ellison, T. M. Reineke, *Green Chem.* **2021**, *23*, 6863.
- [229] V. S. D. Voet, J. Guit, K. Loos, *Macromolecular rapid communications* **2021**, *42*, e2000475.
- [230] S. M. Scott, Z. Ali, *Micromachines* **2021**, *12*.
- [231] R. Chaudhary, P. Fabbri, E. Leoni, F. Mazzanti, R. Akbari, C. Antonini, *Prog Addit Manuf* **2023**, *8*, 331.

- [232] *Additive Manufacturing*, Elsevier **2021**.
- [233] E. Skliutas, S. Kasetaitė, L. Jonušauskas, J. Ostrauskaite, M. Malinauskas, *Opt. Eng.* **2018**, *57*, 1.
- [234] C. J. Thrasher, J. J. Schwartz, A. J. Boydston, *ACS applied materials & interfaces* **2017**, *9*, 39708.
- [235] L. Wu, L. Zhao, M. Jian, Y. Mao, M. Yu, X. Guo, *RPJ* **2018**, *24*, 1500.
- [236] Y. Wu, H. Su, M. Li, H. Xing, *Journal of biomedical materials research. Part A* **2023**, *111*, 527.
- [237] Z. Zhao, X. Tian, X. Song, *J. Mater. Chem. C* **2020**, *8*, 13896.
- [238] E. Yang, S. Miao, J. Zhong, Z. Zhang, D. K. Mills, L. G. Zhang, *Polymer reviews (Philadelphia, Pa.)* **2018**, *58*, 668.
- [239] Y. Zhu, C. Romain, C. K. Williams, *Nature* **2016**, *540*, 354.
- [240] J. Guit, M. B. Tavares, J. Hul, C. Ye, K. Loos, J. Jager, R. Folkersma, V. S. Voet, *ACS Appl. Polym. Mater.* **2020**, *2*, 949.
- [241] C. Lu, C. Wang, J. Yu, J. Wang, F. Chu, *ChemSusChem* **2020**, *13*, 893.
- [242] Q. Ma, D. Mohawk, B. Jahani, X. Wang, Y. Chen, A. Mahoney, J. Y. Zhu, L. Jiang, *ACS Appl. Polym. Mater.* **2020**, *2*, 4666.
- [243] M. Lebedevaite, J. Ostrauskaite, E. Skliutas, M. Malinauskas, *J of Applied Polymer Sci* **2020**, *137*, 2130.
- [244] A. Barkane, O. Platnieks, M. Jurinovs, S. Kasetaitė, J. Ostrauskaite, S. Gaidukovs, Y. Habibi, *Polymers* **2021**, *13*.
- [245] S. Briede, A. Barkane, M. Jurinovs, V. K. Thakur, S. Gaidukovs, *Current Opinion in Green and Sustainable Chemistry* **2022**, *35*, 100626.
- [246] A. Barkane, M. Jurinovs, S. Briede, O. Platnieks, P. Onufrijevs, Z. Zelca, S. Gaidukovs, *3D Printing and Additive Manufacturing* **2022**, *16*, 171.
- [247] A. M. Borrero-López, D. B. Guzmán, J. A. González-Delgado, J. F. Arteaga, C. Valencia, U. Pischel, J. M. Franco, *ACS Sustainable Chem. Eng.* **2021**, *9*, 11032.

- [248] P. Li, Z. Chu, Y. Chen, T. Yuan, Z. Yang, *Progress in Organic Coatings* **2021**, *159*, 106398.
- [249] Z. Wang, M. S. Ganewatta, C. Tang, *Progress in Polymer Science* **2020**, *101*, 101197.
- [250] E. Constant, O. King, A. C. Weems, *Biomacromolecules* **2022**, *23*, 2342.
- [251] A. C. Weems, K. R. Delle Chiaie, J. C. Worch, C. J. Stubbs, A. P. Dove, *Polym. Chem.* **2019**, *10*, 5959.
- [252] N. Zhang, X. Hou, X. Cui, L. Chai, H. Li, H. Zhang, Y. Wang, T. Deng, *Journal of Cleaner Production* **2021**, *296*, 126492.
- [253] B. T. White, V. Meenakshisundaram, K. D. Feller, C. B. Williams, T. E. Long, *Polymer* **2021**, *223*, 123727.
- [254] S. Cousinet, A. Ghadban, E. Fleury, F. Lortie, J.-P. Pascault, D. Portinha, *European polymer journal* **2015**, *67*, 539.
- [255] M. S. Lima, C. S. M. F. Costa, J. F. J. Coelho, A. C. Fonseca, A. C. Serra, *Green Chem.* **2018**, *20*, 4880.
- [256] S. Pandey, B. S. Rajput, S. H. Chikkali, *Green Chem.* **2021**, *23*, 4255.
- [257] M. Lomelí-Rodríguez, J. R. Corpas-Martínez, S. Willis, R. Mulholland, J. A. Lopez-Sanchez, *Polymers* **2018**, *10*.
- [258] O. Llorente, A. Barquero, M. Paulis, J. R. Leiza, *Progress in Organic Coatings* **2022**, *172*, 107137.
- [259] J. Lu, J. Li, H. Gao, D. Zhou, H. Xu, Y. Cong, W. Zhang, F. Xin, M. Jiang, *World journal of microbiology & biotechnology* **2021**, *37*, 16.
- [260] S. Feng, Z. Jiang, Z. Qiu, *Polymers* **2022**, *15*.
- [261] Z. Wei, C. Zhou, Y. Yu, Y. Li, *RSC Adv.* **2015**, *5*, 42777.
- [262] M. Lomelí-Rodríguez, M. Martín-Molina, M. Jiménez-Pardo, Z. Nasim-Afzal, S. I. Cauët, T. E. Davies, M. Rivera-Toledo, J. A. Lopez-Sanchez, *J. Polym. Sci. Part A: Polym. Chem.* **2016**, *54*, 2876.
- [263] M. Jouyandeh, H. Vahabi, N. Rabiee, M. Rabiee, M. Bagherzadeh, M. R. Saeb, *emergent mater.* **2022**, *5*, 603.

- [264] T. Robert, S. Friebel, *Green Chem.* **2016**, *18*, 2922.
- [265] S. Wang, Y. Wu, J. Dai, N. Teng, Y. Peng, L. Cao, X. Liu, *European polymer journal* **2020**, *123*, 109439.
- [266] V. V. Panic, S. I. Seslija, I. G. Popovic, V. D. Spasojevic, A. R. Popovic, V. B. Nikolic, P. M. Spasojevic, *Biomacromolecules* **2017**, *18*, 3881.
- [267] M. Maturi, C. Pulignani, E. Locatelli, V. Vetri Buratti, S. Tortorella, L. Sambri, M. Comes Franchini, *Green Chem.* **2020**, *22*, 6212.
- [268] J. Dai, S. Ma, N. Teng, X. Dai, X. Shen, S. Wang, X. Liu, J. Zhu, *Ind. Eng. Chem. Res.* **2017**, *56*, 2650.
- [269] V. Vetri Buratti, A. Sanz de Leon, M. Maturi, L. Sambri, S. I. Molina, M. Comes Franchini, *Macromolecules* **2022**, *55*, 3087.
- [270] J.-T. Miao, S. Peng, M. Ge, Y. Li, J. Zhong, Z. Weng, L. Wu, L. Zheng, *ACS Sustainable Chem. Eng.* **2020**, *8*, 9415.
- [271] J. Dai, S. Ma, Y. Wu, L. Han, L. Zhang, J. Zhu, X. Liu, *Green Chem.* **2015**, *17*, 2383.
- [272] A. Pellis, P. A. Hanson, J. W. Comerford, J. H. Clark, T. J. Farmer, *Polym. Chem.* **2019**, *10*, 843.
- [273] A. Kuenz, Y. Gallenmüller, T. Willke, K.-D. Vorlop, *Applied microbiology and biotechnology* **2012**, *96*, 1209.
- [274] B. C. Saha, G. J. Kennedy, M. J. Bowman, N. Qureshi, N. N. Nichols, *Biocatalysis and Agricultural Biotechnology* **2022**, *43*, 102418.
- [275] N. Čuk, M. Steinbücher, N. Vidmar, M. Ocepek, P. Venturini, *Coatings* **2023**, *13*, 1779.
- [276] A. B. D. Nandiyanto, R. Ragadhita, M. Fiandini, *Indonesian J. Sci. Technol* **2022**, *8*, 113.
- [277] M. G. González, J. C. Cabanelas, J. Baselga, in *Infrared Spectroscopy - Materials Science, Engineering and Technology* (Ed.: T. Theophanides), InTech **2012**.
- [278] T. Y. Lee, T. M. Roper, E. Jonsson, I. Kudyakov, K. Viswanathan, C. Nason, C. Guymon, C. Hoyle, *Polymer* **2003**, *44*, 2859.
- [279] L. Sollka, K. Lienkamp, *Macromolecular rapid communications* **2021**, *42*, e2000546.

- [280] S. Akbari, A. Root, M. Skrifvars, S. K. Ramamoorthy, D. Åkesson, *J Polym Environ* **2023**.
- [281] U. Shaukat, E. Rossegger, S. Schlögl, *Polymer* **2021**, *231*, 124110.
- [282] J. Saroia, Y. Wang, Q. Wei, M. Lei, X. Li, Y. Guo, K. Zhang, *Int J Adv Manuf Technol* **2020**, *106*, 1695.
- [283] M. Hofmann, *ACS macro letters* **2014**, *3*, 382.
- [284] M. Nadgorny, A. Ameli, *ACS applied materials & interfaces* **2018**, *10*, 17489.
- [285] B. C. Gross, J. L. Erkal, S. Y. Lockwood, C. Chen, D. M. Spence, *Analytical chemistry* **2014**, *86*, 3240.
- [286] R. L. Truby, J. A. Lewis, *Nature* **2016**, *540*, 371.
- [287] T. D. Ngo, A. Kashani, G. Imbalzano, K. T. Nguyen, D. Hui, *Composites Part B: Engineering* **2018**, *143*, 172.
- [288] B. Cao, N. Boechler, A. J. Boydston, *Polymer* **2018**, *152*, 4.
- [289] W. Associates, *Wohlers report 2016: 3D printing and additive manufacturing state of the industry annual worldwide progress report*, Wohlers Associates, Fort Collins (Colo.) **2016**.
- [290] S. Tibbits, *Archit Design* **2014**, *84*, 116.
- [291] A. Ahmed, S. Arya, V. Gupta, H. Furukawa, A. Khosla, *Polymer* **2021**, *228*, 123926.
- [292] Z. Zhang, K. G. Demir, G. X. Gu, *International Journal of Smart and Nano Materials* **2019**, *10*, 205.
- [293] M. Y. Khalid, Z. U. Arif, R. Noroozi, A. Zolfagharian, M. Bodaghi, *Journal of Manufacturing Processes* **2022**, *81*, 759.
- [294] A. Kotikian, R. L. Truby, J. W. Boley, T. J. White, J. A. Lewis, *Advanced materials (Deerfield Beach, Fla.)* **2018**, *30*.
- [295] H. Yang, W. R. Leow, T. Wang, J. Wang, J. Yu, K. He, D. Qi, C. Wan, X. Chen, *Advanced materials (Deerfield Beach, Fla.)* **2017**, *29*.
- [296] Z. Ding, C. Yuan, X. Peng, T. Wang, H. J. Qi, M. L. Dunn, *Science advances* **2017**, *3*, e1602890.

- [297] A. Lendlein, S. Kelch, *Angew. Chem. Int. Ed.* **2002**, *41*, 2034.
- [298] D. Crespy, R. M. Rossi, *Polym. Int.* **2007**, *56*, 1461.
- [299] A. S. Gladman, E. A. Matsumoto, R. G. Nuzzo, L. Mahadevan, J. A. Lewis, *Nature materials* **2016**, *15*, 413.
- [300] H. Meng, G. Li, *Polymer* **2013**, *54*, 2199.
- [301] Y. Dong, S. Wang, Y. Ke, L. Ding, X. Zeng, S. Magdassi, Y. Long, *Adv. Mater. Technol.* **2020**, *5*, 2000034.
- [302] R. Marcombe, S. Cai, W. Hong, X. Zhao, Y. Lapusta, Z. Suo, *Soft matter* **2010**, *6*, 784.
- [303] Z. Varga, G. Filipcsei, A. Szilágyi, M. Zrínyi, *Macromol. Symp.* **2005**, *227*, 123.
- [304] M. Hossain, D. K. Vu, P. Steinmann, *Arch Appl Mech* **2015**, *85*, 523.
- [305] G. Li, X. Chen, F. Zhou, Y. Liang, Y. Xiao, X. Cao, Z. Zhang, M. Zhang, B. Wu, S. Yin, Y. Xu, H. Fan, Z. Chen, W. Song, W. Yang, B. Pan, J. Hou, W. Zou, S. He, X. Yang, G. Mao, Z. Jia, H. Zhou, T. Li, S. Qu, Z. Xu, Z. Huang, Y. Luo, T. Xie, J. Gu, S. Zhu, W. Yang, *Nature* **2021**, *591*, 66.
- [306] M. Sitti, *Nat Rev Mater* **2018**, *3*, 74.
- [307] A. K. Bastola, M. Hossain, *Materials & Design* **2021**, *211*, 110172.
- [308] L. V. Nikitin, D. G. Korolev, G. V. Stepanov, L. S. Mironova, *Journal of Magnetism and Magnetic Materials* **2006**, *300*, e234-e238.
- [309] K. Zimmermann, V. A. Naletova, I. Zeidis, V. A. Turkov, E. Kolev, M. V. Lukashevich, G. V. Stepanov, *Journal of Magnetism and Magnetic Materials* **2007**, *311*, 450.
- [310] P. V. Komarov, P. G. Khalatur, A. R. Khokhlov, *Polymers for Advanced Techs* **2021**, *32*, 3922.
- [311] L. Vítková, L. Musilová, E. Achbergerová, R. Kolařík, M. Mrlík, K. Korpasová, L. Mahelová, Z. Capáková, A. Mráček, *International journal of molecular sciences* **2022**, *23*.
- [312] A. K. Bastola, N. Rodriguez, M. Behl, P. Soffiatti, N. P. Rowe, A. Lendlein, *Materials & Design* **2021**, *202*, 109515.
- [313] M. Mrinalini, S. Prasanthkumar, *ChemPlusChem* **2019**, *84*, 1103.

- [314] S. Li, H. Bai, R. F. Shepherd, H. Zhao, *Angew. Chem. Int. Ed.* **2019**, 58, 11182.
- [315] D. Schönfeld, D. Chalissery, F. Wenz, M. Specht, C. Eberl, T. Pretsch, *Molecules (Basel, Switzerland)* **2021**, 26.
- [316] L. Hines, K. Petersen, G. Z. Lum, M. Sitti, *Advanced materials (Deerfield Beach, Fla.)* **2017**, 29.
- [317] X. Kuang, D. J. Roach, J. Wu, C. M. Hamel, Z. Ding, T. Wang, M. L. Dunn, H. J. Qi, *Adv. Funct. Mater.* **2019**, 29, 1805290.
- [318] X. Liu, J. Liu, S. Lin, X. Zhao, *Materials Today* **2020**, 36, 102.
- [319] M. Cianchetti, C. Laschi, A. Menciassi, P. Dario, *Nat Rev Mater* **2018**, 3, 143.
- [320] A. Lendlein, O. E. C. Gould, *Nat Rev Mater* **2019**, 4, 116.
- [321] Y. S. Lui, W. T. Sow, L. P. Tan, Y. Wu, Y. Lai, H. Li, *Acta biomaterialia* **2019**, 92, 19.
- [322] R. Ahamed, S.-B. Choi, M. M. Ferdous, *Journal of Intelligent Material Systems and Structures* **2018**, 29, 2051.
- [323] Q. Cao, Q. Fan, Q. Chen, C. Liu, X. Han, L. Li, *Mater. Horiz.* **2020**, 7, 638.
- [324] K. J. Merazzo, A. C. Lima, M. Rincón-Iglesias, L. C. Fernandes, N. Pereira, S. Lanceros-Mendez, P. Martins, *Mater. Horiz.* **2021**, 8, 2654.
- [325] M. Rafiee, R. D. Farahani, D. Therriault, *Advanced science (Weinheim, Baden-Wuerttemberg, Germany)* **2020**, 7, 1902307.
- [326] M. R. Jolly, J. D. Carlson, B. C. Muñoz, *Journal of Intelligent Material Systems and Structures* **1996**, 5, 607.
- [327] J. Carlson, M. R. Jolly, *Mechatronics* **2000**, 10, 555.
- [328] P. Allia, G. Barrera, P. Tiberto, T. Nardi, Y. Leterrier, M. Sangermano, *Journal of Applied Physics* **2014**, 116, 113903.
- [329] J. Amici, P. Allia, P. Tiberto, M. Sangermano, *Macromol. Chem. Phys.* **2011**, 212, 1629.
- [330] C. Albornoz, E. E. Sileo, S. E. Jacobo, *Physica B: Condensed Matter* **2004**, 354, 149.
- [331] Q. Ze, X. Kuang, S. Wu, J. Wong, S. M. Montgomery, R. Zhang, J. M. Kovitz, F. Yang, H. J. Qi, R. Zhao, *Advanced materials (Deerfield Beach, Fla.)* **2020**, 32, e1906657.

- [332] T. N. Do, H. Phan, T.-Q. Nguyen, Y. Visell, *Adv. Funct. Mater.* **2018**, 28, 1800244.
- [333] S. Di Zhang, Y. C. Zhai, Z. F. Zhang, *AMR* **2011**, 287-290, 2032.
- [334] M. A. Moreno, J. Gonzalez-Rico, M. L. Lopez-Donaire, A. Arias, D. Garcia-Gonzalez, *Journal of Magnetism and Magnetic Materials* **2021**, 224, 109148.
- [335] A. K. Bastola, M. Hossain, *Composites Part B: Engineering* **2020**, 200, 108348.
- [336] A. Hooshiar, A. Payami, J. Dargahi, S. Najarian, *Mechanical Systems and Signal Processing* **2021**, 161, 107918.
- [337] S. Xuan, Y. Xu, T. Liu, X. Gong, *International Journal of Smart and Nano Materials* **2015**, 6, 135.
- [338] Y. Xu, G. Liao, T. Liu, in *Nanofluid Flow in Porous Media* (Eds.: M. Sheikholeslami Kandelousi, S. Ameen, M. Shaheer Akhtar, H.-S. Shin), IntechOpen **2020**.
- [339] L. A. Makarova, Y. Alekhina, A. S. Omelyanchik, D. Peddis, V. V. Spiridonov, V. V. Rodionova, N. S. Perov, *Journal of Magnetism and Magnetic Materials* **2019**, 485, 413.
- [340] M. D'Auria, D. Davino, R. Pantani, L. Sorrentino, *Smart Mater. Struct.* **2016**, 25, 55014.
- [341] A. Hodaiei, O. Akhlaghi, N. Khani, T. Aytas, D. Sezer, B. Tatli, Y. Z. Menciloglu, B. Koc, O. Akbulut, *ACS applied materials & interfaces* **2018**, 10, 9873.
- [342] A. Dey, I. N. Roan Eagle, N. Yodo, *JMMP* **2021**, 5, 69.
- [343] M. A. S. R. Saadi, A. Maguire, N. T. Pottackal, M. S. H. Thakur, M. M. Ikram, A. J. Hart, P. M. Ajayan, M. M. Rahman, *Advanced materials (Deerfield Beach, Fla.)* **2022**, 34, e2108855.
- [344] J. J. Restrepo, H. A. Colorado, *Journal of Composite Materials* **2020**, 54, 647.
- [345] Y. Kim, H. Yuk, R. Zhao, S. A. Chester, X. Zhao, *Nature* **2018**, 558, 274.
- [346] A. Amirov, A. Omelyanchik, D. Murzin, V. Kolesnikova, S. Vorontsov, I. Musov, K. Musov, S. Khashirova, V. Rodionova, *Processes* **2022**, 10, 2412.
- [347] D. Kokkinis, M. Schaffner, A. R. Studart, *Nature communications* **2015**, 6, 8643.
- [348] A. K. Bastola, M. Paudel, L. Li, *Polymer* **2018**, 149, 213.

- [349] L. Lu, P. Guo, Y. Pan, *Journal of Manufacturing Science and Engineering* **2017**, *139*, 137.
- [350] E. M. Palmero, J. Rial, J. de Vicente, J. Camarero, B. Skårman, H. Vidarsson, P.-O. Larsson, A. Bollero, *Science and technology of advanced materials* **2018**, *19*, 465.
- [351] C. Huber, C. Abert, F. Bruckner, M. Groenefeld, S. Schuschnigg, I. Teliban, C. Vogler, G. Wautischer, R. Windl, D. Suess, *Scientific reports* **2017**, *7*, 9419.
- [352] J. A. Cuenca, K. Bugler, S. Taylor, D. Morgan, P. Williams, J. Bauer, A. Porch, *Journal of physics. Condensed matter an Institute of Physics journal* **2016**, *28*, 106002.
- [353] J. H. Kim, S. Lee, M. Wajahat, H. Jeong, W. S. Chang, H. J. Jeong, J.-R. Yang, J. T. Kim, S. K. Seol, *ACS nano* **2016**, *10*, 8879.
- [354] S. Lantean, G. Barrera, C. F. Pirri, P. Tiberto, M. Sangermano, I. Roppolo, G. Rizza, *Adv. Mater. Technol.* **2019**, *4*, 1900505.
- [355] S. Lantean, I. Roppolo, M. Sangermano, M. Hayoun, H. Dammak, G. Rizza, *Additive Manufacturing* **2021**, *47*, 102343.
- [356] S. Lantean, I. Roppolo, M. Sangermano, M. Hayoun, H. Dammak, G. Barrera, P. Tiberto, C. F. Pirri, L. Bodelot, G. Rizza, *Adv. Mater. Technol.* **2022**, *7*, 2200288.
- [357] E. Rossegger, R. Höller, K. Hrbinič, M. Sangermano, T. Griesser, S. Schlögl, *Adv Eng Mater* **2022**.
- [358] E. Rossegger, R. Höller, D. Reisinger, J. Strasser, M. Fleisch, T. Griesser, S. Schlögl, *Polym. Chem.* **2021**, *12*, 639.
- [359] C. Hinczewski, S. Corbel, T. Chartier, *Rapid Prototyping Journal* **1998**, *4*, 104.
- [360] J.-H. Lee, C.-M. Um, I. Lee, *Dental materials official publication of the Academy of Dental Materials* **2006**, *22*, 515.
- [361] N. B. Cramer, C. N. Bowman, *J. Polym. Sci. A Polym. Chem.* **2001**, *39*, 3311.
- [362] M. Sahin, S. Ayalur-Karunakaran, J. Manhart, M. Wolfahrt, W. Kern, S. Schlögl, *Adv Eng Mater* **2017**, *19*.

Curriculum Vitae

Ines Cazin

Education

- 2020 - Present** **Doctoral Program at the Montanuniversität Leoben (Austria)**
Doctoral thesis: Synthesis of stimuli-responsive polymers for the preparation of complex 3D objects with spatially resolved functionalities.
- 2015 – 2017** **Master of Science, Applied Chemistry**
Faculty of Chemical Engineering and Technology, University of Zagreb, Zagreb (Croatia)
Master's thesis: Novel Heterogeneous Photoredox Transformations Using Organic Materials.
- 2011 – 2015** **Bachelor of Science, Applied Chemistry**
Faculty of Chemical Engineering and Technology, University of Zagreb, Zagreb (Croatia)
Bachelor's thesis: L – ascorbic Acid and its Derivatives.

Work experience

- 01/2020 – Present** **Researcher and PhD Student**
Polymer Competence Center Leoben (PCCL), Leoben (Austria)
Project: Synthesis of stimuli-responsive polymers for the preparation of complex 3D objects with spatially resolved functionalities.
- 10/2018 – 10/2019** **Research Assistant**
KU Leuven, Department of Chemistry, Leuven (Belgium)
Project: Versatile Nanostructured Functionalization of 2D Carbon Surfaces.
- 02/2018 – 09/2018** **Research Assistant**
KU Leuven, Department of Pharmaceutical and Pharmacological Sciences, Leuven (Belgium)
Project: Imaging the Link Between Metabotropic and Ionotropic Communication.

Research experience

- 02/2023 – 04/2023** **Visiting PhD Student**
Helios TBLUS, d.o.o., Domžale (Slovenia)
Project: Synthesis of Bio-Based Resin.
- 09/2021 – 12/2021** **Visiting PhD Student**
Polytechnic University of Turin, Turin (Italy)
Project: 3D Printing of Magneto-responsive Polymeric Materials.
- 03/2017 – 09/2017** **Student Researcher**
Max Planck Institute of Colloids and Interfaces, Potsdam (Germany)
Master's thesis: Novel Heterogeneous Photoredox Transformations Using Organic Materials.
- 07/2015 – 10/2015** **Student Researcher**
University of Namur, Unit of Organic Chemistry, NAMUR MEDICINE & Drug Innovation Center (NAME DIC), Namur (Belgium)
Project: Flow Synthesis of Combretastatine A-4.
- 02/2014 – 06/2015** **Student Researcher**
Faculty of Chemical Engineering and Technology, Department of Organic Chemistry, University of Zagreb, Zagreb (Croatia)
Project: Synthesis and Cytostatic Evaluations of Novel Nitrogen Heterocycles Library.
- 09/2014 – 10/2014** **Student Trainee**
Ruder Bošković Institute, Division of Organic Chemistry and Biochemistry, Zagreb (Croatia)
Project: Synthesis of Octapeptides and Disaccharides.

Research grant

- **Deutscher Akademischer Austauschdienst (DAAD) Research Scholarship** for 7 months stay in the group of Prof. Peter H. Seeberger at Max Planck Institute of Colloids and Interfaces, Germany (2017).

List of publications

- (1) A. M. Macan, A. Harej, **I. Cazin**, M. Klobučar, V. Stepanić, K. Pavelić, S. K. Pavelić, D. Schols, R. Snoeck, G. Andrei, S. Raić-Malić, *European journal of medicinal chemistry* **2019**, *184*, 111739.
- (2) **I. Cazin**, E. Rossegger, G. La Guedes de Cruz, T. Griesser, S. Schlögl, *Polymers* **2020**, *13*.
- (3) **I. Cazin**, M. O. Gleirscher, M. Fleisch, M. Berer, M. Sangermano, S. Schlögl, *Additive Manufacturing* **2022**, *57*, 102977.
- (4) **I. Cazin**, E. Rossegger, I. Roppolo, M. Sangermano, P. Granitzer, K. Rumpf, S. Schlögl, *RSC advances* **2023**, *13*, 17536.
- (5) **I. Cazin**, K. Plevová, W. Alabiso, E. Vidović, S. Schlögl, *Adv Eng Mater* **2024**.
- (6) **I. Cazin**, M. Ocepek, J. Kecelj, A. S. Stražar, S. Schlögl, *Materials* **2024**, *17*, 1890.

Other skills

- Research expertise:** Organic synthetic chemistry, medicinal chemistry, flow chemistry, photochemistry, surface science, polymer chemistry.
- Computer skills:** Microsoft Office, ChemDraw, MestreNova, Origin, SPIP™, Opus, SciFinder.
- Language:** English (Fluent), German (A2), Italian (Limited), Croatian (Native).
- Interests:** Science and technology, science communication blogs, music (playing classical and acoustic guitar), history, hiking.